DESIGN, CONTROL AND USER EVALUATIONS OF A SELF-ALIGNING KNEE EXOSKELETON

by
ÇAĞATAY IRMAK

Submitted to the Graduate School of Engineering and Natural Sciences
in partial fulfillment of
the requirements for the degree of Master of Science

Sabancı University
July 2022

ABSTRACT

DESIGN, CONTROL AND USER EVALUATIONS OF
A SELF-ALIGNING KNEE EXOSKELETON

ÇAĞATAY IRMAK

Mechatronics Engineering, Master's Thesis, July 2022

Thesis Supervisor: Prof. Volkan Patoğlu

Keywords: Physical human-robot interaction, rehabilitation robotics, interaction control, series elastic actuation, force-feedback exoskeletons, self-alignment, compliant mechanisms, human subject experiments.

The demand for the treatment and rehabilitation of lower and upper extremities is expected to increase due to various reasons, such as the growing world population and increasing neurological disorders. Robot-assisted rehabilitation is preferred for the administration of physical therapies, as repetitive and physically demanding rehabilitation treatments can be delivered with high intensity and accuracy, while simultaneously ensuring the safety of patients. Furthermore, these devices can provide quantitative measurements of patient progress thanks to their integrated sensors and administer customized assistance to satisfy the individual needs of each patient.

In this thesis, we present a self-aligning robot-assisted knee exoskeleton to improve the mobility of patients. The knee exoskeleton features self-alignment based on a compliant mechanism to ensure the ergonomic movements of the knee. Thanks to this self-aligning property, the knee exoskeleton enables the translational movements of the knee joint in the sagittal plane, in addition to the main flexion/extension movements. Furthermore, a Bowden cable-based series elastic actuator is utilized for the remote placement of the actuators while enabling high-fidelity interaction control.

As a novel feature, a large stroke XY-stage compliant mechanism is proposed to address the misalignment problem between the human knee joint and the exoskeleton. A compliant mechanism with high rotational and low translational stiffness levels is designed such that the self-alignment mechanism can be implemented in a compact and light-weight form, while featuring no backlash and friction. Through the compliant alignment mechanism, a close match between the human knee joint and the exoskeleton joint axes is achieved by automatically aligning the joint axis of the exoskeleton, such that parasitic interaction forces induced on the user are minimized.

A Bowden cable-driven series elastic actuator is utilized for the knee exoskeleton to actively control the interaction torques applied to the knee joint, such that assistance torques can be provided to the user. Bowden cable transmission enables the actuator and harmonic reduction units to be placed at a remote location, enabling the exoskeleton to feature low mass and inertia and relieving the user from the burden of carrying this weight. Thanks to its series elastic actuation, the knee exoskeleton displays high-fidelity torque tracking performance, while also featuring active back-driveability within the control bandwidth and passive compliance for excitations above this bandwidth.

We also present a comprehensive set of human subject experiments designed to evaluate the ergonomic improvements provided by the self-alignment feature of the knee exoskeleton. The results of these human subject experiments provide evidence that the self-alignment feature of the knee exoskeleton decreases the parasitic interaction forces due to misalignment and ensures that the exoskeleton does not significantly interfere with the knee kinematics.

ÖZET

KENDİNDEN HİZALAMALI DİZ DIŞ İSKELETİNİN TASARIMI, KONTROLÜ VE KULLANICI DEĞERLENDİRMELERİ

ÇAĞATAY IRMAK

Mekatronik Mühendisliği, Yüksek Lisans Tezi, Temmuz 2022

Tez Danışmanı: Prof. Dr. Volkan Patoğlu

Anahtar Kelimeler: Fiziksel insan-robot etkileşimi, rehabilitasyon robotları, etkileşim kontrolü, seri elastik eyleme, kuvvet geri-beslemeli dış iskelet, kendinden hizalama, Bowden kablolu güç iletimi, esnek mekanizmalar, insanlı deneyler.

Kalabalıklaşan dünya nüfusu, nörolojik sorunlar ve yaralanmalar gibi çeşitli nedenlerle alt ve üst ekstremitelerin tedavi ve rehabilitasyonuna olan ihtiyaç artmaktadır. Robot destekli rehabilitasyon, fizyoterapilerdeki yoğun egzersizleri, yüksek yoğunluk ve doğrulukla tekrarlayarak güvenli bir şekilde uygulayabildiği için sıklıkla tercih edilmektedir. Ayrıca bu cihazlar, sensörleri sayesinde hastanın tedavisindeki ilerlemenin nicel ölçümlerini yaparak hastaya özel yardım sağlayabilmektedir.

Bu tezde, hastaların hareket kabiliyetini arttıran kendinden hizalamalı bir robot destekli diz dış iskeleti sunuyoruz. Diz dış iskeleti, tasarımında yer alan kendinden hizalamalı esnek mekanizması sayesinde, fleksiyon/ekstansiyon hareketlerine ek olarak, sagital düzlemde öteleme hareketlerine de olanak sağlayarak, dizin hareketlerinin ergonomik bir şekilde olmasını sağlar. Ayrıca, Bowden kablolu seri elastik eyleyici kullanımı sayesinde motor ve dişli ünitesi dizden uzağa yerleştirilebilir ve yüksek başarımlı etkileşim kontrolü sağlanabilir.

İnsan diz eklemi ile dış iskelet arasındaki hizalanma sorununu çözmek için X ve Y yönlerinde yüksek hareket alanına sahip olan özgün bir esnek mekanizma önerilmiştir. Yüksek dönme ve düşük öteleme esnekliğine sahip olan bu mekanizma, boşluk ve sürtünme içermeyen seviyede, kompakt ve hafif bir biçimde hayata geçirilebilecek şekilde tasarlanmıştır. Kendinden hizalamalı esnek mekanizma sayesinde, dış iskeletin dönme ekseni otomatik olarak hizalanarak, insan dizinin ve dış iskeletin eksenleri arasında eşleşme sağlanır. Böylece kullanıcının dizine etki eden istenmeyen etkileşim kuvvetleri azaltılır.

Diz eklemine uygulanan etkileşim torklarını aktif olarak kontrol etmek için Bowden kablo tahrikli bir seri elastik eyleyici kullanılmıştır. Bowden kablo iletimi, motor ve

harmonik dişli ünitelerinin daha avantajlı bir yere yerleştirilmesini sağlayarak, dış iskeletin daha düşük kütle ve atalete sahip olmasını sağlar ve kullanıcıyı bu ağırlığı taşıma zorunluluğundan kurtarır. Diz dış iskeleti, seri elastik eyleyicisi sayesinde yüksek duyarlılıkta tork kontrol performansı sergilerken, aynı zamanda kontrol bant genişliği içinde aktif geri sürülebilirlik ve bu bant genişliğinin girdiler içinse pasif uyumluluk sağlar.

Diz dış iskeletinin kendinden hizalamalı özelliğinin sağladığı ergonomik iyileştirmeleri değerlendirmek için kapsamlı insanlı deneyler tasarlanmıştır. Bu insanlı deneylerin sonuçları, diz dış iskeletinin kendinden hizalanma özelliğinin, hatalı hizalanma nedeniyle oluşan istenmeyen etkileşim kuvvetlerini azalttığına ve dış iskeletin oturup kalkma ve yürüyüş kinematiğini önemli ölçüde etkilemediğine dair istatiksel öneme sahip kanıtlar sunmaktadır.

ACKNOWLEDGEMENTS

I have been very lucky to encounter very important teachers who made me beyond a few levels up, in the critical times of my educational life. My primary school teacher İpek Mert, my high school psychics teacher Mehmet Dalkılıç, and my master supervisor Prof. Dr. Volkan Patoğlu.

Firstly, I need to express my deepest gratitude to my supervisor Prof.Volkan Patoğlu. In the research, he always give all the ideas in his mind, and support and improve all the ideas of students. He always push to do better in research; and also in everything; if you cant give up, you can win even Palme Dor de Cannes with setup videos.

I would like to thank committee members of this thesis: Assist. Prof. Melih Türkseven and Assist. Prof. Ramazan Ünal, for their time, interest, and insightful questions, and helpful comments to fulfill the potential of this work.

I also would like to thank İlker Sevgen, Yavuz Tokgöz, Süleyman Tutkun for their technical support.

I would like to thank Dr. Mustafa Yalçın, Dr. Alper Ergin, and Dr. Gökay Çoruhlu for their help and for sharing their experiences and technical knowledge.

I would like to thank my old lab members: Umut Çalışkan who is warm leader with helpful and kind attitude as a senior of HMI lab when I was started; Özge Orhan who is one of the best presenter I have ever seen, it was very enjoyable to work with her in the bicycle project because she is positive, hardworking collective team player and leader; Ayhan Aktaş who is very humble, warm; Uğur Mengilli who always supports and helps me.

I would also thank Ali Bonab and Ali Yaşar. We are like brothers in a home 7/24. We experienced so many enjoyable times in İstanbul. Eating, eating, eating, walking, talking up to 3 every night, watching Formula 1, diving into plum trees, getting lost at google maps... Ali Yaşar is one of the most helpful person I have seen. Ali Bonab is a hardworking professional who always supports me. I hope we will have good memories in Toscany also.

I want to thank my labmate Deniz Ece Susuz for her helpfulness in any work in the lab. Also, I wanna thank my labmate Melike Cezayirlioğlu so that she dived into plum and mulberry trees with us.

I would also thank Mehmet Emin Mumcuoğlu and Can Önol. I feel very lucky to meet Mehmet Emin because he is perfect team player with his humble, helpful,

easygoing personality. He always improves the efficiency of his teammate. Can is the one of the warmest person that I have ever seen, I really fell very lucky to meet him. He is very humble and helpful unconditionally. He always gives positive energy to the social environment. Playing chess, walking, talking, diving into music lists and mulberry trees... I also like his sportive and musical sides. I hope we will do too many hikings in the mountains, mountain and road bicycling in the future.

I would also thank Emre Cemal Gönen. Thanks to him, I can adapt very easily to my master journey. He is a very very colorful, humble, and easygoing person. He is at the level of share all the material he have without selfishness. He is a really good collective team player and hardworking pioneer leader who is perfect at task planing. I feel lucky to spend time with him socially also because he always give you positive energy. I think that it would be very productive and enjoyable engineering team with Özge, Cemal and Mehmet Emin. In the future I hope we can work together for some projects, even for hobby projects.

I would also like thank Ömer Burak Aladağ, Harun Tolasa, Taylan Özgür Kenanoğlu and Alperen Kenan for having enjoyable times inside and outside HMI lab. I need to specially thanks to Harun Tolasa for helping me in statistical analysis. I can talk with Burak forever.

I would also thank for my HMI grass field friends athletic Selimoviç Selim İz, Nouer Sıla Akpınar, Xavi Umut Celal Kenanoğlu, and İniesta Bilal Çatkın. We had enjoyable times with them inside and outside campus. I need to especially thanks to Umut and Bilal for their valuable opinions and helps in HMI.

I also would like to thank Ece Kurt, Gökan Alcan, Müge Fidan, Naida Fetic, and Ömer Kemal Adak. Naide is a hardworking and very helpful professional who always gives me motivation. Kemal abi is very positive talkative person, I really thanks him for giving positive energy to our lab.

I also wanna thanks to FC Barcelona culture, because their philosophy gives me important points of view for engineering such as focusing on collective working while enjoying, not giving up until deadline last minute, to be able to know you can not win every time.

També vull donar les gràcies a la cultura del FC Barcelona, perquè la seva filosofia em dona uns punts de vista importants per a l'enginyeria com centrar me en el treball collectiu tot gaudint, no renunciar a la data límit d'última hora, per poder saber que no es pot guanyar cada cop.

Last but foremost I would like to thank my precious parents Şehriban Irmak, Cemal Irmak and my sister İlkay Irmak for their invaluable love and support. I also wanna thanks my grand mothers Elif Irmak, Sakine Sütçü and my grand father İsmail Irmak. I also wanna thanks my uncles Erdal Irmak, Kemal Irmak, Murat Sütçü, Erkan Sütçü, they have always been very warm to me as if my big brothers. Also, I also wanna thanks my aunts Sabire Sütçü, Sırmalı Gültürk and Saliha Eroğlu; my mom and aunts they all are admirable crichton, strong and hardworking womens who always seek for their rights. I hug my cousins Mirvet Sütçü, Alev Sütçü Yılmaz, Mesude Gültürk Gençay, Melahat Gültürk, Yıldız Gültürk, Kenan Eroğlu, Uğur Eroğlu, Işılay Sütçü, İnci Sütçü, Zerrin Sütçü, Sedef Sütçü, and Çınar Irmak; my nephews Asya Gençay, Aras Gençay, Deyan Sütçü, Eda Maria Sütçü, and İlay Yılmaz.

I would like to acknowledge the financial support provided by The Scientific and Technological Research Council of Turkey (TÜBİTAK) through their grant 216M200.

To my beloved big family

LIST OF ABBREVIATIONS

TABLE OF CONTENTS

LIST OF TABLES

LIST OF FIGURES

Chapter 1

INTRODUCTION

1.1 Robot-Assisted Rehabilitation

Robotic exoskeletons are especially interesting for assistance and rehabilitation because of their correspondence with users, higher flexibility, and the possibility for use in at-home settings. Exoskeletons created for medical uses have a long history, with the first active walking exoskeleton being created by Miomir Vukobratovic in Belgrade, during the late 1960s and early 1970s. Due to their size and weight, these early concepts, however, largely proved to be infeasible. Actuator technology has historically placed restrictions on exoskeleton development, with weight being the main issue. Battery technology is a secondary issue as batteries with high energy density are needed to power an mobile exoskeleton.

Exoskeletons have become substantially more feasible over the past two decades thanks to advancements in actuator and battery technology. This has greatly benefited research on rehabilitative exoskeletons. Since then, numerous full-body exoskeletons have been created, including research-based exoskeletons, like Berkeley's BLEEX, and exoskeletons created by for-profit companies, such as Raytheon and ReWalk exoskeletons.

A large number of these exoskeletons were initially intended for military usage. For example, DARPA funds were used for the initial development of both BLEEX and Sarcos exoskeletons. But, as is the case with Sarcos, the same technology is also currently being repurposed for more civil and commercial uses. Although these full-body exoskeletons are stunning, their high cost and complexity prevent them from capturing a wide target market.

Focusing on only helping a few joints is an alternative approach and significantly

more cost-effective technique in the field of rehabilitation. Hip and knee flexion and extension, as well as ankle dorsi and plantar flexion are commonly focused joints.

Kong, et al. [16] describe an assistive knee device based on this methodology. A spur gear and a worm gear are assembled to the Brushed DC motor in order to supply the torque required for human assistance. They converted their actuator into a compact Rotary Series Elastic Actuator (cRSEA) by inserting a rotary spring between the spur and warm gears in order to precisely control and adjust the torque generated by the exoskeleton. The spring's deflections are used to determine torques. The main advantage of this system is to enable an energy buffer between the human and the actuator by filtering motor noise. The main disadvantage of this system is spring-related hysteresis.

1.2 Anatomy of Human Knee

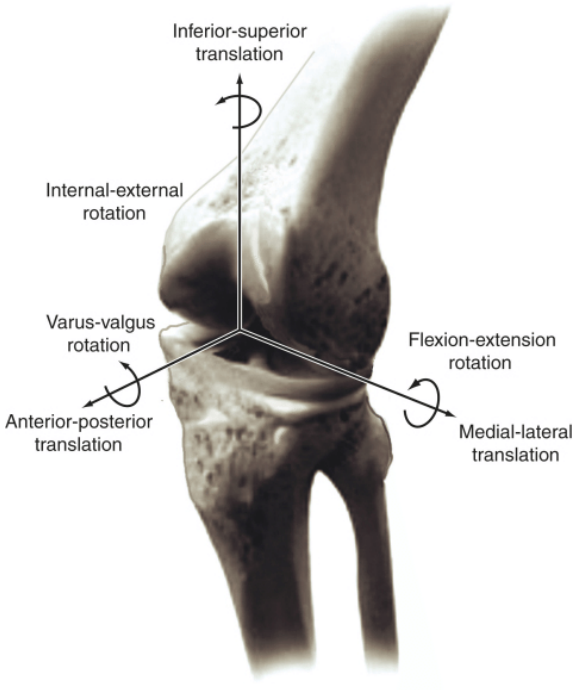

Figure 1.1 Six degrees of freedom of human knee joint [1]

It is possible to create a precise six degrees of freedom (DoF) kinematic model of the human knee joint [17]. However, strong ligaments and muscles restrain most of these DoFs, significantly limiting the range of motion of this joint. This makes it possible to accurately characterize knee kinematics using simplified knee joint models with less DoF [18].

Although the main motion of the knee in the sagittal plane is flexion-extension, the human knee in this plane cannot be accurately described by a simple revolute joint. Considerable anterior-posterior translations are caused by the tibia and femur rolling, with motions above 19 mm in the sagittal plane [19, 20, 21]. The physical structure of the femur and tibia, as well as the geometry of the articulated surfaces, have a significant impact on the precise nature of anterior-posterior translations, which are linked to the knee's rotational flexion-extension. Therefore, this anterior-posterior motion is unique to each individual.

As well as these motions in the sagittal plane, the human knee joint can also rotate internally and externally up to 50 degrees when the human knee is extended. However, the human knee's capacity to rotate both internally and externally is severely constrained when it is fully extended or supporting the body weight [22].

1.3 Joint Misalignment Problem

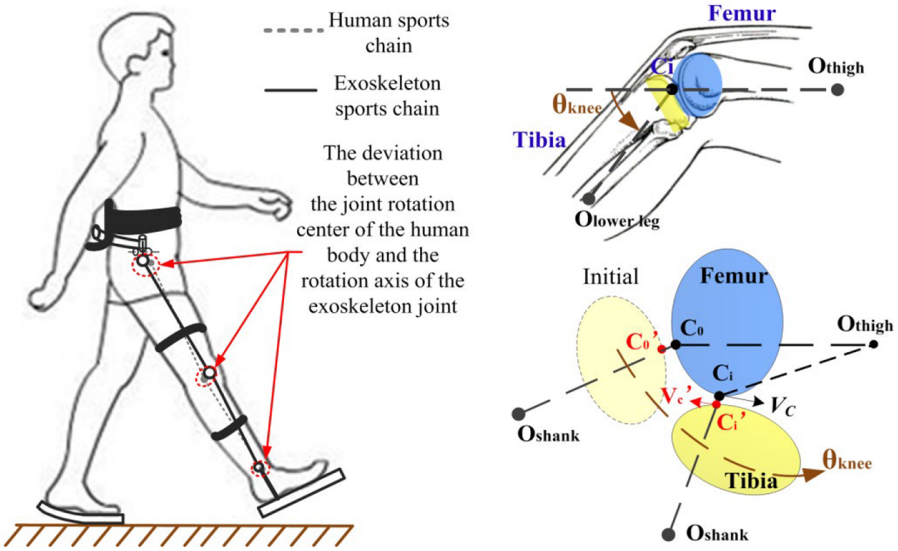

Figure 1.2 Misalignment between human knee and exoskeleton [2]

Designing ergonomic rehabilitation robots utilizing exoskeleton technology is an active research area. Exoskeletons are linked to human limbs at several points of contact, and they move in synchronization with human joints. These devices are favored because they can control the torques of targeted joints and measure the corresponding movements of every joint individually.

For exoskeleton-type robots, the alignment of the robot axes with human joint axes is a critical design consideration. Human joints' complex kinematics make it impossible to model them as simple combination of kinematic pairs. The positions of human joints cannot be determined from the outside, the exoskeleton's location relative to the human limb varies for each attachment, all of which causes misalignment [23, 24].

The misaligned joint axis of an exoskeleton causes the patient to feel undesired parasitic forces at the joint and attachment parts which can lead to pain, suffering, and even long-term damage under repeated usage. The axis misalignment that causes compensatory motions is the most significant factor since the adverse nature of these motions can slow healing and impair real-world usage of the limb [25].

1.4 Contributions

In this thesis, we present a self-aligning robot-assisted knee exoskeleton to improve the mobility of patients. The knee exoskeleton features self-alignment based on a compliant mechanism to ensure the ergonomic movements of the knee. Thanks to this self-aligning property, the knee exoskeleton enables the translational movements of the knee joint in the sagittal plane, in addition to the main flexion/extension movements. Furthermore, a Bowden-cable based series elastic actuator is utilized for the remote placement of the actuators while enabling high-fidelity interaction control. We present a comprehensive set of human subject experiments designed to evaluate the ergonomic improvements provided by the self-alignment feature.

The contributions of this study can be listed as follows:

- As a novel feature, a large stroke XY-stage compliant mechanism is proposed to address the misalignment problem between the human knee joint and the exoskeleton. A compliant mechanism with high rotational and low translational stiffness is designed such that the self-alignment mechanism can be implemented in a compact and light-weight form, while featuring no backlash and friction. Through the compliant alignment mechanism, a close match between the human knee joint and the exoskeleton joint axes is achieved by automatically aligning the joint axis of the exoskeleton, such that parasitic interaction forces induced on the user is minimized.

- A compact rotational complaint series elastic element has been designed and implemented for use with the Bowden cable-driven series elastic actuation. The Bowden cable transmission enables the actuator and harmonic reduction units to be placed at a remote location, enabling the exoskeleton to feature lower mass and inertia and relieving the user from the burden of carrying this weight.

- The interaction control of the knee exoskeleton has been implemented and experimentally verified. It has been shown that through its series elastic actuation, the knee exoskeleton displays high-fidelity torque tracking performance, while also featuring active back-driveability within its control bandwidth and passive compliance for excitations above this bandwidth.

- A comprehensive set of human subject experiments has been designed and implemented to evaluate the ergonomic improvements provided by the self-alignment feature of the knee exoskeleton.

- Quantitative and qualitative evaluations of user performance have been collected through motion capture devices, force sensors mounted at the user interaction points, and usability questionnaires. Evidence has been provided indicating that the self-alignment feature of the knee exoskeleton decreases the parasitic interaction forces due to misalignment and ensures that the exoskeleton does not significantly interfere with gait kinematics.

1.5 Outline

The rest of the thesis is organized as follows:

Chapter 2 presents a review of the state-of-art of knee exoskeletons and overviews the compliant mechanisms in the literature.

Chapter 3 presents the design requirements of the knee exoskeleton, details mechatronic design of the proposed knee exoskeleton, analysis of the compliant self-aligning mechanism and the compliant torsional spring, and experimental characterization of the system.

Chapter 4 presents the interaction control of the knee exoskeleton. In particular, velocity sourced-impedance control of series elastic actuator and experimental characterization of active back-driveability and torque tracking performance of the system are provided.

Chapter 5 presents the experimental setup and details the experimental procedure used for the human subject experiments with the knee exoskeleton. Quantitative and qualitative results from the experiments evaluating the effect of self-alignment on ergonomy are presented.

Chapter 6 concludes the thesis and discusses future research directions.

Chapter 2

Related Work

In this chapter, a comprehensive review of related work in the literature about knee exoskeletons and compliant mechanisms is presented.

2.1 Review of Knee Exoskeletons

Knee exoskeletons can be studied in terms of actuation and power transmission, sensor and control system, human-exoskeleton attachment, and joint alignment.

2.1.1 Actuator and Transmission Designs

Efficiency, portability and output torque are directly affected by actuator and power transmission design [26]. There are active, quasi-active, and passive actuated knee exoskeletons and active ones are the most commonly used [3].

Figure 2.1 Different actuation ways [3].

2.1.1.1 Active Actuation and Transmission

As well as the most used action type is electrical, pneumatic and hydraulic actuation are also used for exoskeletons.

Different transmission ways such as cable drives, belt drives, and gear drives can be used with electrical actuation that have high precision and controllability. Bowden cable transmission that enables actuation unit to be placed remote is implemented by [27, 28]. However, this way introduces high friction to the system. Also, Capstan cable is implemented by [29], while cable-pulley and belt are implemented by [30, 31]. Moreover, gear drives are also implemented by using different mechanisms such as 4-bar linkage [32, 33] and 5-bar linkage [34]. Note that these kind of rigid drives are bulky, heavy and uncomfortable for exoskeleton user.

Pneumatic actuation are generally used for grounded type exoskeletons. Pump and air compressor are placed remote, and pneumatic artificial muscle [35] and pneumatic cylinder can be used for transmission.

Although hydraulic actuation systems are complex and have large oil pump system, they are suitable for load carrying exoskeletons [3].

2.1.1.2 Quasi-passive and Passive Actuation and Transmission

A spring is typically used for quasi-passive or passive actuation. Those actuation types are popular these days thanks to a less complicated design with low volume and inertia.

Elliott et al. [36, 37] used a knee device with clutch-spring for the quasi-passive actuation storing and releasing energy during running. To store and release energy, Dollar et al. [38] employed a spring carriage, and Rogers et al. [39] employed an air spring. A pulley, tendon, and spring-based variable stiffness mechanism were used by Shamaei et al. [40, 41] for the weight assistance.

In order to store and release energy after the knee angle passed 60 degrees, Chaichaowarat et al. [42, 43] used a planar spiral spring and a 4-bar linkage for the passive actuation. Teflon and compression spring with an eccentric pulley were employed by Yuan et al. [44] and Li et al. [45] to aid in weight assistance. In order to retain the bio mechanical energy lost at the knee during the descent part of a squatting cycle and release it during the ascending phase, Ranaweera et al. [46] used pulley disks, wire cables and springs.

2.1.2 Control Systems

Sensing and control systems significantly affect the exoskeletons' accuracy, efficiency, smoothness, and wear comfort.

Recent works about rehabilitation training have highlighted the significance of the motion intention of humans [26]. In the high level controller, data gathered from sensors in the human body, exoskeleton, or interaction force/torque sensors between them can be used to predict motion intention and implement a suitable control strategy. Position, velocity, force/torque, and impedance control of actuators are made at the low-level controller using the desired trajectory coming from the high-level controller.

Impedance control, as opposed to position/velocity control and force/torque control, can control not just the position/velocity or the force/torque but their relationship, governing the interaction between the knee exoskeleton and the human, so that comfort and coordination of human and machine can be improved. A general structure of impedance control can be seen in Figure 2.2.

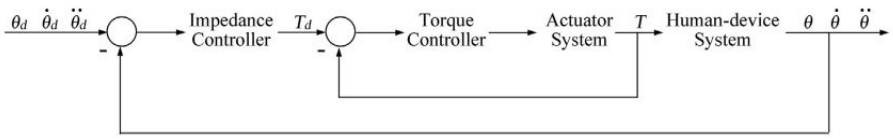

Figure 2.2 Typical cascaded impedance control system [3].

2.1.2.1 Control System Based on Wearable Sensors

In this type high-level controller structures, signals measured from human body is used. Skin surface EMG [47, 4, 48] and the electroencephalogram (EEG) [49, 50] are the most commonly used signals.

EEG-controlled exoskeleton technology has advanced significantly in the previous years [51, 52]. The BETTER project used exoskeletons or gait orthoses along with brain signals to enhance the physical rehabilitation of individuals with gait abnormalities due to amyotrophic lateral sclerosis, spinal cord injury or stroke [53, 54]. EMG signals are also employed in this study to operate the lower limb exoskeleton, whereas EEG signals are used to discrete directives, such as the intended action [55, 56].

There are still several drawbacks for commonly used EEG-based interfaces in the estimation of motion intention [26]. The primary drawbacks of wearable EEG measuring technology are the balance between training time and accuracy, their rela-

tively high sensitivity, and the overlapping of distinct electrical activity produced by various brain regions [57, 58].

There are a lot of studies about the EMG signals to diagnose human disorders and to track the healing of patient [59]. Thanks to linearity between the EMG signal and the joint torque [47, 59], it is also possible to estimate the intention effectively using relatively weak EMG signals. The calibration of the EMG signals is one of the key problems that must be resolved when utilizing the EMG signals to predict human intention.

Fleischer et al. [59, 4] used human musculoskeletal model and EMG signals for walking intention. EMG signals are recorded at the chosen muscles that control the flexion and extension motion of the knee joint. Pose sensors are utilized in addition to EMG sensors to record the wearer's postures. Estimation of torques are done by using the EMG data and EMG-to torque function. The forward dynamics of the human body model is then applied to the torques to determine the necessary angular accelerations for the knee joints.

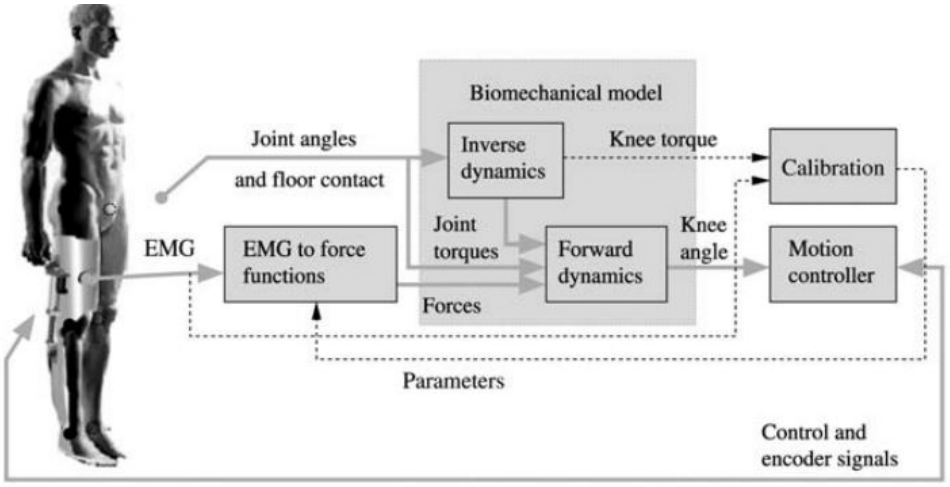

Figure 2.3 EMG based control of exoskeleton robot [4].

2.1.2.2 Control Systems Based on Interaction Torque Measurements

In this type of controls systems, the interaction torque can be directly measured from the attachment area, while it can be calculated by using the deformation of torsional elastic part and its stiffness.

The floor reaction force (FRF) is used by HAL-5 [60] for the estimation of the motion intention. Three phases of the walking motion are used while assisting a particular patient: swing, landing, and support phase. Reference torque trajectories can be estimated for each phase during assistance.

Exoskeletons have been utilized under impedance control, also. The exoskeleton supplies an interaction torque to assist the human to track natural gait when their movement deviates from it. This is called assist as needed. A virtual tunnel which enables foot to deviate a certain range from desired trajectory was designed [61]. The deviation area and the impedance force can both be modified by changing the width of the virtual tunnel.

2.1.2.3 Control Systems Based on Exoskeleton Sensors

For this type control systems, sensors on exoskeleton are used. Typically, this type of control system is created using the models of exoskeletons or the human body. To estimate human motion intention, the BLEEX exoskeleton [62] uses torque sensors which are placed at the hip, knee, and ankle joints. Particularly, a high degree of sensitivity is required for the control system to react to the forces and torques applied by the wearer. To improve sensitivity, the dynamics of exoskeleton is modelled by using realistic model of exoskeleton and wearer's inertia. The wearer can move the exoskeleton legs with little force thanks to the gravity compensation and the sensitivity amplification approach.

2.1.3 Human-Exoskeleton Attachments

Figure 2.4 a) lateral-support layout; b) improved lateral-support layout; c) two-side-support layout; d) anterior/posterior-support layout [3]

The user's comfort is greatly impacted by the human attachment interfaces that deliver the torque from the actuator to the knee. Distributing the torque and minimizing the undesired tangential forces are necessary [3]. Two key factors affect the design: the configuration and the layout of the attachment parts [63].

2-attachment points and 4-attachment points constitute a large partion of the attachment configuration. Witte et al. [28] placed the attachment bands slightly

above the knee and slightly above the ankle for 4-attachment points. In order to ensure knee flexion clearance, [63] positioned the proximal calf band and distal thigh band as close to the knee as possible. The distal lower leg band was placed above the ankle, while the proximal thigh band was put close to the pelvis. Kardan et al. [64] positioned the thigh band at 0.3 m above the knee and the shank band at 0.25 m below the knee for 2-attachment points. The attachment bands were placed at 0.10 m and 0.18 m above and below the knee, respectively by Maeda et al. [65]. About half of the knee exoskeleton design in the literature includes 4-attachment points [3].

As shown in Figure 2.4, there are four different types of mechanical frame layouts based on where the support is located: lateral-support layout, improved-lateral-support layout, two-side-support layout, and anterior/posterior-support layout.

The mechanical structure on the lateral side of the lower limb is known as the lateral support layout. As a drawback of lateral support layout, parasitic forces can be increased since torque passes through flexible attachment parts. Examples of this layout can be seen in Wehbi et al. [66], Felix et al. [67] [68], Nikitczuk et al. [69], and Shan et al. [70].

To minimize parasitic forces, improved lateral support layout, which enables translational movements in sagittal plane of knee, is used by Rifai et al. [30] [31], Luo et al. [71], Celebi et al. [27], ONYX (Lockheed Martin Inc.), Keeogo (B-Temia Inc.), Levitation (Sping-Loaded Technology Levitation Inc.), and Elevate Robotic Ski Xo (Roam Ski Inc.).

To decrease undesired parasitic forces another layout is two-side-support layout which places a mechanical support structure on the lower limb's central side. However, Chandrapal et al. [72] and Ranaweera et al. [46] revealed that this design could result in interference between two legs.

Another layout type is anterior/posterior-support layout, which places a mechanical support structure on the lower limb's anterior or posterior side. Configuration of this layout is complicated compared with other layouts. Examples of this layout can be seen at anterior/posterior-support layout means the mechanical Kardan et al. [64] [73], Liao et al. [34], and Sridar et al. [74] [75].

Lateral-support layout and improved-lateral-support-layout are mostly used according to [3].

2.1.4 Knee Joint Designs

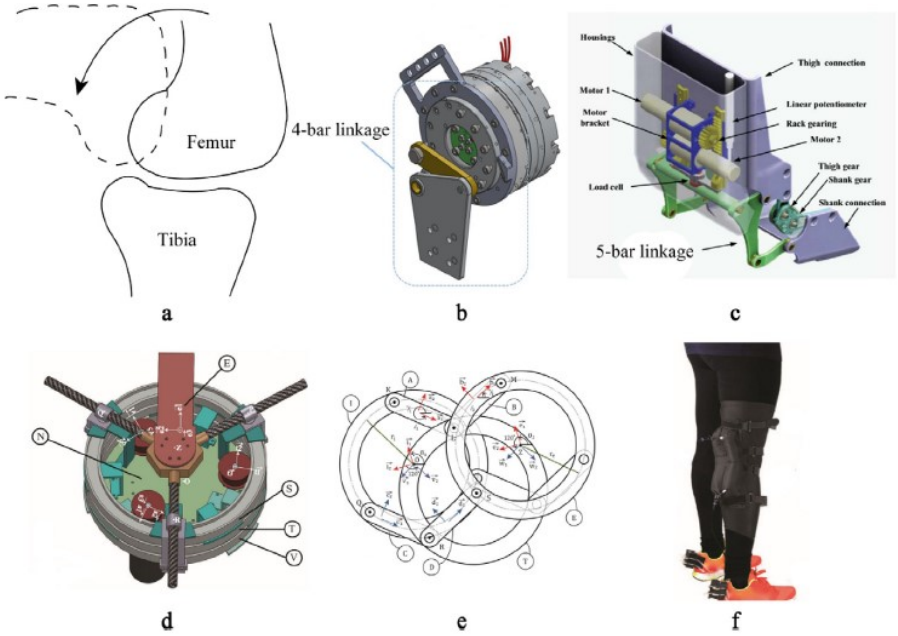

Figure 2.5 Different mechanisms to solve misalignment problem [3].

Knee exoskeletons can also be compared in terms of their joint kinematics. To solve misalignment problem between human knee and exoskeleton, there are different approaches.

To minimize misalignment, one way is to design a mechanism mimicking polycentric motion of human knee. Four-bar mechanism [76, 77, 32, 33, 42, 43], five-bar linkage with gear meshing mechanism [34, 78, 45], and rolling joint [63] are used.

Celebi et al. [27] use under-actuated Schmidt coupling mechanism which directly transmits torque and enables passive translational movements. Furthermore, Ergin et al. [29] uses 3-RRP mechanism with three active DoF.

Soft structured designs are used to minimize misalignment, such as Sridar et al. [75, 74]. Moreover, Saccares et al. [79, 80] utilize 6 DoFs by using two articulated parallelograms and a universal joint in iT-knee for self-aligning between human knee and exoskeleton. The flexion and extension are actively controlled in the knee exoskeleton of Witte [28] while the motion of the other 5 DoFs are passively allowed thanks to compliance in these directions.

According to [3], misalignment problems are not considered in the design of most knee exoskeletons.

2.1.4.1 Advantages/Disadvantages of Different Approaches to Misalignment Compensation

Two of the misalignment compensation approaches are based on just adjusting the length of exoskeleton links or the position of thigh-shank cuffs [81, 82]. Although these approaches are generally used in the exoskeletons designed with revolute joint to minimize initial mismatch, due to the anatomy of human joints, the mismatch becomes problematic when the rotation starts [83].

Another misalignment compensation approach makes use of self-aligning mechanisms [27, 84, 63, 85]. Thanks to these mechanisms, undesired interactions forces can be reduced, but these mechanisms may introduce additional inertia and result in more complex designs and control less [86].

Another misalignment compensation approach is to use passive DoFs at the human-exoskeleton interface [87, 88, 89]. This method can also decrease undesired interaction forces. Not focusing on minimizing assistive torques is the disadvantage of this method [86].

Fixation design of brace is another approach for misalignment compensation [90]. The advantage of this approach is to increase torque/force transmission and to reduce undesired interaction forces.

2.1.5 Proposed Self-Aligning Knee Exoskeleton

In Table 2.1 and Table 2.2, self-aligning knee exoskeletons have been compared in terms of application area, actuation, transmission, sensors, DoFs, control system, mass, motion range, and human subject experiments. As it can be seen from this comparison, our study provides more comprehensive human subject experiments for the locked/unlocked case, interaction forces, and evaluate comfort on a large number of volunteers.

AssistOn-Knee is a non-compliant version of the knee exoskeleton proposed in this thesis. AssistOn-Knee actively controls the flexion and extension motion of knee, as well as passively enabling translational motions of instantaneous center of rotation. The motion of device is restricted in the sagittal plane for compact and lightweight design [27]. To solve the misalignment problem, a rigid Schmidt mechanism is used in the joint. This planar parallel mechanism has one rotational DoF and two translational DoF. To be able to place motor and reduction unit remotely, Bowden cable transmission is used. Also, compression springs are used to implement a series elastic actuator. AssistOn-Knee has a range of motion from -10 to 170 degrees. The translational workspace of self aligning mechanism of AssistOn-Knee covers a circle with 24 mm radius. AssistOn-Knee has 35.5 Nm continuous torque output.

Major difference between the proposed self aligning knee exoskeleton and AssistOn-Knee is due to the design of the self-aligning joint design. Instead of using a relatively bulky rigid Schmidt coupling, a novel compliant XY stage has been used in the proposed design. Furthermore, instead of utilizing linear helical springs, a compliant rotational mechanism has been designed as the series elastic element.

Overall, the compliant design enables for more compact and light-weight implementations, while minimizing friction and backlash. However, the compliant XY stage introduces some stiffness against the passive translations, which has been minimized to enable high levels of passive self-alignment.

Table 2.1 Related works on self-aligning knee exoskeleton in terms of application area, actuation, transmission, sensing system, and DoF

Study	**Application**	**Actuation**	**Transmission**	**Sensing system**	**DoF**
Our study	**Knee rehabilitation**	**Brushed DC motor**	**Gear and Bowden cable**	**Optical encoder**	**3**
Wang et al. [91]	Stance phase of walking assistance	Brushed DC motor	2 stage timing belt	IMU sensor	4
Celebi et al. [27]	Knee flexion/ extension assistance	Brushed DC motor	Gear and Bowden cable	3 optical encoders	2
Tang et al. [85]	Rehabilitation	-	Driving cable	-	3
Choi et al. [92]	Promotion active daily lives for elderly	Brushless DC motor	Timing belt, pulley, and ball screw	3 encoders, torque sensor and IMU sensors	3
Niu et al. [84]	Rehabilitation	Linear motor	Five bar mechanism	Pressure sensor	3
Sarkisian et al. [93]	Rehabilitation	Linear motor	Slider	Position sensor	3
Cai et al. [94]	Rehabilitaiton	Stepper motor	Cable drive, and friction drive disk	Torque sensor, precision potentiometer	6
Saccares et al. [79]	Sit to stand assistance	Brusless DC motor	Gear	Torque sensor	6
Ergin et al. [29]	Knee rehabilitation	Brushed DC motor	Belt and 3-RRP rings	Optical encoders	3
Kim et al. [32]	Walking and sit to stand assistance	Brusless DC motor	Gear and four bar mechanism	FSR, torque sensor and encoder	2
Lee et al. [95]	Walking assitance for personal usage	Brusless DC motor	Timing belt, rouing pulley, and steel cable	Pressure sensor	2

Table 2.2 Related works on self-aligning knee exoskeleton in terms of control system, mass, motion range, locked/unlocked test, comfort test, and volunteer number

Study	**Control system**	**Mass (kg)**	**Motion range (degree)**	**Locked/ unlocked tested?**	**Interaction forces captured?**	**Comfort rated?**	**Volunteer number**
Our study	**Velocity sourced impedance control**		**-10-170**	**Yes**	**Yes**	**Yes**	**8**
Wang et al. [91]	Torque control	3.2	-	Yes	No	No	-
Celebi et al. [27]	Torque control	1.4	-10 - 170	No	No	No	1
Tang et al. [85]	-	-	-	No	No	No	-
Choi et al. [92]	Torque control	-	0-160	No	No	No	-
Niu et al. [84]	-	1.6	-	No	Yes	No	1
Sarkisian et al. [93]	Torque control	-	-	Yes	Yes	Yes	14
Cai et al. [94]	Torque control	-	-100-100	No	Yes	No	1
Saccares et al. [79]	Torque control	3.75	0-120	No	Yes	No	-
Ergin et al. [29]	Impedance control	-	0-90	No	No	No	-
Kim et al. [32]	Force, damping, position, and impedance control	3.5	0-120	No	No	No	1
Lee et al. [95]	-	2.4	0-159	No	Yes	No	1

2.2 Review of Compliant Mechanisms

Structures known as compliant mechanisms offer guided motion through the elastic deformation of the compliant constituent parts. Compliant mechanisms can be produced very compact and light-weight structures and are commonly easier to fabricate than conventional mechanisms that make use of various types of joints. They are also virtually frictionless, do not experience backlash or wear. As a result, they offer smooth and consistent guided motion, require low maintenance and potentially indefinite life [96, 97]. Thanks to these advantages, compliant mechanisms have wide range of application areas.

Compliant mechanisms should have low stiffness in the intended path's direction, also known as the degree of freedom (DoF), and higher stiffness in all other directions, also known as the degree of constraint (DoC).

Compliant flexure hinge mechanisms can be categorized into two groups: leaf spring (flexure beam) and notch type as it can be seen in Figure 2.6. Notch type mechanisms have higher DoC and lower DoF stiffness as compared to leaf spring mechanisms. Also, notch type mechanisms are vulnerable to fatigue deformation and stress concentration [5].

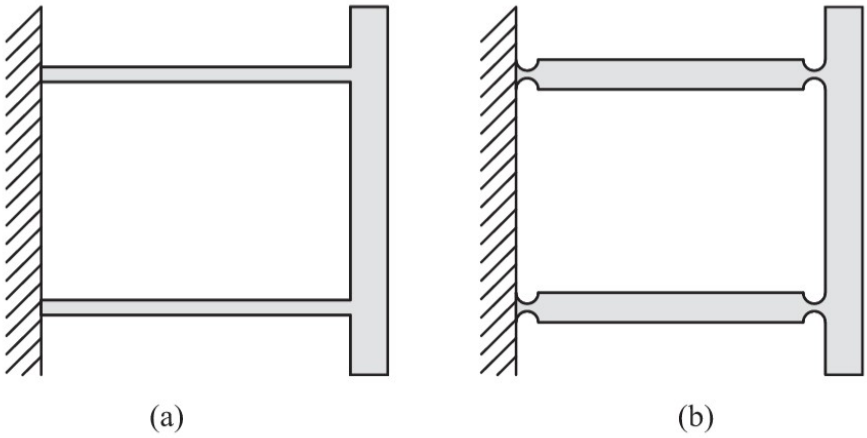

Figure 2.6 Leaf spring and notch type flexure hinges, respectively [5]

Beam based parallelograms have very important advantages. Their manufacturing and assembly is relatively easy. By serially connecting, DoF direction stiffness can be reduced and workspace can be increased. Also, by parallel and symmetrically connecting these mechanisms, DoC direction stiffness can be increased. Moreover, thanks to the well known force-displacement relationship of beams, their mathematical modeling is relatively easy.

Since the behavior of a flexure beam is well known, different combinations of them have been developed to compose more complex compliant structures. For different purpuses, the parallelogram (P) [98, 99], double-parallelogram (DP) [100, 101], and double double-parallelogram (DP-DP) [102, 103] have been proposed as can be seen in Figure 2.7.

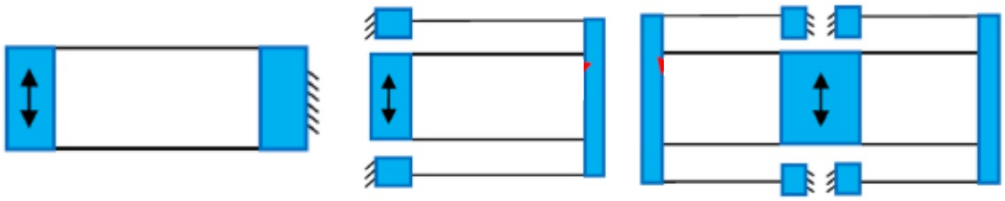

Figure 2.7 the parallelogram (P), double-parallelogram (DP), DP-DP, with order

Moreover, as it can be seen in Figure 2.8, rigid parts can be added between beams to increase DoC direction stiffness [6]. However, manufacturing of these type mechanism becomes harder and DoF direction stiffness becomes larger.

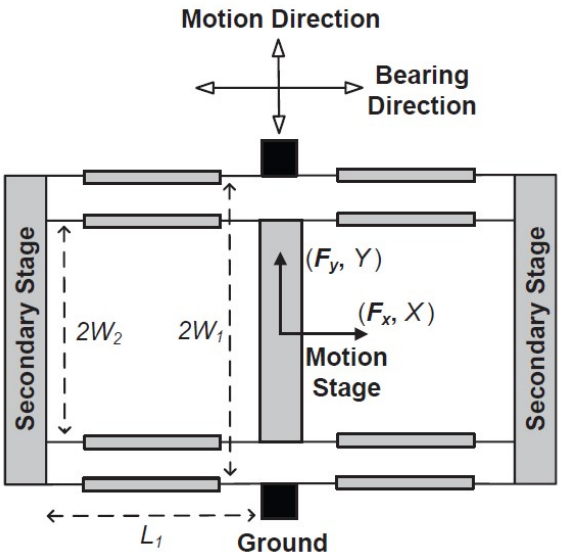

Figure 2.8 DP-DP with rigid parts [6]

2.2.1 Compliant XY Stage Mechanisms

Planar compliant mechanism that translates along X and Y directions can be designed by connecting the compliant parallelograms in different configurations according to design requirements like workspace, DoC and DoF direction stiffnesses, and load bearing capacity. The most used configurations in the literature is to connect multi stage parallelograms symmetrically and serially in a planar manner. For

example, monolithic XY stage mechanism is made of 3 stage multi parallelograms [7] in the Figure 2.9. It has centimeter range workspace.

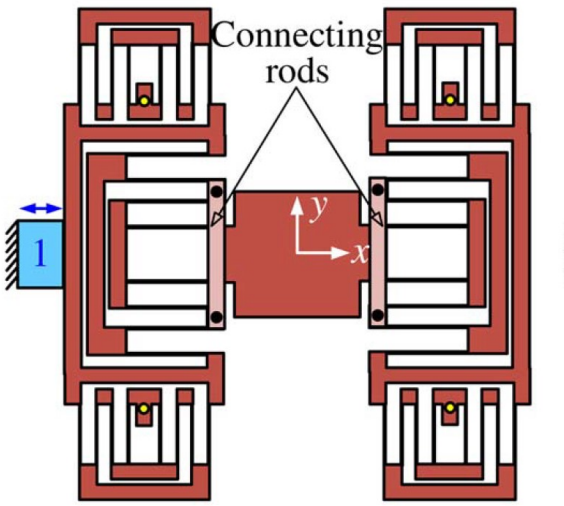

Figure 2.9 monolithic XY stage mechanism [7].

Note that this mechanism have large workspace, but its size is too large. To solve this problem, compliant Oldham mechanism in Figure 2.10 uses different configuration for planar motion. It is designed by connecting two paired double parallelogram serially with 90 degree offset [8]. The design's planarity makes it ideal for manufacturing-restricted applications such as micro/mesoscale power transmissions. Thanks to its relatively compact structure, this mechanism is very suitable for exoskeleton's joint designs. By using multistage parallelograms, its workspace can be increased.

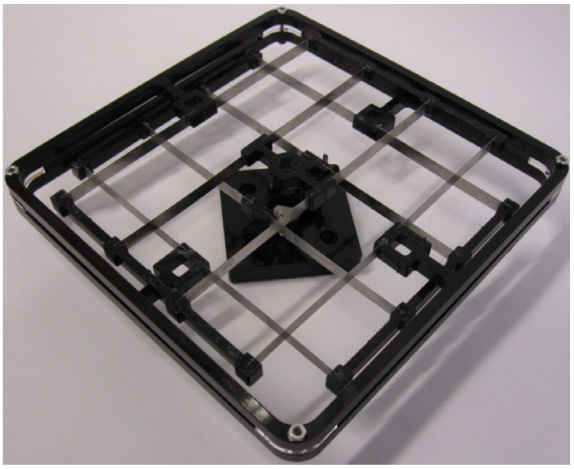

Figure 2.10 Compliant Oldham Coupling [8].

Moreover, a notch-type compliant XY stage in Figure 2.11 is designed for translations in the x and y axes [9]. This mechanism has large workspace also, but it has

relatively low fatigue life due to notch type structure.

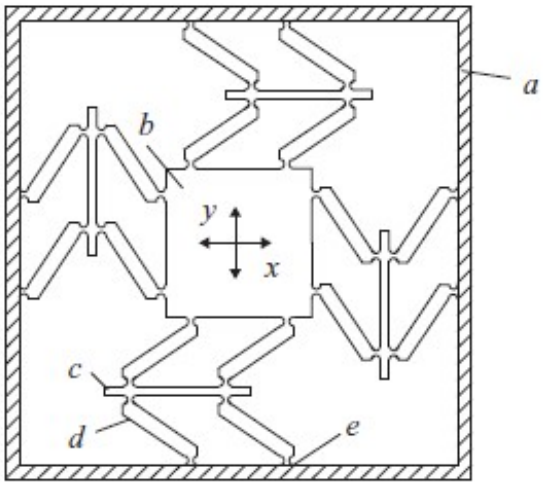

Figure 2.11 Notch-type compliant XY stage [9].

The HexFlex in Figure 2.12 that is a single-layer, multi-axis spatial positioning control mechanism is used for both macro and micro applications that demand precise positioning [9]. Note that fatigue life of those kind of notch type compliant mechanism is not good compered to beam based compliant mechanisms.

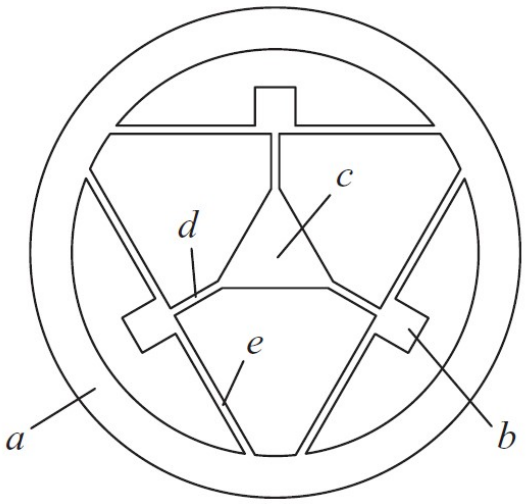

Figure 2.12 Hexflex [9].

2.2.2 Compliant Rotary Motion Mechanisms

Cross-axis flexural pivot in Figure 2.13 has two flexible beams that are at an certain angle. Since the rotation axis also translate, this mechanism should be restricted at that point for some application like series elastic actuation. Also, for many applications, sizes of this mechanism becomes too large especially in the out of plane direction.

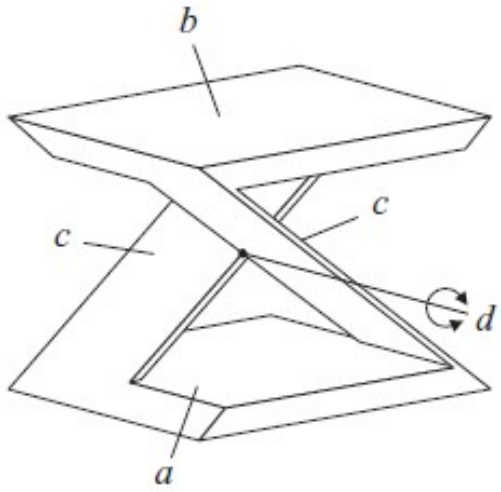

Figure 2.13 Cross-axis flexural pivot [9].

To solve axial shift problem, flexure beams can be connect co-axially. Large Angle Flexure Pivot (LAFP) in Figure 2.14 propose a mechanism that has large workspace up to 180° with a very low center shift about 10 m [10]. However, its allowable torque capacity is about 0.5 Nm.

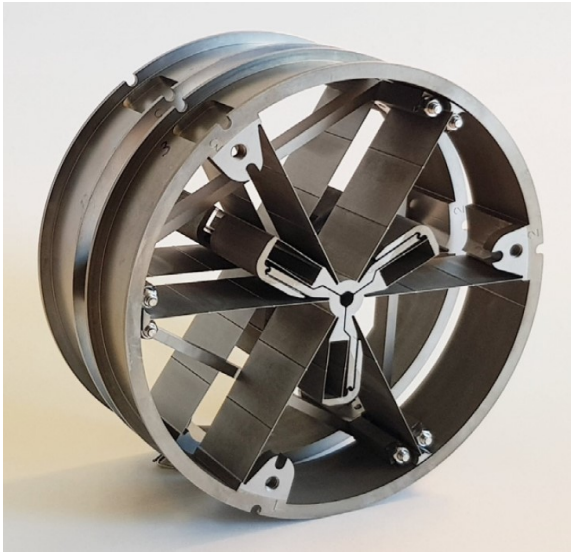

Figure 2.14 Cross-axis flexural pivot [10].

To increase allowable torque capacity, the number of beams can be increased and truncated beams can be used. In the open-source robotic leg prosthesis [11], a spring disk that is produced with Al 7075 is proposed, as it can be seen in Figure 2.15. This compliant element has 4.3 mm thickness and 10 cm diameter. Stiffness of this compact design is about 100 Nm/rad and it has 15 Nm torque bearing capacity. Thanks to high torque bearing capacity, this mechanism is very suitable for torque sensing at exoskeleton's knee joint.

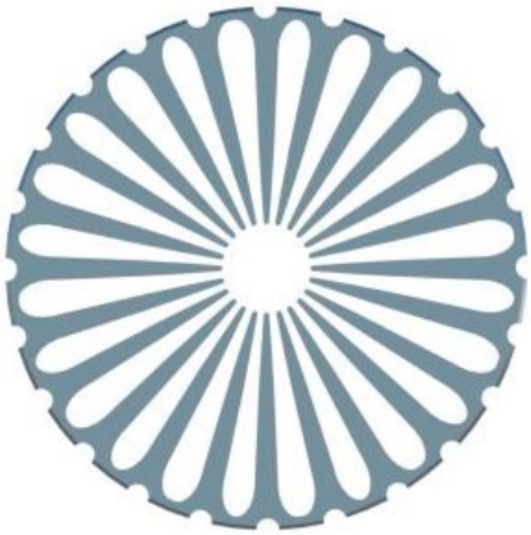

Figure 2.15 Spring disk [11].

Chapter 3

Mechatronic Design

In this chapter, the design requirements and the detailed mechatronic design of the proposed knee exoskeleton, the analysis of the compliant self-aligning mechanism and the compliant torsional spring, and the experimental characterization of the system are presented.

3.1 Design Requirements

Rehabilitation robot design is challenging from different aspects, including guaranteeing safety, adjustability, and ergonomy.

The mechatronic design and the interaction control of the exoskeleton affects the safety of physical human-robot interaction. The part of exoskeleton that interacts with human has to be light-weight with low inertia, and the actuators and joints must have low friction and backlash [104]. Knee exoskeleton workspace must be singularity free in the necessary range of motion so that natural gait is not restricted. The coupled stability of interaction with human must be ensured in the control of the exoskeleton. There exists fundamental limitations causing strict limits on stable control gains in the closed-loop force control [105], [106].

Ergonomy is another important factor to consider throughout the design process. The connections between the human and exoskeleton should be flexible outside the human limb and lack of any sharp ridges to prevent hurting patients. Moreover, the exoskeleton should not need too much mental and physical effort to operate.

Other important factors include the adjustability and ease of usage. For example, gait exoskeletons should be customized to a patient in a short period of time to ensure minimal donning and doffing duration.

3.1.1 Torque and Power Requirements

A healthy person may exert an average of 80 Nm during walking and 200 Nm during running [107]. The walking torque is used as a baseline, since the knee exoskeleton is designed as a rehabilitation device for patients. Moreover, sit to stand tasks require a maximum torque of 82.6 Nm. Based on these two investigations, it can be concluded that an average patient needs about 80 Nm of torque to accomplish the majority of daily knee movements. To be effective, an assistive device does not necessarily need to supply all of the torque. Too much torque can be harmful for patients, because it would enable the exoskeleton to entirely override their muscles rather than just directing and assisting them. The majority of knee exoskeletons for mobile walking assistance are designed to deliver up to 30% of the users' own muscle torque, that is about 24 Nm.

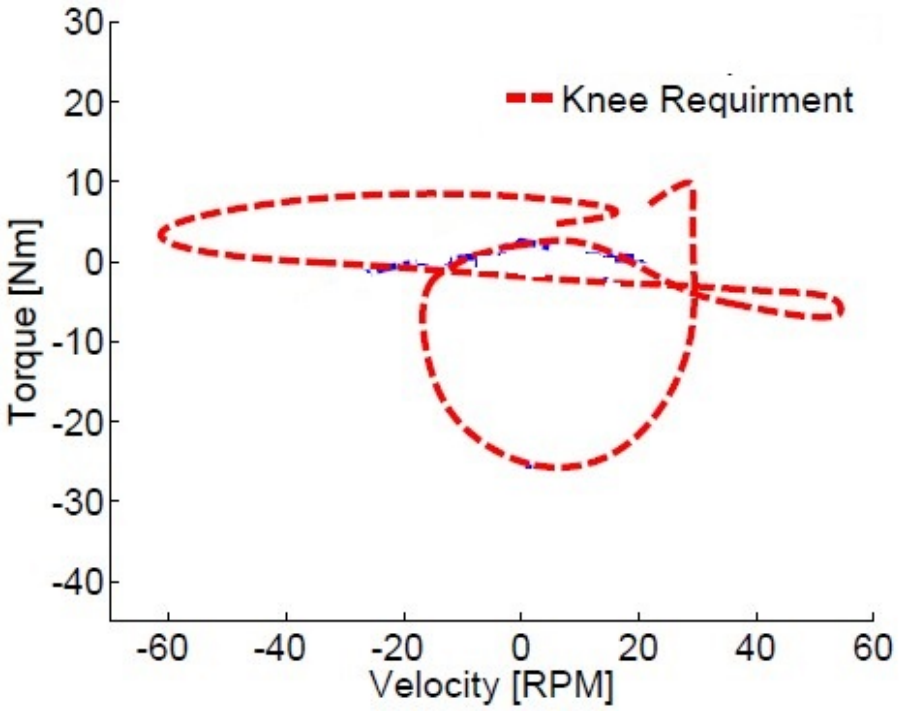

Figure 3.1 Torque requirement of knee joint[12]

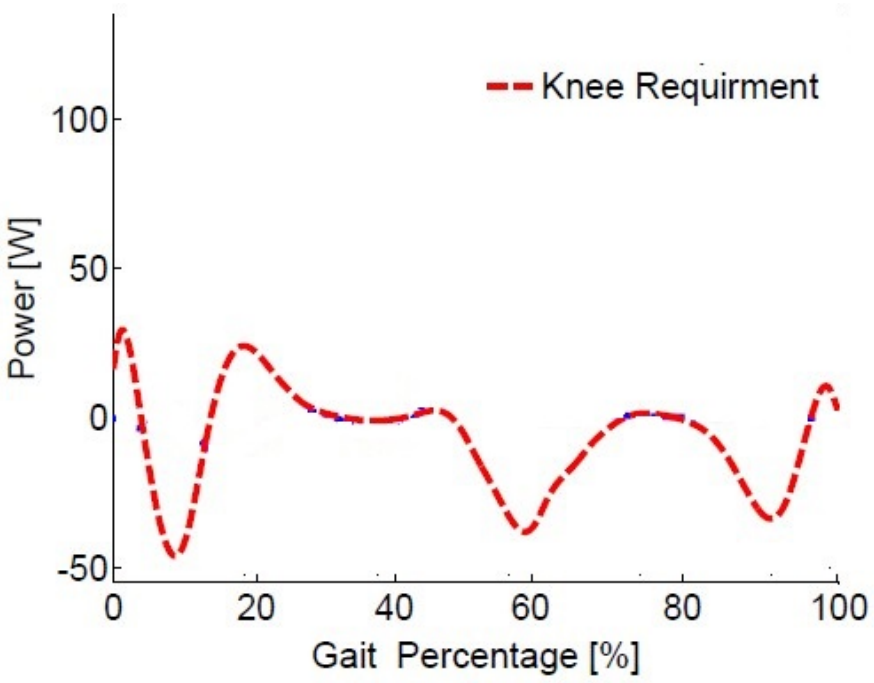

Figure 3.2 Power requirement of knee joint [12]

3.1.2 Design Requirements for the Compliant Self-Aligning Mechanism

In the self-aligning knee exoskeleton, a compliant mechanism is used for the motions in sagittal plane instead of a rigid Schmidt coupling. The design requirements for this compliant mechanism are determined as follows:

- It should have at least [-19mm, 19mm] workspace along X and Y directions.
- It should have as low stiffness as possible along X and Y directions to enable high passive backdrivability.
- It should have a rotational stiffness that is at least 10 times higher than the rotational stiffness of the compliant element of the series elastic actuator.
- It should support at least 30 N along translational directions to ensure sufficient load-bearing capacity.

3.2 Design of the Self-Aligning Knee Exoskeleton

The knee exoskeleton features a self-alignment mechanism based on a compliant mechanism to ensure the ergonomic movements of the knee. Thanks to this self-aligning property, the knee exoskeleton enables the translational movements of knee joint in the sagittal plane, in addition to the main flexion/extension movements.

As it can be seen from Figure 3.3, a large stroke XY-stage compliant mechanism is utilized to address the misalignment problem between the human knee joint and the exoskeleton. A compliant mechanism with high rotational and low translational stiffness is designed such that the self-alignment mechanism can be implemented in a compact and light-weight form, while featuring no backlash and friction. Series elastic element is based on a compliant torsional spring with 218.4 Nm/rad rotational stiffness.

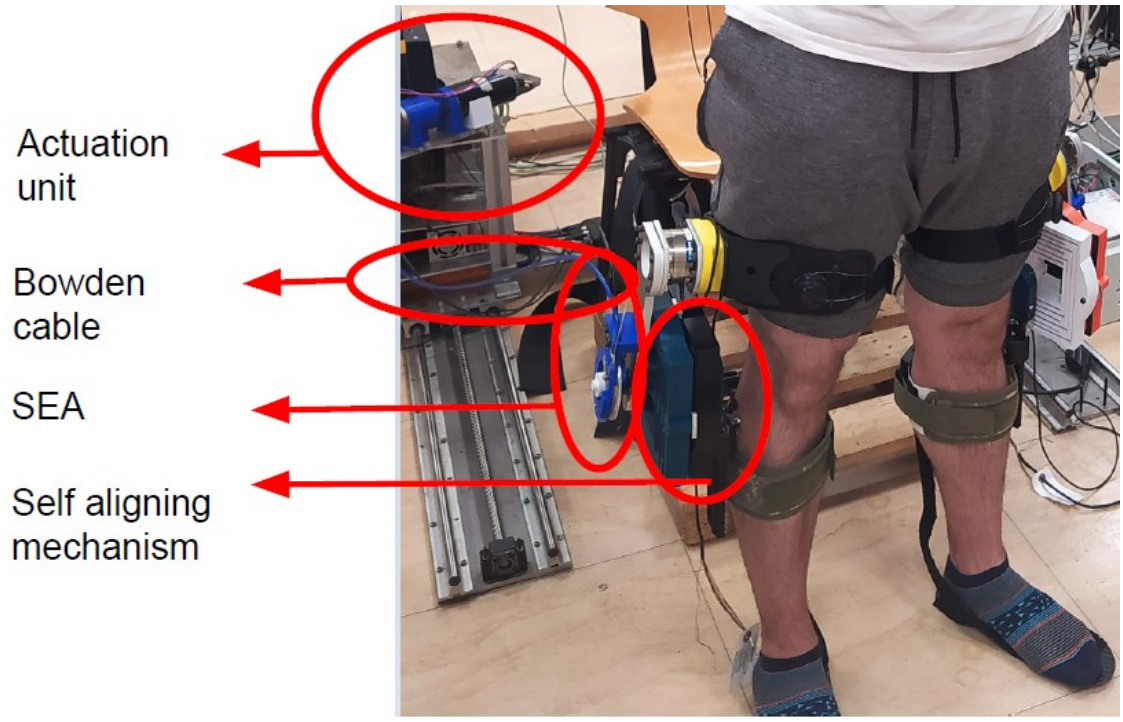

Figure 3.3 The self-aligning knee exoskeleton

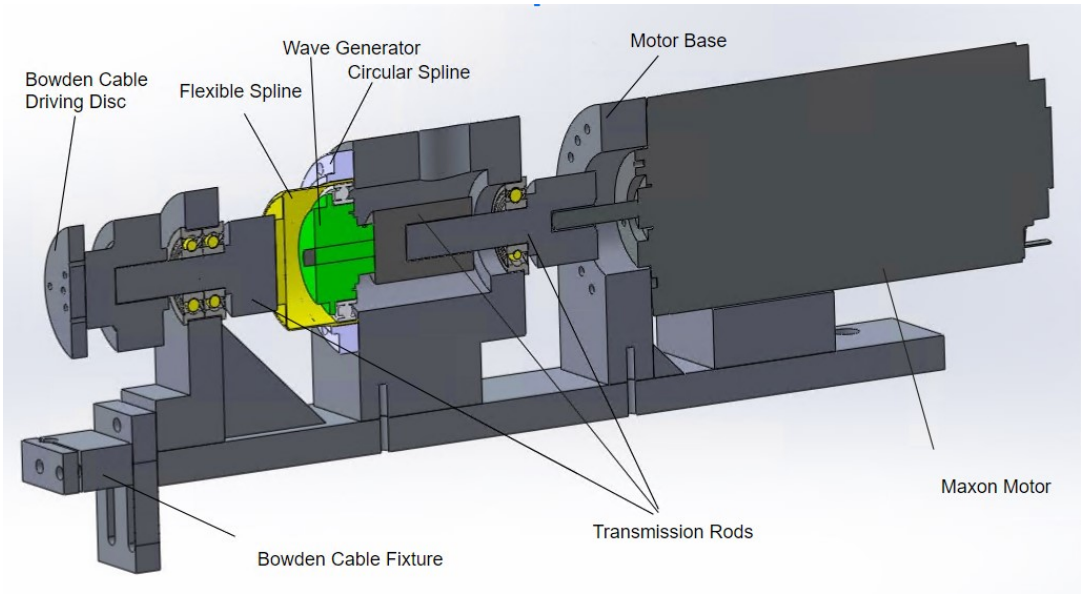

Figure 3.4 Solid model of the remote actuation unit

A Bowden cable-based series elastic actuator is utilized for remote placement of the actuators while enabling high-fidelity interaction control. The remote actuation unit in Figure 3.4 includes a 200 W brushed DC motor with an 500 count per count optical encoder, a harmonic derive with 1:50 reduction ratio. Moreover, there exist a 4:7 disk ratio between actuation unit and series elastic element. As a result, up to 43.84 Nm continuous torque can be generated by the system.

3.3 Design of the Compliant Mechanisms

3.3.1 Compliant XY Stage of the Self-Aligning Mechanism

Due to the large workspace and low transitional stiffness requirements of the self-aligning mechanism, a serially connected multistage parallelogram compliant mechanism is selected as the underlying compliant kinematics. To increase the rotational stiffness and to decrease parasitic motions, a symmetrical parallel connection of two multistage double parallelogram mechanisms is preferred. Note that since the behavior of a flexure beam is well studied, the analytical modeling of multi-stage xy mechanism is possible.

3.3.2 Stiffness Modelling of Multistage Parallelogram

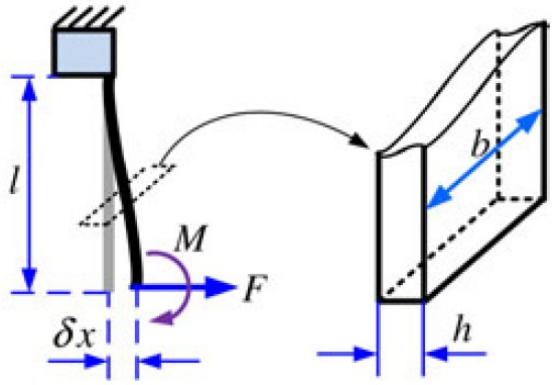

Figure 3.5 Force and displacements in single beam

Force-displacement relationship of a single beam in the beam constraint model can be simplified for fixed end boundary conditions as follows [108, 109]

$$\delta x = \frac{Fl^3}{12EI}. \tag{3.1}$$

where E is the Young's modulus of the material, b is the out-of-plane thickness, h is the in-plane thickness, l is the beam length, and area moment of inertia is given by $I = bh^3/12$.

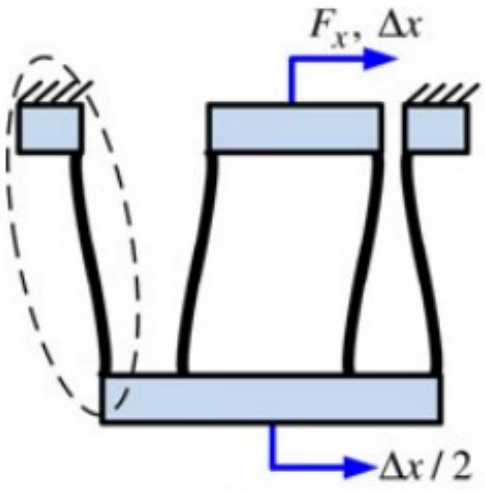

Figure 3.6 Forces and displacements in double parallelogram

The transverse stiffness of a double parallelogram is presented in [109] as

$$K_{DP} = \frac{Ebh^3}{l^3}. \tag{3.2}$$

While the rotational stiffness of double parallelogram is shown as [110]

$$K_{\tau,DP} = \frac{2\beta_1^2\beta_2^2 k_e}{\left(\beta_1^2 + \beta_2^2\right)}. \tag{3.3}$$

where β_i is the vertical distance of the i^{th} beam to the center, and $k_e = \frac{12l^2}{h^2}$.

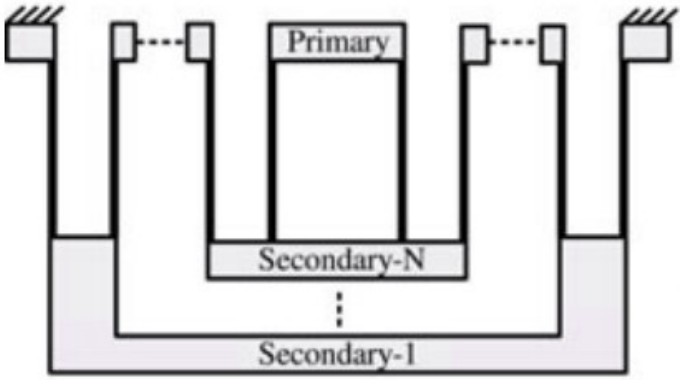

Figure 3.7 Multistage compound DP

The transverse stiffness of a multistage compound double parallelogram (DP) is derived as [109]

$$K_{mDP} = \frac{Ebh^3}{N_n l^3}. \tag{3.4}$$

Accordingly, since they are serially connected, the rotational stiffness of the multi-stage compound DP can be derived as

$$K_{\tau,mDP} = \frac{2\beta_1^2\beta_2^2 k_e}{N_n\left(\beta_1^2+\beta_2^2\right)}. \tag{3.5}$$

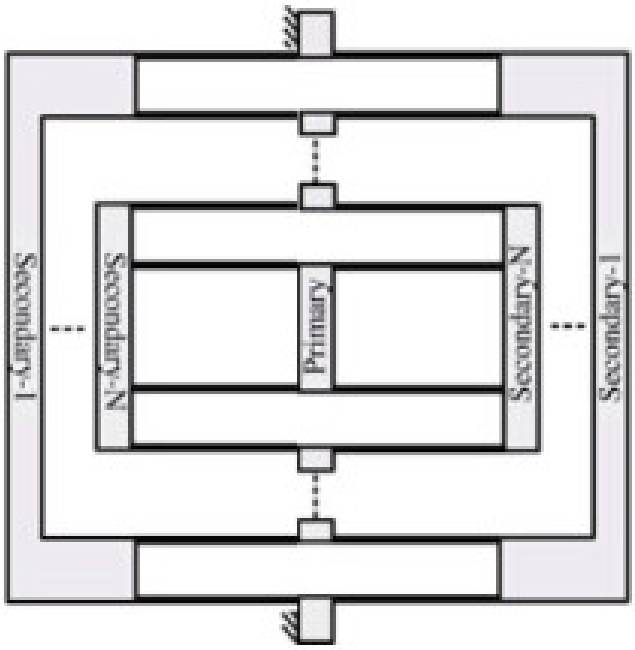

Figure 3.8 Multistage compound DP-DP

The transverse stiffness of a multistage compound DP-DP as shown in Figure 3.8 becomes [109]

$$K_{mDPDP} = \frac{2Ebh^3}{N_n l^3}. \tag{3.6}$$

Accordingly, since they are symmetrically parallel connected, the rotational stiffness of a multistage compound DP-DP can be shown to be

$$K_{\tau,mDPDP} = \frac{4\beta_1^2\beta_2^2 k_e}{N_n\left(\beta_1^2+\beta_2^2\right)}. \tag{3.7}$$

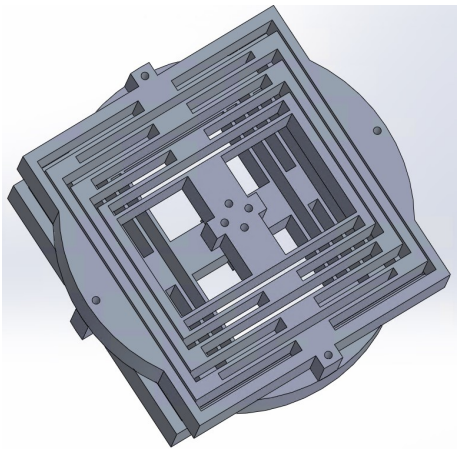

Figure 3.9 Solid model of the compliant self-aligning mechanism

The translational stiffnesses of the overall compliant XY stage mechanism along the X and Y directions are identical and equal to

$$K_{x,XY\,stage} = K_{y,XY\,stage} = K_{mDPDP} = \frac{2Ebh^3}{N_n l^3}. \tag{3.8}$$

Moreover, since two multistage compound DP-DP are connected serially, the rotational stiffness of the overall compliant XY stage mechanism becomes

$$K_{\tau,XY\,stage} = \frac{2\beta_1^2\beta_2^2 k_e}{N_n\left(\beta_1^2+\beta_2^2\right)}. \tag{3.9}$$

3.3.3 Workspace and Maximum Force Capacity of Multistage Parallelogram

The maximum deflection of the compliant XY stage mechanism can be determined as

$$\Delta x_{\max} = \frac{F_{\max}}{K} = \frac{\sigma_{\max} l^2}{3Eh}. \tag{3.10}$$

where $\sigma_{\max}$ is the yield strength. The maximum deflection also characterizes the maximum force limit, based on the stiffness of the mechanism.

3.3.4 Optimization of the Design Variables

To satisfy the minimum workspace and the maximum force/torque requirements, to ensure as low transitional stiffness as possible and a sufficient level rotational stiffness, an optimization of the design variables of the compliant XY stage is performed.

In this optimization problem, the cost function is taken as the translational stiffness of the multistage DP-DP mechanism. The minimum workspace and rotational stiffness values are imposed as constraints.

The design variables are taken as the length (l) and in-plane and out of plane thicknesses (h and b, respectively) of the beams.

The design parameters are selected as the material properties (E and yield strength ($\sigma_{\max}$)), the vertical distance of the beam to the center (β), and the number of DP stages (N_n). Note that the number of DP stages is selected as three, since for the knee exoskeleton, the mechanism becomes too bulky for larger number of stages. Due to production costs, PLA is used as the underlying material for prototyping.

The optimization problem can be expressed as:

$$\text{minimize } K = \frac{2Ebh^3}{N_n l^3}$$

$$\text{subject to } \frac{2\beta_1^2\beta_2^2 k_e}{N_n\left(\beta_1^2+\beta_2^2\right)} > 2000 Nm/rad$$

$$\Delta x_{\max} = \frac{\sigma_{\max} l^2}{3Eh} > 19mm$$

$$0 < l < 45mm$$

$$0 < b < 25mm$$

$$0 < h < 3mm$$

A grid search technique is used to solve the optimization problem. The optimal design variables are determined as follows:

- The thickness of the beams (h): 2 mm
- The length of the beams (l): 43 mm
- The width of the beams (b): 25 mm

As a result of this design optimization, the compliant mechanism possesses the following properties that satisfy design requirements:

- Transverse stiffness: 3.93 N/mm

- Rotational stiffness: 2179.1 Nm/rad
- Workspace: 19.51 mm
- Maximum allowable force: 76.7 N

3.3.5 Alternative Optimal Designs using Different Materials

Due to EDM production cost of Al7075, PLA material has been chosen for the prototype implementation. In this subsection, some alternative optimal designs for different materials are presented in Table 3.1. More compact and strong compliant mechanisms can be implemented with materials with low elastic modulus and high yield strength. For example, as it can be seen from table, much more compact designs are possible if titanium is used.

Table 3.1 Alternative Optimal Designs for Different Materials

Material	**Thickness of beam [mm]**	**Width of beam [mm]**	**Length of beam [mm]**	**Stiffness [N/mm]**	**Rotational stiffness [Nm/rad]**	**Workspace [mm]**
PLA	2	25	43	3.93	2179.1	19.5
Al7075	0.3	8.5	28.8	0.46	2858.9	19.4
Steel	0.3	10	32.8	0.04	2046.8	19.2
Titanium	0.3	5	27.2	0.51	2029.9	19.1

3.3.6 Experimental Verification of the Translational Stiffness

A prototype of the self-alignment mechanism has been built using PLA material. Its workspace has been characterized as 19.5 mm, as it can be seen from Figure 3.10.

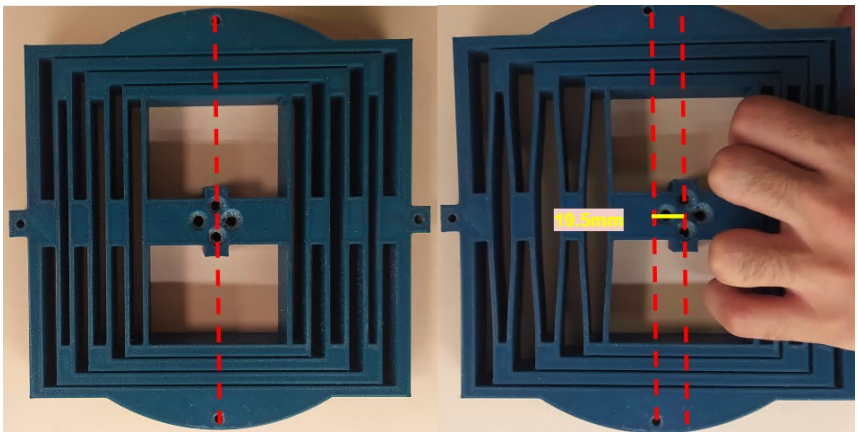

Figure 3.10 Workspace verification of self aligning mechanism

Also, its translational stiffness has been characterized as 3.73 N/mm with $R^2 = 0.995$, as it can be seen from Figure 3.11.

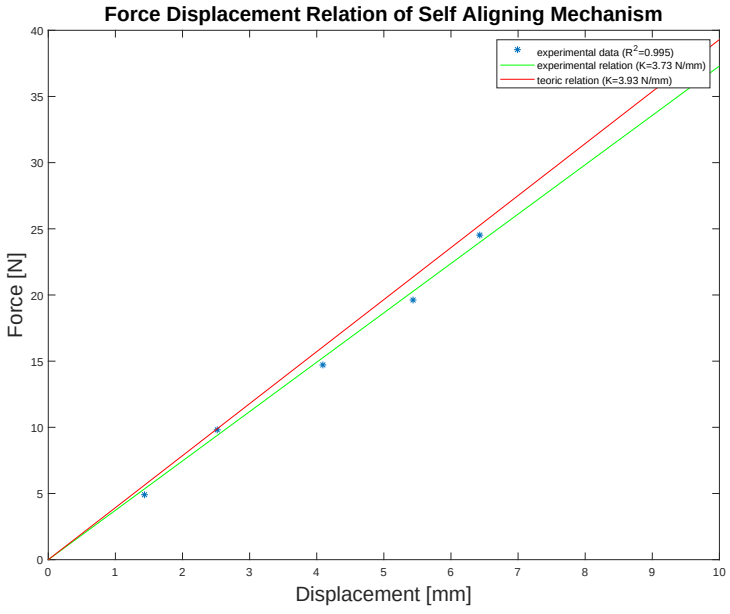

Figure 3.11 Experimental translational stiffness verification of self aligning mechanism

Moreover, its torsional stiffness has been characterized as 218.4 Nm/rad with $R^2 = 0.997$, as it can be seen from Figure 3.12.

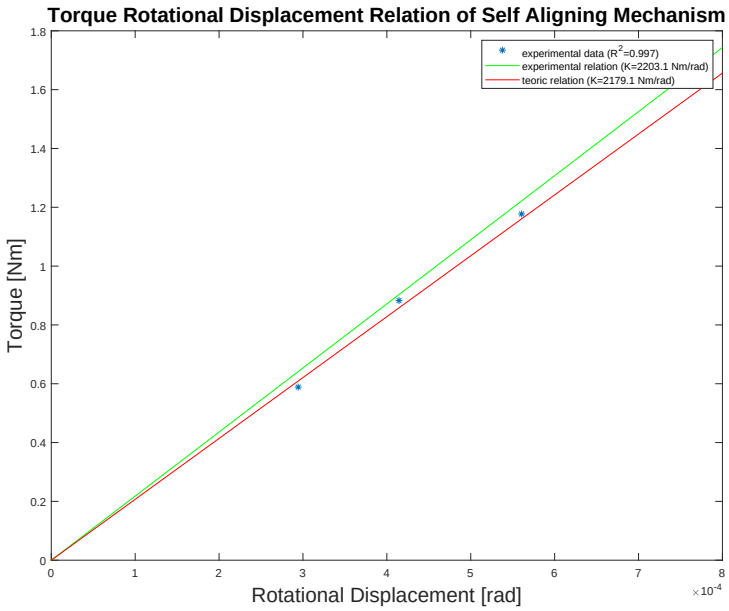

Figure 3.12 Experimental torsional stiffness verification of self aligning mechanism

3.3.7 Compliant Torsional Mechanism

The compliant torsional mechanism has been designed based on the series elastic element presented in [11]. The compliant torsional mechanism in Figure 3.13 has been customized for the self-aligning knee exoskeleton by changing number of beams and thickness of mechanism for the required rotational stiffness of 200 Nm/rad which is close to the maximum torsional stiffness of the human knee [111] and 25 Nm maximum torque. In particular, 10 trapezoidal beams are used with the thickness of 6 mm made of Al 7075 material.

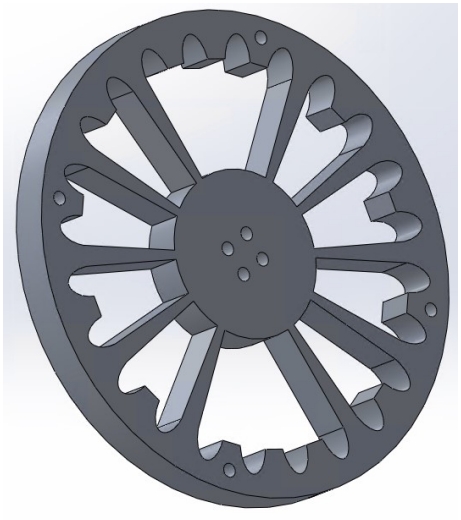

Figure 3.13 Solid model of the compliant torsional stiffness mechanism

3.3.8 Experimental Verification of the Torsional Stiffness

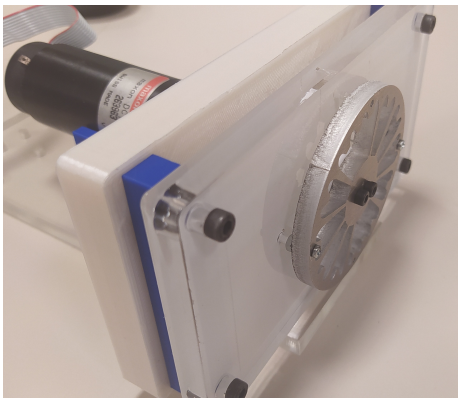

Figure 3.14 Experimental verification setup for compliant torsional stiffness mechanism

The torsional stiffness of compliant torsional mechanism has been calculated by applying sinusoidal torques (0.4 Nm, 0.8 Nm, and 1.2 Nm) under different frequencies (0.5 Hz, 1 Hz, and 2 Hz) via experimental setup in Figure 3.14. As it can be seen from figure 3.15, the torsional stiffness of the compliant mechanism has been calculated as 218.4 Nm/rad for 0.5 Hz with $R^2 = 0.995$, 218.7 Nm/rad for 1 Hz with $R^2 = 0.997$, and 218.2 Nm/rad for 2 Hz with $R^2 = 0.991$, respectively. Therefore, any frequency dependent stiffening/softening effect has not been observed.

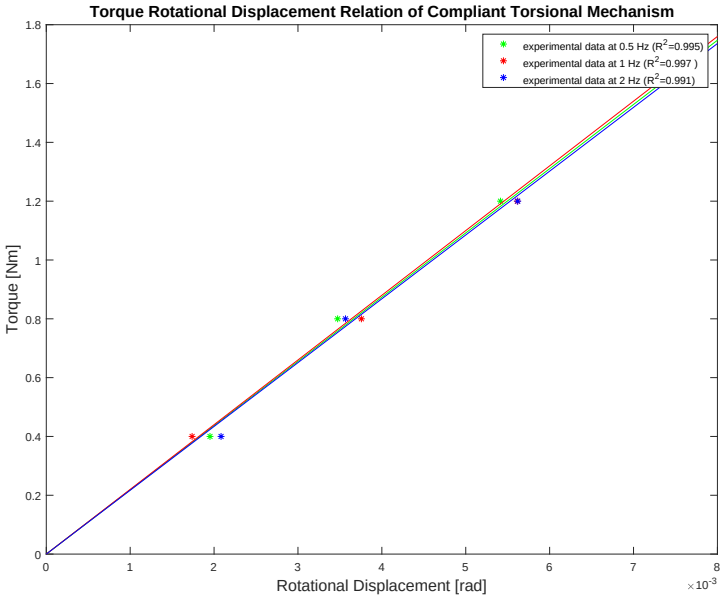

Figure 3.15 Experimental verification of compliant torsional stiffness mechanism for different frequencies

Note that under/overestimation of stiffness of SEA changes the stiffness that is rendered by velocity sourced impedance control; but underestimation of stiffness in model reference force control is a necessary condition for passivity, as shown in [112].

3.4 Specifications of the Knee Exoskeleton Prototype

Table 3.2 presents the specifications results of the compliant self-aligning knee exoskeleton. The continuous end-effector torque output is determined as 4 Nm for the PLA based prototype. The end-effector resolutions are calculated as 0.09° for rotations since the optical encoder on the compliant element has 1000 cpr resolution.

A compliant rotary mechanism with 218.4 Nm/rad are used to estimate joint torque with resolution of 0.3 Nm. The exoskeleton possesses a translational workspace of -19.5 mm - 19 mm along the X and Y directions, while it is capable of performing up to 180° rotations about the perpendicular axis.

Table 3.2 Specifications of the Knee Exoskeleton Prototype

Criteria	X	Y	Z
Cont. Torque	N/A	N/A	4 Nm
Max. Speed	N/A	N/A	43.5 rpm
Min. Res. Torque	N/A	N/A	0.3 Nm
Translational Stiffness	3.73 N/mm	3.73 N/mm	N/A
Rotational Stiffness	N/A	N/A	218.4 Nm/rad
Resolution	N/A	N/A	0.09 [°]
Workspace	-19.5-19.5 mm	-19.5-19.5 mm	$-10° - 170°$

Chapter 4

Interaction Control of the Knee Exoskeleton

In this chapter, the high and low-level controllers designed for interaction control are presented.

4.1 High-Level Controller

High-level controllers are implemented for the sit-to-stand and walking tasks. The desired torque profiles based on the knee angles are determined as the input to the low-level impedance/torque controller.

4.1.1 High-Level Controller for the Sit-to-Stand Task

Due to coupled stability challenges, position-based torque controllers are preferred for sit-to-stand tasks, rather than a time-based or EMG-based controllers [13].

Using the knee torque as a function of the knee angle allows for timing flexibility and consistency during power transmission, and reduces the errors in the knee torque. This technique performs very similarly to a gravity compensation scheme if it is assumed that the hip is fixed. Also, the implementation of a position-dependent controller is relatively easy because there is no need for additional sensors to estimate the task cycle.

To be effective, an assistive device does not necessarily need to supply all of the torque. Too much torque can be harmful for patient because it would enable the exoskeleton to entirely override their muscles rather than just directing and assisting them. The majority of knee exoskeletons are made to deliver up to 30% of the

wearer's own muscle torque [113]. Therefore, the weight normalized torque-angle curve for able-bodied sit-to-stand is used for the torque-knee angle relationship [114] with 30% scaling. In this plot, shown in Figure 4.1, there is a quick increase in torque right after seat-off. To solve this problem, a initial torque is added and slope of the curve is flattened.

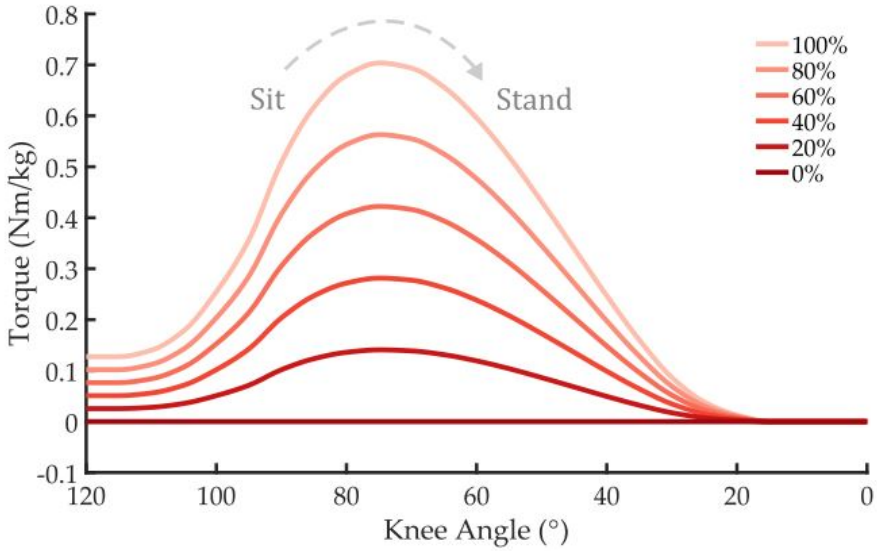

Figure 4.1 Torque profile for a sit-to-stand task [13]

4.1.2 High-Level Controller for the Walking Task

Position dependent controllers can also be used for walking tasks, thanks to their advantages, such as not needing additional sensors to estimate the walking phase, and providing timing flexibility, consistency during power transmission, and less error in the knee torque. The torque-position curve of walking is computed using musculoskeletal simulation of recorded walking experiments by using OpenSim software [14].

As shown in Figure 4.2, the weight normalized torque-angle curve for able-bodied walking is used for the torque-knee angle relationship [14] with 30% scaling.

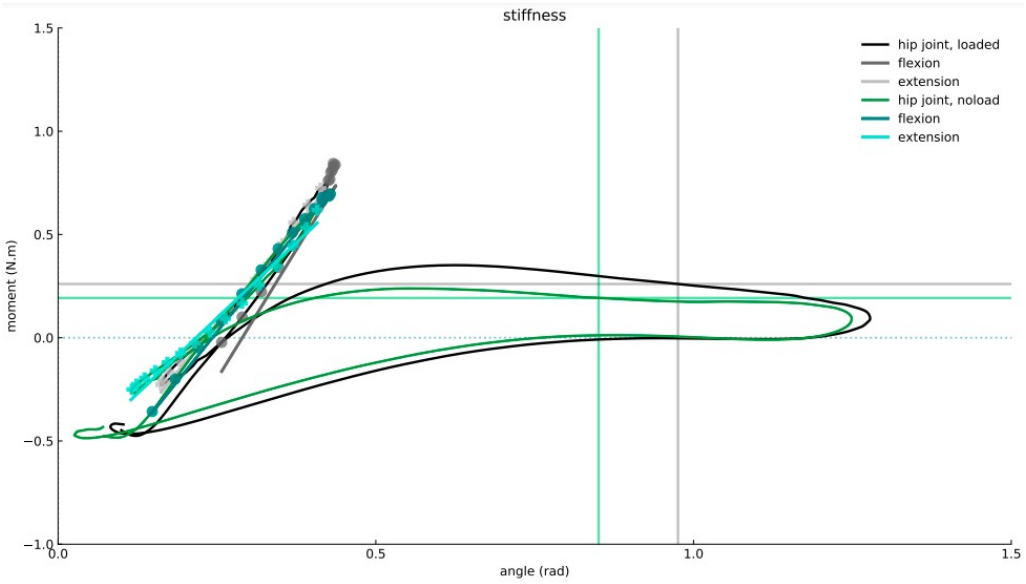

Figure 4.2 Normalized torque-angle curve for the walking task [14]

4.1.3 Limitations of Position Dependent High Level Controllers

The sudden rise in torque that occurs after standing is one of the drawbacks of position depended sit-to-stand controller [115]. Since the timing of torque is very responsive to the chair height and the rotational knee position, a sudden increase in torque during assistance may become uncomfortable.

Due to the possibility of excessive deflection of the self aligning mechanism, applying torques on the right axial position can become harder. This may introduce more undesired forces on the knee muscles.

Moreover, the proposed high-level controllers depend on the position of the human knee and the weight of the user, therefore customized torques cannot be applied.

Assist-as-needed control strategy that provides assistance in case of an important deviation from the desired motion is commonly used in rehabilitation. As opposed to the position based strategy, it improves the active participation of the user, so learning and healing has the potential to improve [116].

Furthermore, as compared to the position based high level controller, a high-level controller that uses the shank's orientation, as in iT-Knee [80], may provide more effective assistance to the knee when performing quasi-static motions with different body postures and knee loading.

4.2 Low-Level Controller

4.2.1 Series Elastic Actuation

Thanks to the Bowden cable transmission, the actuator and harmonics drive unit can be placed remotely, therefore inertia exerted on human knee can be reduced. However, harmonic drive and Bowden cable introduces high friction, so the actuation are not passively backdriveable.

A compliant element is added between Bowden cable-driven disk and the end effector to reduce output impedance and to enable high fidelity force/torque control. This control approach is known as Series Elastic Actuation (SEA) [117, 118]. By measuring the deflection of this compliant element via a digital encoder, force/torque sensing is implemented. The stiffness of this compliant element of SEA is (about an order of magnitude) lower compared to conventional force/torque sensors, so the force/torque control gains can be selected much higher for more responsive and robust force/torque control against disturbances. Thanks to SEA, low cost actuation, reduction and transmission systems that have friction and stiction can be used. Also, this approach eliminates the requirement for expensive force/torque sensor with high precision, and precise robust force/torque control can be implemented through the robust motion control of the deflections of the compliant element.

Because motion controllers with high gains can be applied, the system behaves as a motion source within device's motion control bandwidth, without the need for high precision actuators or transmission components. SEA assures active backdrivability within device's force/torque control bandwidth. Furthermore, the series elastic element of SEA functions as a physical filter for the frequencies above this bandwidth.

There is a trade-off between the force/torque control bandwidth and the force/torque resolution in the design of SEA. By using more compliant elements in SEA, the force/torque resolution can be increased, but, on the other hand, the force/torque control bandwidth decreases [106]. Relatively low control bandwidths are sufficient for exoskeletons as the bandwidths of patients are lower [119].

4.2.1.1 Velocity Control Bandwidth

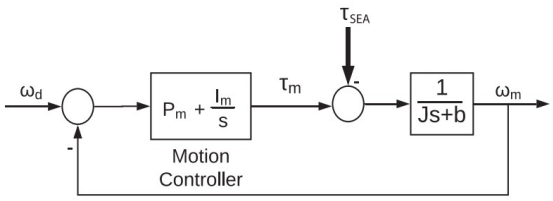

Figure 4.3 Inner loop velocity controller [15]

To determine the inertia J and the damping b of device, a close loop system identification is performed by applying sinusoidal velocity inputs in frequencies ranging from 0.1 Hz to 20 Hz. The velocity controller gains P_m and I_m have been tuned for robust motion control, and are known. No external torque has been applied during the system identification and motion controller rejects the torque on SEA that acts as a disturbance. The transfer function of system from the desired velocity to the measured velocity can be modelled as follows

$$\frac{\omega_m}{\omega_d} = \frac{P_m s + I_m}{Js^2 + (P_m + b)\, s + I_m}. \tag{4.1}$$

By using System Identification Toolbox of Matlab, the transfer function is estimated as

$$TF_{est} = \frac{0.0589s + 3.525}{0.00231s^2 + 0.1929s + 3.525}. \tag{4.2}$$

The stiffness of device has been already identified as K=218.4 Nm/rad in Chapter 3. Using the estimated transfer function, inertia and damping of device can be found as presented in Table 4.1.

Table 4.1 Velocity controller gains and identified system parameters

Symbol	**Value**
J	0.0023 kgm^2
b	0.1340 Nms/rad
K	218.4 Nm/rad
P_m	0.0589 Nms/rad
I_m	3.525 Nm/rad

The cut off frequency of inner velocity controller is 24 Hz, as it can be seen from Figure 4.4.

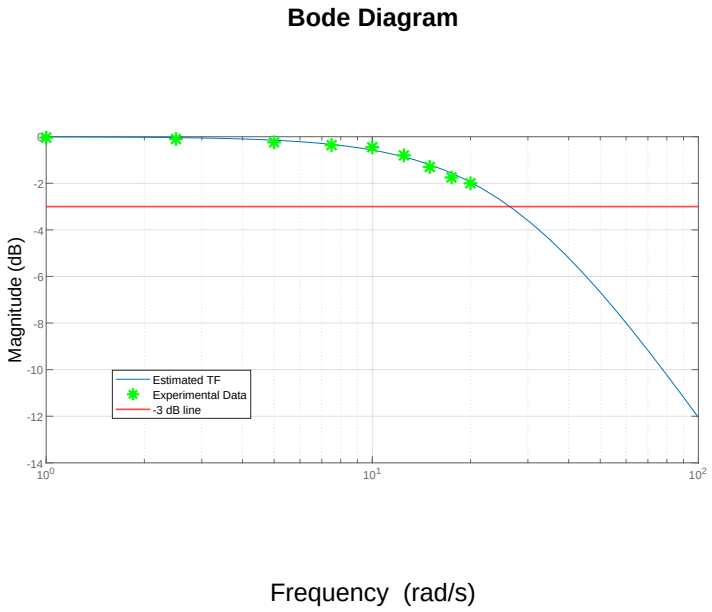

Figure 4.4 Experimental system identification of device

4.2.1.2 Torque Tracking Performance and Bandwidth

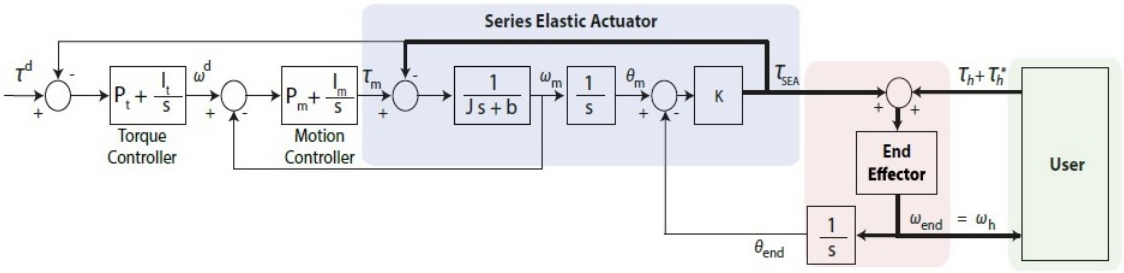

Figure 4.5 Torque controller [15]

The torque controller gains, P_m and I_m, have been tuned to maximize the torque control bandwidth. The motion controller gains have already been tuned for robust motion control to reject the disturbances. The controller gains are presented from Table 4.2.

Table 4.2 Controller gains used for torque control characterization

Symbol	**Value**
P_m	0.0589 Nms/rad
I_m	3.525 Nm/rad
P_t	0.072 rad/Nms
I_t	0.375 rad/s^2Nm

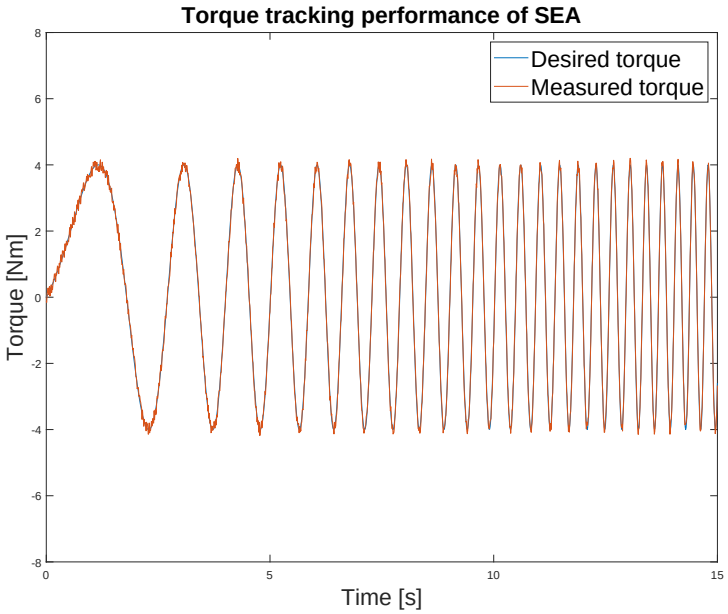

Figure 4.6 Torque tracking performance

The torque tracking performance of SEA under the cascaded torque controller for the chirp input with 4 Nm amplitude and frequencies from 0.1 to 5 Hz is presented in Figure 4.6. SEA displays a maximum of 0.3 Nm tracking error with RMSE of 2.4%.

The torque control bandwidth has been characterized as 11 Hz by applying chirp input with 4 Nm amplitude and frequency range from 0.1 to 15 Hz.

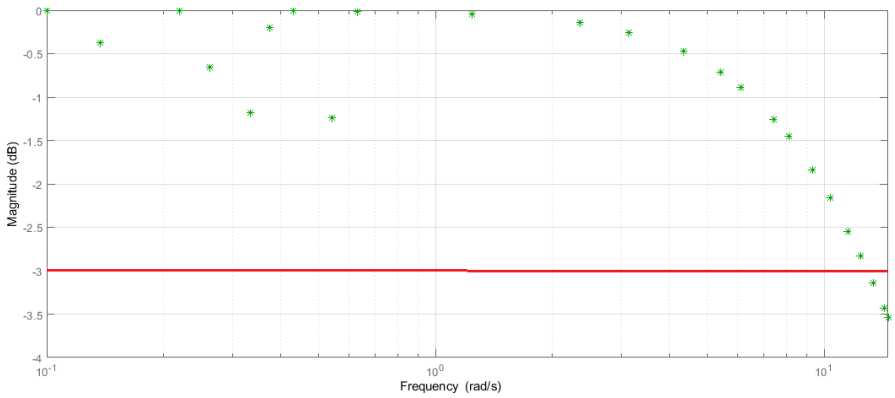

Figure 4.7 Torque control bandwidth

4.2.2 Velocity-Sourced Impedance Controller

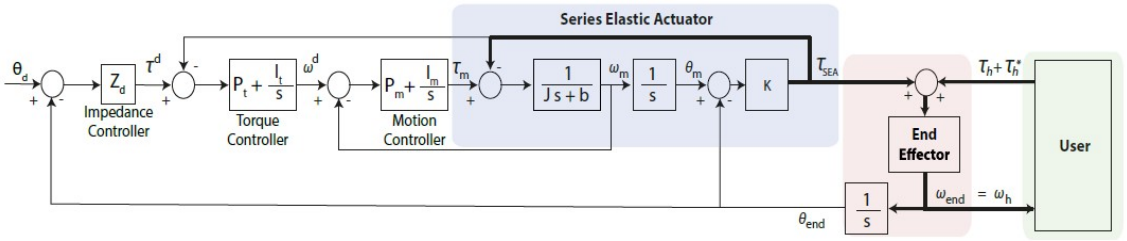

Figure 4.8 Velocity sourced impedance controller [15]

To control SEA to provide assistance, velocity-sourced impedance controller (VSIC) has been used as the low-level controller. The velocity-sourced impedance controller consists of an inner-most velocity control loop, an intermediate torque control loop and an outer-most impedance control loop. The inner most velocity control loop handles friction and stiction and makes the device behave as an ideal motion source. In the intermediate loop, interaction force/torque is controlled by using the deflection of compliant element of SEA. Constant disturbances can be dealt with by closed-loop control thanks to the use of integrator gains [119]. Moreover, tuning of controllers in VSIC is relatively easy since the dynamic model of actuator is not required [15].

As it can be seen from Figure 4.8, in the inner velocity controller and intermediate torque controller, PI controllers are used, which are $P_m - I_m$ for motion and $P_t - I_t$ for torque control. Also, an impedance controller with the desired impedance Z_d around the equilibrium point θ_d of end-effector is used at the outermost loop to generate references to the torque controller.

Since exoskeletons interact with humans, it should be safe. The coupled stability

of controlled SEA and human is necessary for the interaction safety. Human may be assumed as passive element in closed loop analysis, since it is assumed that human does not intentionally try to destabilize the system [120, 121]. As a result, if the passivity of SEA under velocity sourced impedance control is guaranteed, the coupled stability of the human and exoskeleton can be achieved.

To select gains that guarantee coupled stability via passivity for SEA under VSIC, theoretical bounds for null impedance and spring rendering have been presented by Tosun and Patoglu [15].

In Equation (4.3), passivity condition for null space rendering is presented [15].

$$J < \frac{(P_m + b)(1 + P_m P_t)}{P_m I_t + P_t I_m} \wedge b < \frac{P_t I_m}{I_t} \tag{4.3}$$

where J is the motor inertia and b is the motor damping.

In Equation (4.4), passivity conditions for spring rendering are presented [15].

$$J < \frac{(P_m + b)(\Delta K P_m P_t + K)}{\Delta K (P_m I_t + P_t I_{\mathrm{m}})} \wedge b < \frac{P_t I_{\mathrm{mi}}}{I_t} \wedge K_d < K_d^{\max} \tag{4.4}$$

where K_d is desired virtual stiffness and K_d^{max} is maximum renderable stiffness, $\Delta K := K - K_d$ and $K_d^{\max} = K\frac{\beta}{\beta + \alpha K}$, $\alpha = P_m I_t + P_t I_m$, and $\beta = P_t I_m^2 - b I_m I_t$.

Considering the controller gains used for the knee exoskeleton presented in Table 4.2 and the plant parameters in Table 4.1, it can be shown that coupled stability of interaction is ensured for VSIC. In Equation 4.5, the passivity of null space rendering has been verified. Moreover, in Equation 4.6, the passivity of spring rendering of 60 Nm/rad has been verified.

$$0.0023 < 0.6876 \wedge 0.134 < 0.6768 \tag{4.5}$$

$$0.023 < 0.9469 \wedge 0.134 < 0.2538 \wedge 60 < 136.69 \tag{4.6}$$

4.2.2.1 Spring Rendering Performance

The virtual stiffness levels of 60 Nm/rad and 120 Nm/rad were used as the desired stiffness under VSIC. Known static torques from 0.5 Nm to 2 Nm were applied to the end-effector. Then, the rendered stiffness levels were calculated by using the angular displacement of the end-effector. The rendered stiffness is 61.43 Nm/rad with RMSE 5.2% $R^2 = 0.996$ for 60 Nm/rad desired stiffness. while the rendered stiffness is 121.56 Nm/rad with RMSE 9.2% $R^2 = 0.979$ for 120 Nm/rad desired stiffness.

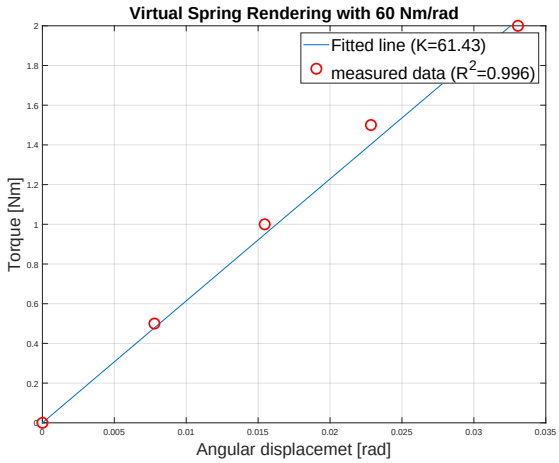

Figure 4.9 Spring rendering with 60 Nm/rad

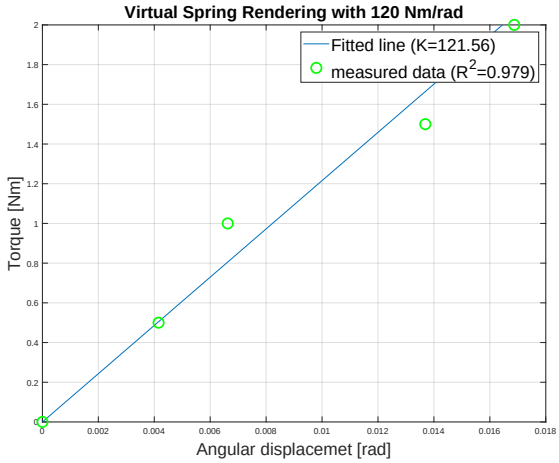

Figure 4.10 Spring rendering with 120 Nm/rad

4.2.2.2 Null Space Rendering Performance

The active back-driveability of SEA has been determined for null space rendering under VSIC. SEA aims to provide zero torque under this controller. To be able to provide small torques, a potato chip is commonly used to evaluate active backdrive-ability. In particular, the end-effector was pushed by a potato chip without breaking it. Figure 4.11 presents that a maximum of 0.69 Nm is require to drive the system.

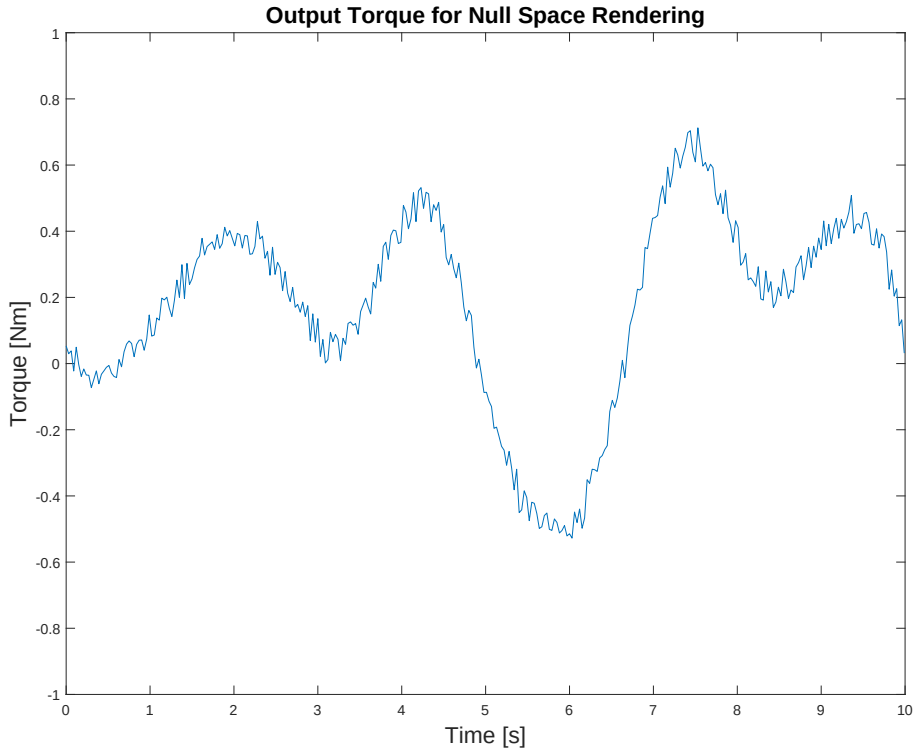

Figure 4.11 Chip test

Chapter 5

Human Subject Experiments

In this chapter, we present the experimental setup and detail the experimental procedure used for the human subject experiments with the compliant knee exoskeleton. The quantitative and qualitative results of the experiments evaluating the effect of self-alignment on ergonomy are presented.

5.1 Experimental Setup

The experimental setup consists of a compliant self-aligning knee exoskeleton, a treadmill, a chair, a Cortex Metalyzer 3B spirometry device to capture metabolic energy consumption, an i-Sens inertial motion capture system, and two 6-axis ATI force sensors to capture the interaction forces at the human connected interface, as can be seen in Figure 5.1.

Figure 5.1 Cortex Metalyzer 3B spirometry device, I-sens inertial motion capture system, ATI force sensor

5.2 Participants

Eight healthy volunteers participated in the experiments. None of the participants had any sensory-motor impairment or gait disorders, and all participants signed a consent form approved by the IRB of Sabanci University. Moreover, volunteers with BMI indices lower than 18 or higher than 30 were not allowed to participate in the study. In Figure 5.2, a volunteer who don the self-aligning exoskeleton and motion capture sensors can be seen.

Before the experiments began, the knee exoskeleton was explained to the volunteers, and they were given an emergency stop button in case they felt unsafe or uncomfortable.

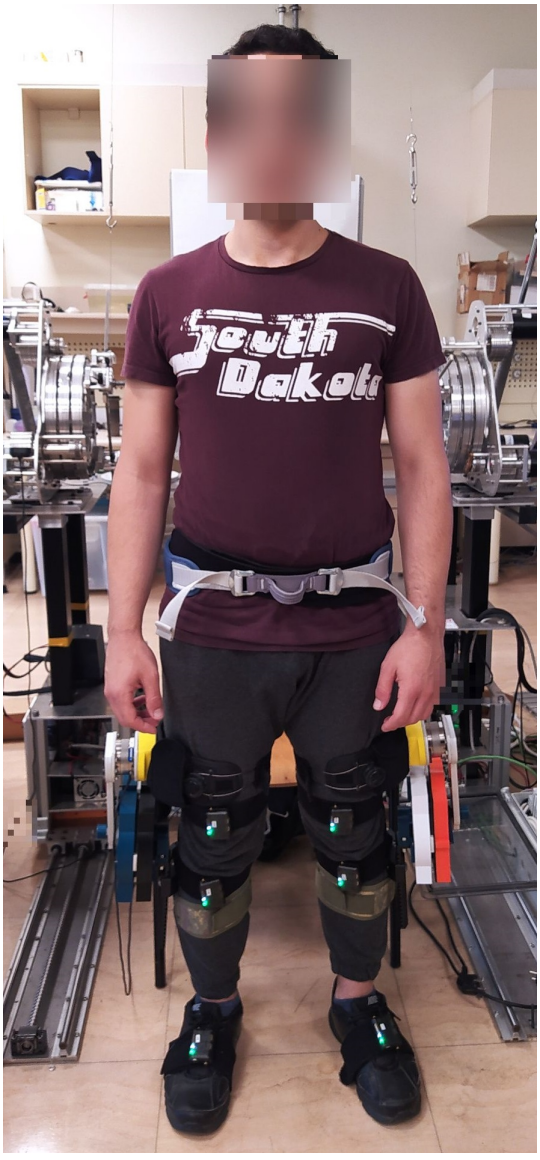

Figure 5.2 A volunteer during a sit-to-stand task

5.3 Hypothesis

The following hypothesis are tested.

Hypothesis 1: The self-aligning property of the knee exoskeleton significantly improves the users' ergonomy of its users and their perceived comfort, while reducing the interaction forces with the device for all tasks.

Hypothesis 2: The self-aligning knee exoskeleton does not significantly interfere with the natural sit-to-stand and walking kinematics of its users.

5.4 Tasks and Experimental Conditions

Sit-to-stand and walking tasks were used to conduct for the ergonomy evaluation experiments of the self-aligning mechanism. For each task, the following experimental conditions were tested:

- $C_{locked_{non}}$**: Self-aligning locked and no assistance**: The self-aligning mechanism is locked and no assistance torque is provided.
- $C_{locked_{un}}$**: Self-aligning unlocked and no assistance**: The self-aligning mechanism is unlocked and no assistance torque is provided.

5.5 Experimental Protocol for the Evaluation of Self-Alignment

5.5.1 Sit-to-Stand Task

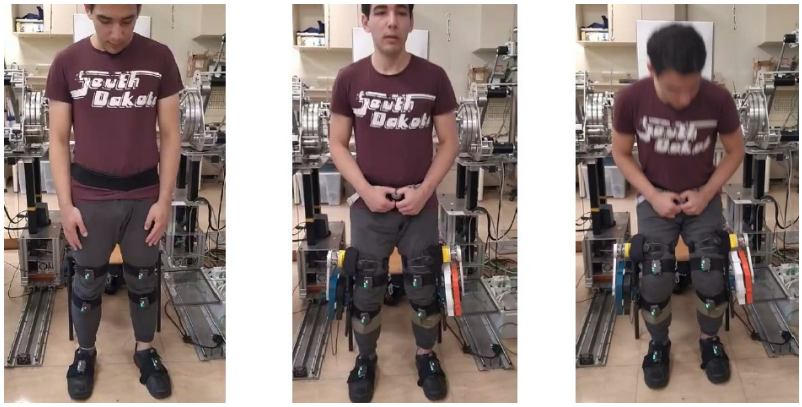

Figure 5.3 Sit to stand task

The inertial motion capture system was donned by volunteers to record kinematics of their lower limbs, and the force sensor was attached to the upper brace of the knee exoskeleton to record interaction forces/torques.

At the beginning of each session (under the locked and unlocked conditions), volunteers tried 3 to 5 sit-to-stand transitions to familiarize themselves with this condition. First, 20 sit-to-stand tasks were asked to be performed by volunteers before donning the knee exoskeleton. Then, the volunteers tried 20 sit-to-stand tasks from a standard-height chair (46 cm tall) under locked/unlocked condition.

Volunteers were blinded to the conditions (locked or unlocked). Randomly, the self-aligning mechanism was left unlocked to begin the testing for half of the volunteers. At the end of each task, a questionnaire was filled by the volunteers. The System Usability Scale (SUS) was used as the questionnaire. Between two sessions, volunteers were given a rest for 3 minutes, as can be seen in Figure 5.4.

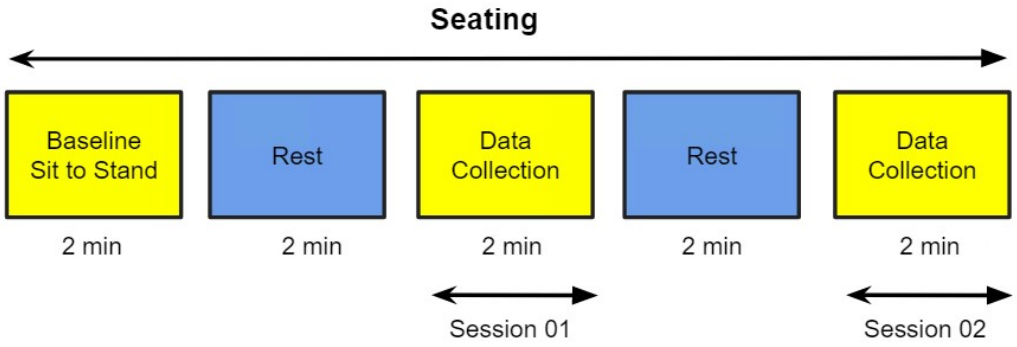

Figure 5.4 Experimental protocol of sit to stand task without assistance

5.5.1.1 Experimental Protocol for the Walking Task

Figure 5.5 Walking task

In the walking task, there were two sessions (locked and unlocked conditions) presented in a randomized order, in addition to the initial baseline session. For the baseline session, 2 minutes walking of volunteers were recorded before the donning device. In each session, kinematic and interaction force data collection started immediately. Two minutes breaks were scheduled between the sessions to minimize any fatigue effects and to lock/unlock the self-aligning mechanism, as can be seen in Figure 5.6. Kinematic data is collected from the first 30 seconds of each session.

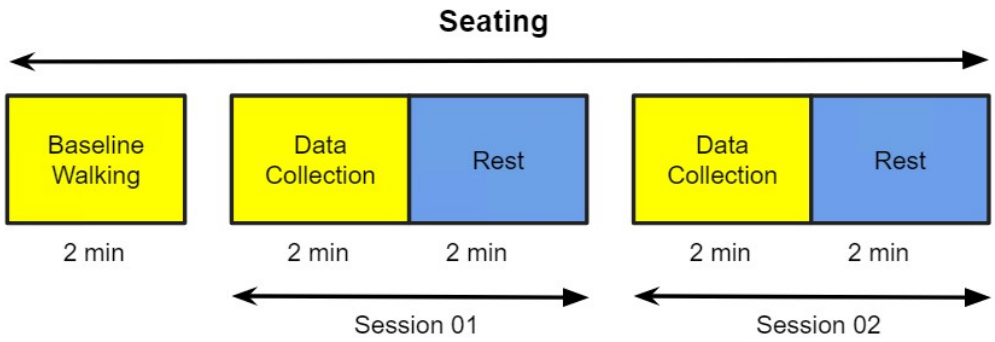

Figure 5.6 Experimental protocol of walking task without assistance

5.6 Performance Metrics

The effectiveness of the exoskeleton's interactions with participants and the significance of allowing for self-alignment of exoskeleton with human knee during sit-to-stand and walking tasks were assessed by using a variety of quantitative and qualitative metrics.

The range of motion during flexion/extension of the knee was measured by the motion capture system and the exoskeleton. For the walking task, gait kinematics data captured by I-sens were also compared for different conditions. To understand the self-aligning mechanisms effects for all tasks, interaction forces were recorded by using ATI mini 56 force sensors attached to upper knee brace.

As a qualitative metric, volunteers were asked to fill a questionnaire for System usability scale (SUS) to evaluate their subjective preferences for the device. Also, comfort levels were asked to volunteers to compare without exoskeleton, self-aligning locked and unlocked cases.

5.7 Statistical Analysis

One-way repeated measures ANOVA was used to determine significant differences in the quantitative metrics. Box plots are used to show any significant differences. SPSS (ver. 28.0, IBM, New York, USA) was used for statistical analysis.

5.8 Results of Sit to Stand Task

5.8.1 Interaction Forces and Torques

The self-aligning property of the exoskeleton is evaluated by studying the undesired interaction forces. For all experiments, undesired interaction forces were captured by using the force sensor attached to the upper knee brace of the volunteers.

5.8.1.1 Interaction Forces along X Direction

Mean values and standard deviations of undesired interaction forces between the left upper brace and the knee along the x direction is shown in Figure 5.7.

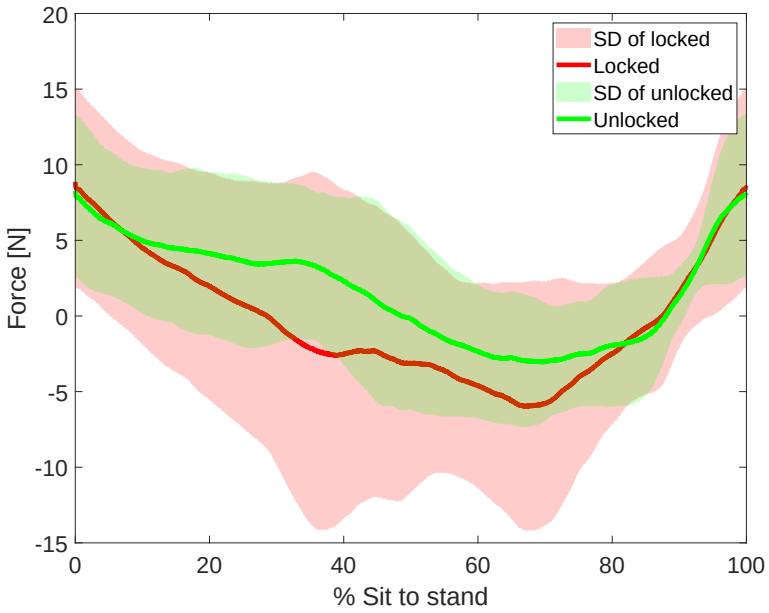

Figure 5.7 Mean values and standard deviations of undesired interaction forces between the left upper brace and the knee along the x direction

Mean values and standard deviations of the maximum of absolute value of the undesired interaction forces between the left upper brace and the knee along the x direction is shown as box plot in Figure 5.8. One-way repeated measures ANOVA

was conducted to study the effect of the self-aligning on the interaction forces along y direction between left knee and exoskeleton. The effect of self-aligning was found to be statistically significant for this forces at $p<0.05$ level ($F(1,14)=4.876$).

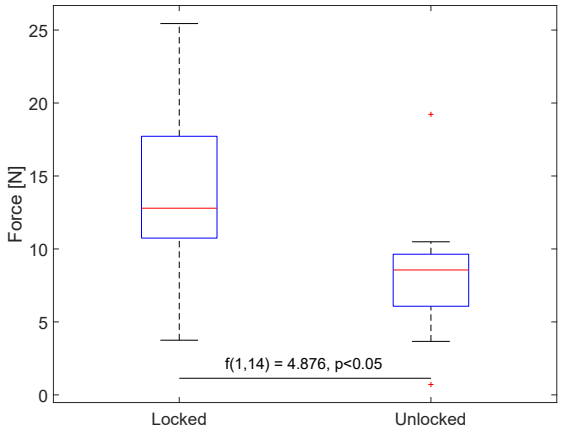

Figure 5.8 Mean values and standard deviations of the maximum of absolute value of the undesired interaction forces between the left upper brace and the knee along the x direction

Table 5.1 Effect size of undesired interaction forces between left upper brace and knee in x direction

	Point Estimate	95 Confidence Interval	
		Lower	Upper
Eta-squared	0,107	0,000	0,403
Epsilon-squared	0,043	-0,071	0,361
Omega-squared Fixed-effect	0,040	-0,067	0,346
Omega-squared Random-effect	0,040	-0,067	0,346

Mean values and standard deviations of undesired interaction forces between the right upper brace and the knee along the x direction is shown in Figure 5.9.

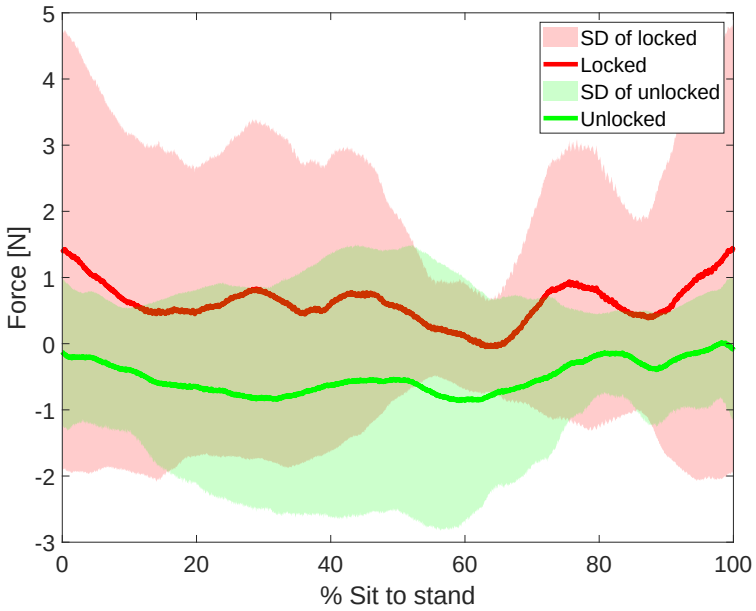

Figure 5.9 Mean values and standard deviations of undesired interaction forces between the right upper brace and the knee along the x direction

Mean values and standard deviations of the maximum of absolute value of the undesired interaction forces between the right upper brace and the knee along the x direction is shown as box plot in Figure 5.10. One-way repeated measures ANOVA was conducted to study the effect of the self-aligning on the interaction forces along y direction between right knee and exoskeleton. The effect of self-aligning was found to be statistically significant for this forces at $p<0.05$ level ($F(1,14)=0.840$).

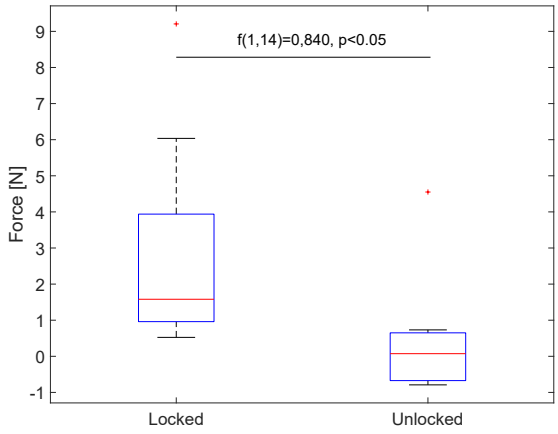

Figure 5.10 Mean values and standard deviations of the maximum of absolute value of the undesired interaction forces between the right upper brace and the knee along the X direction

Table 5.2 Effect size of undesired interaction forces between right upper brace and knee in x direction

	Point Estimate	95 Confidence Interval	
		Lower	Upper
Eta-squared	0,057	0,000	0,343
Epsilon-squared	-0,011	-0,071	0,296
Omega-squared Fixed-effect	-0,010	-0,067	0,282
Omega-squared Random-effect	-0,010	-0,067	0,282

5.8.1.2 Interaction Forces along the Y Direction

Mean values and standard deviations of undesired interaction forces between the left upper brace and the knee along the y direction is shown in Figure 5.11.

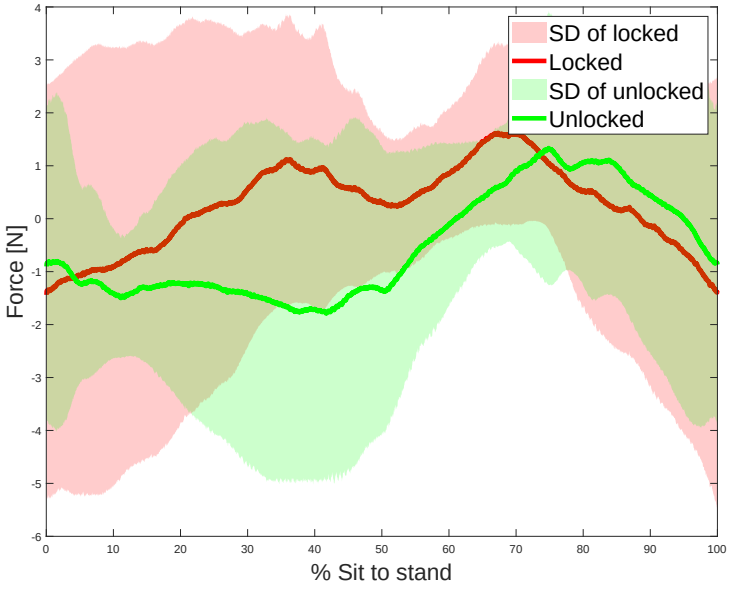

Figure 5.11 Mean values and standard deviations of undesired interaction forces between the left upper brace and the knee along the y direction

Mean values and standard deviations of the maximum of absolute value of the undesired interaction forces between the left upper brace and the knee along the y direction is shown as box plot in Figure 5.12. One-way repeated measures ANOVA was conducted to study the effect of the self-aligning on the interaction forces along y direction between left knee and exoskeleton. The effect of self-aligning was not found to be statistically significant for this forces at $p<0.05$ level ($F(1,14)=0.304$).

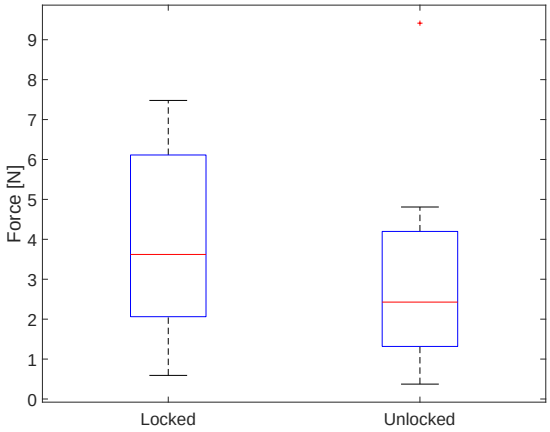

Figure 5.12 Mean values and standard deviations of the maximum of absolute value of the undesired interaction forces between the left upper brace and the knee along the y direction

Mean values and standard deviations of undesired interaction forces between the right upper brace and the knee along the y direction is shown in Figure 5.17.

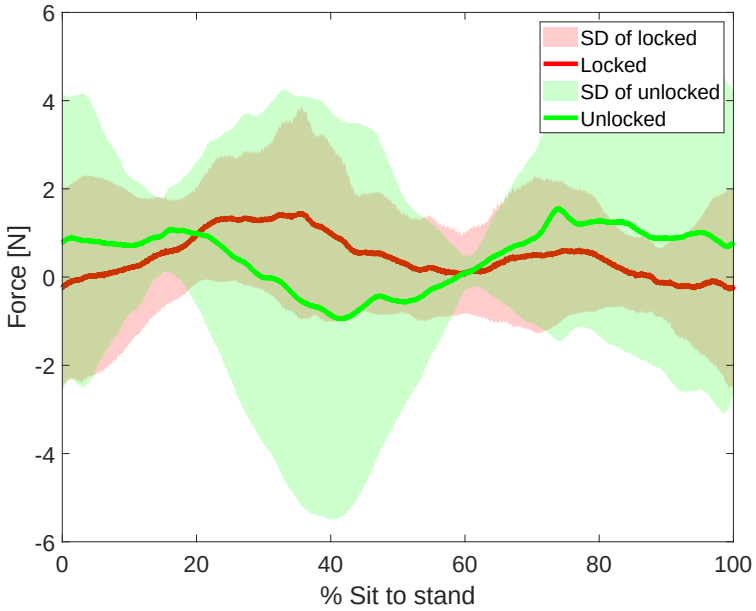

Figure 5.13 Mean values and standard deviations of undesired interaction forces between the right upper brace and the knee along the y direction

Mean values and standard deviations of the maximum of absolute value of the undesired interaction forces between the right upper brace and the knee along the y direction is shown as box plot in Figure 5.14. One-way repeated measures ANOVA

was conducted to study the effect of the self-aligning on the interaction forces along y direction between right knee and exoskeleton. The effect of self-aligning was not found to be statistically significant for this forces at $p<0.05$ level ($F(1,14)=0.125$).

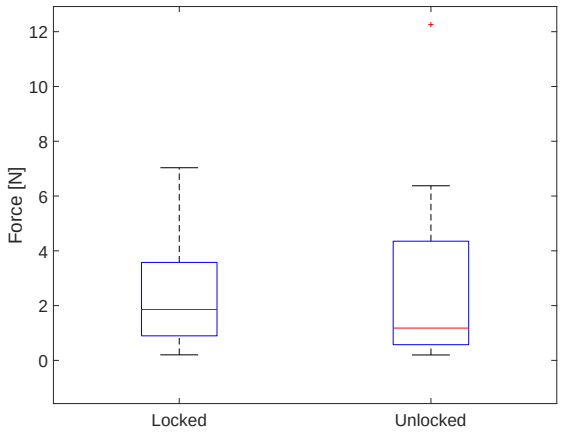

Figure 5.14 Mean values and standard deviations of the maximum of absolute value of the undesired interaction forces between the right upper brace and the knee along the y direction

5.8.1.3 Interaction Forces along the Z Direction

Mean values and standard deviations of undesired interaction forces between the left upper brace and the knee along the z direction is shown in Figure 5.15.

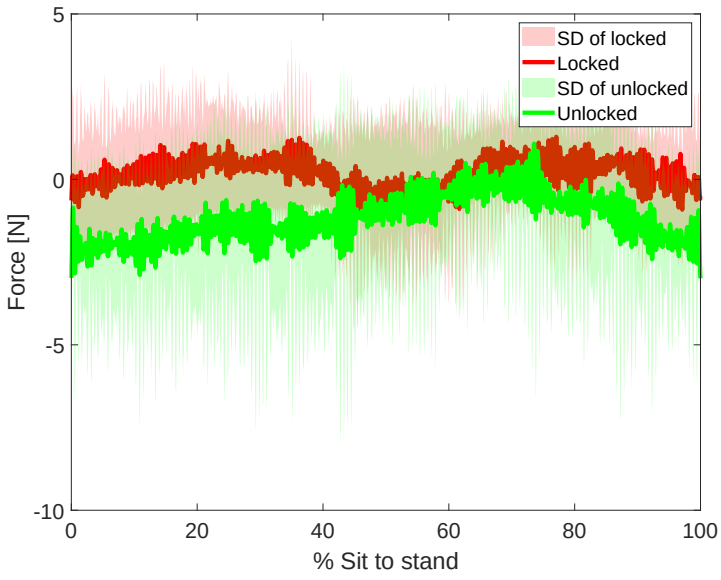

Figure 5.15 Mean values and standard deviations of undesired interaction forces between the left upper brace and the knee along the z direction

Mean values and standard deviations of the maximum of absolute value of the undesired interaction forces between the left upper brace and the knee along the z direction is shown as box plot in Figure 5.16. One-way repeated measures ANOVA was conducted to study the effect of the self-aligning on the interaction forces along z direction between left knee and exoskeleton. The effect of self-aligning was not found to be statistically significant for this forces at $p<0.05$ level ($F(1,14)=0.001$).

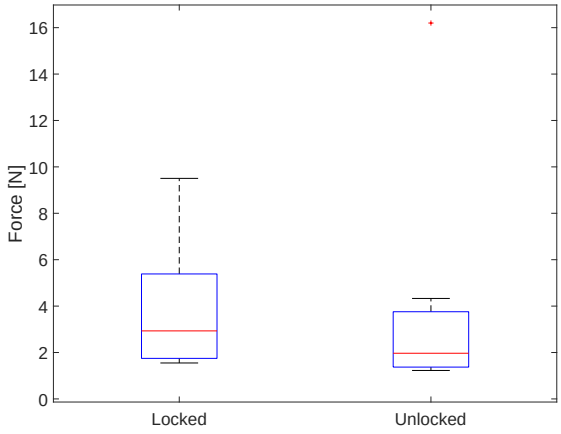

Figure 5.16 Mean values and standard deviations of the maximum of absolute value of the undesired interaction forces between the left upper brace and the knee along the z direction

Mean values and standard deviations of undesired interaction forces between the right upper brace and the knee along the z direction is shown in Figure 5.17.

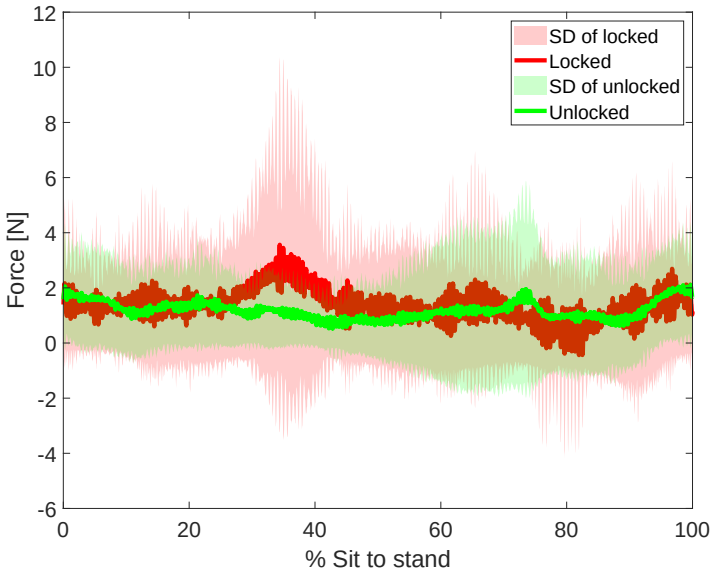

Figure 5.17 Mean values and standard deviations of undesired interaction forces between the right upper brace and the knee along the z direction

Mean values and standard deviations of the maximum of absolute value of the undesired interaction forces between the right upper brace and the knee along the z direction is shown as box plot in Figure 5.18. One-way repeated measures ANOVA was conducted to study the effect of the self-aligning on the interaction forces along z direction between right knee and exoskeleton. The effect of self-aligning was not found to be statistically significant for this forces at $p<0.05$ level ($F(1,14)=0.746$).

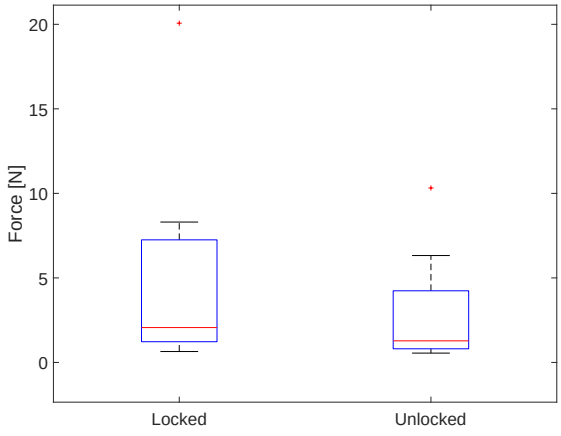

Figure 5.18 Mean values and standard deviations of the maximum of absolute value of the undesired interaction forces between the right upper brace and the knee along the z direction

5.8.1.4 Interaction Torques along the X Direction

Mean values and standard deviations of undesired interaction torques between the left upper brace and the knee along the x direction is shown in Figure 5.19.

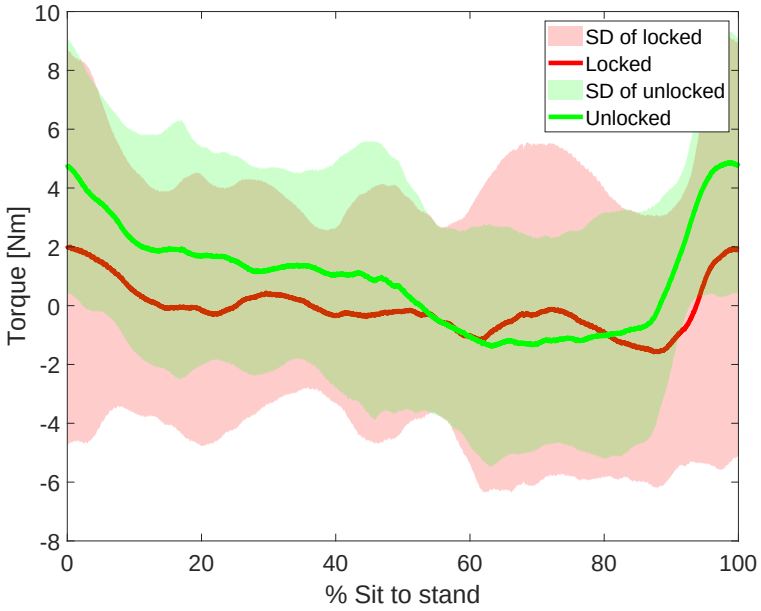

Figure 5.19 Mean values and standard deviations of undesired interaction torques between the left upper brace and the knee along the x direction

Mean values and standard deviations of the maximum of absolute value of the undesired interaction torques between the left upper brace and the knee along the x direction is shown as box plot in Figure 5.20. One-way repeated measures ANOVA was conducted to study the effect of the self-aligning on the interaction torques along x direction between left knee and exoskeleton. The effect of self-aligning was not found to be statistically significant for this torques at $p<0.05$ level ($F(1,14)=0.000$).

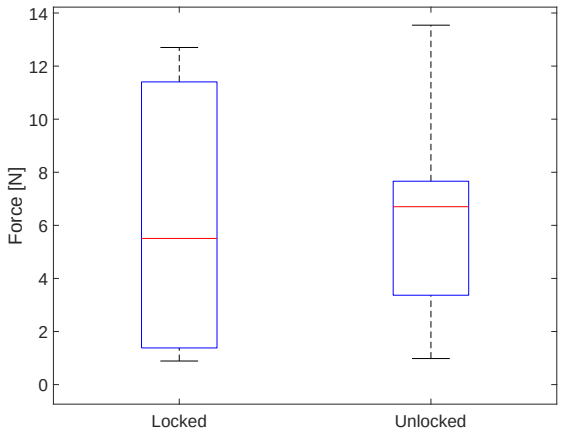

Figure 5.20 Mean values and standard deviations of the maximum of absolute value of the undesired interaction torques between the left upper brace and the knee along the x direction

Mean values and standard deviations of undesired interaction torques between the right upper brace and the knee along the x direction is shown in Figure 5.21.

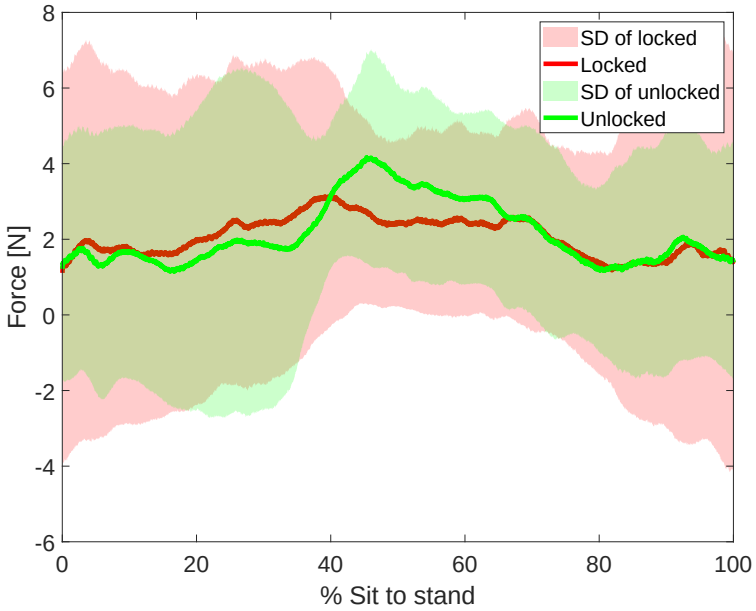

Figure 5.21 Mean values and standard deviations of undesired interaction torques between the right upper brace and the knee along the x direction

Mean values and standard deviations of the maximum of absolute value of the undesired interaction torques between the right upper brace and the knee along the x direction is shown as box plot in Figure 5.22. One-way repeated measures ANOVA

was conducted to study the effect of the self-aligning on the interaction torques along x direction between right knee and exoskeleton. The effect of self-aligning was not found to be statistically significant for this torques at $p<0.05$ level ($F(1,14)=0.034$).

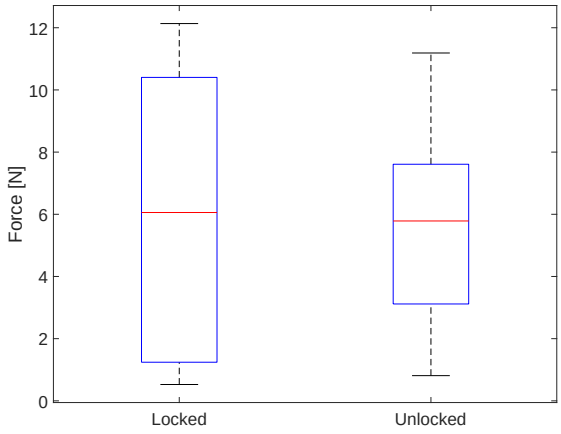

Figure 5.22 Mean values and standard deviations of the maximum of absolute value of the undesired interaction torques between the right upper brace and the knee along the x direction

5.8.1.5 Interaction Torques along the Y Direction

Mean values and standard deviations of undesired interaction torques between the left upper brace and the knee along the y direction is shown in Figure 5.23.

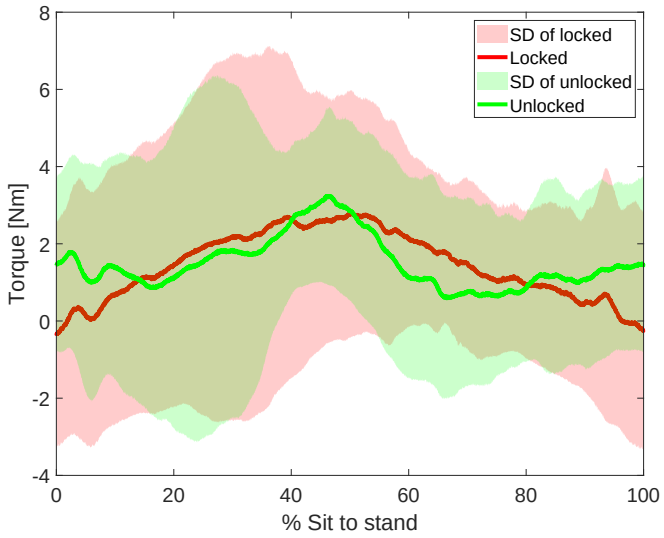

Figure 5.23 Mean values and standard deviations of undesired interaction torques between the left upper brace and the knee along the y direction

Mean values and standard deviations of the maximum of absolute value of the undesired interaction torques between the left upper brace and the knee along the y direction is shown as box plot in Figure 5.24. One-way repeated measures ANOVA was conducted to study the effect of the self-aligning on the interaction torques along y direction between left knee and exoskeleton. The effect of self-aligning was not found to be statistically significant for this torques at $p<0.05$ level ($F(1,14)=0.018$).

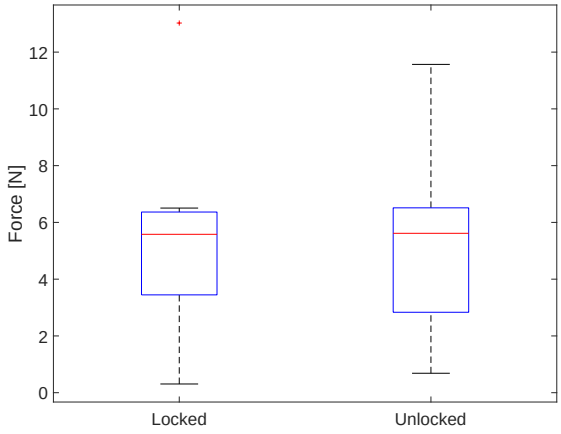

Figure 5.24 Mean values and standard deviations of the maximum of absolute value of the undesired interaction torques between the left upper brace and the knee along the y direction

Mean values and standard deviations of undesired interaction torques between the right upper brace and the knee along the y direction is shown in Figure 5.25.

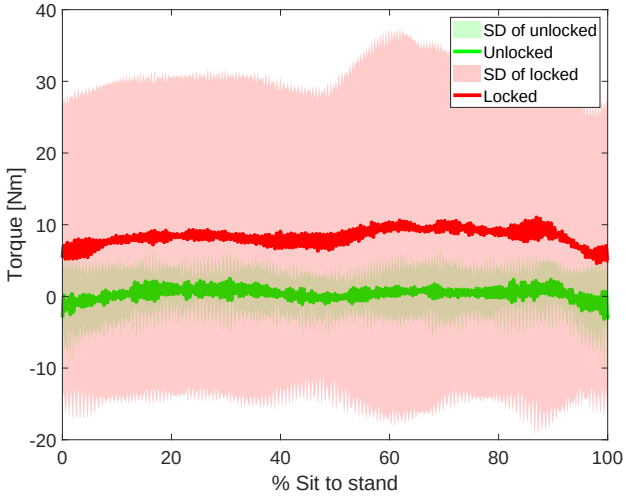

Figure 5.25 Mean values and standard deviations of undesired interaction torques between the right upper brace and the knee along the y direction

Mean values and standard deviations of the maximum of absolute value of the undesired interaction torques between the right upper brace and the knee along the y direction is shown as box plot in Figure 5.26. One-way repeated measures ANOVA was conducted to study the effect of the self-aligning on the interaction torques along y direction between right knee and exoskeleton. The effect of self-aligning was not found to be statistically significant for this torques at $p<0.05$ level ($F(1,14)=0.537$).

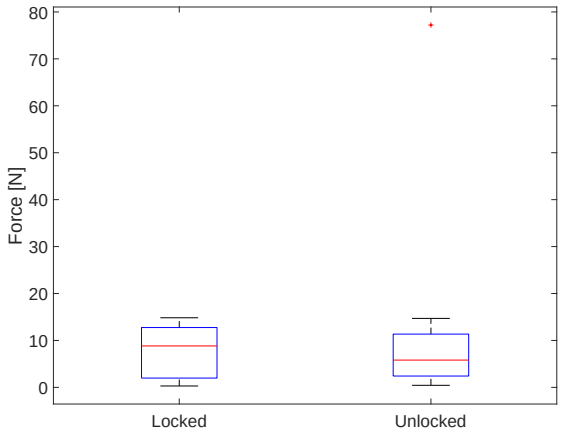

Figure 5.26 Mean values and standard deviations of the maximum of absolute value of the undesired interaction torques between the right upper brace and the knee along the y direction

5.8.1.6 Interaction Torques along the Z Direction

Mean values and standard deviations of undesired interaction torques between the left upper brace and the knee along the z direction is shown in Figure 5.27.

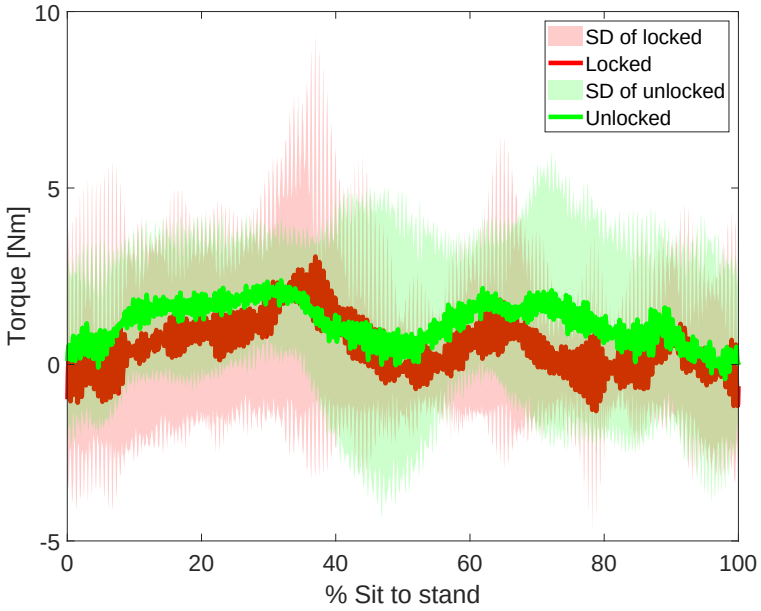

Figure 5.27 Mean values and standard deviations of undesired interaction torques between the left upper brace and the knee along the z direction

Mean values and standard deviations of the maximum of absolute value of the undesired interaction torques between the left upper brace and the knee along the z direction is shown as box plot in Figure 5.28. One-way repeated measures ANOVA was conducted to study the effect of the self-aligning on the interaction torques along z direction between left knee and exoskeleton. The effect of self-aligning was not found to be statistically significant for this torques at $p<0.05$ level ($F(1,14)=0.009$).

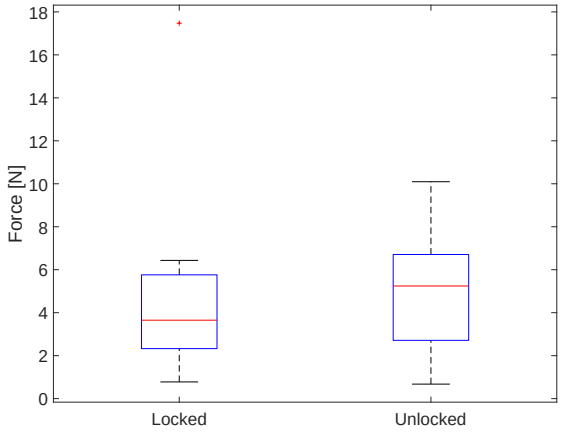

Figure 5.28 Mean values and standard deviations of the maximum of absolute value of the undesired interaction torques between the left upper brace and the knee along the z direction

Mean values and standard deviations of undesired interaction torques between the right upper brace and the knee along the z direction is shown in Figure 5.29.

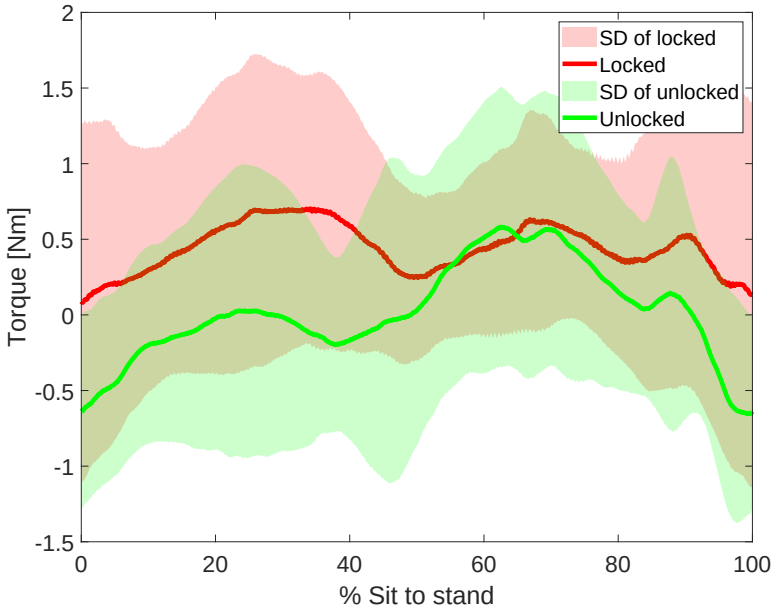

Figure 5.29 Mean values and standard deviations of undesired interaction torques between the right upper brace and the knee along the z direction

Mean values and standard deviations of the maximum of absolute value of the undesired interaction torques between the right upper brace and the knee along the z direction is shown as box plot in Figure 5.30. One-way repeated measures ANOVA

was conducted to study the effect of the self-aligning on the interaction torques along z direction between right knee and exoskeleton. The effect of self-aligning was not found to be statistically significant for this torques at $p<0.05$ level ($F(1,14)=0.447$).

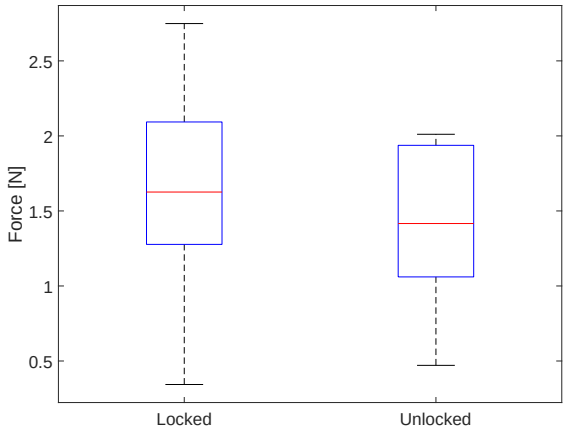

Figure 5.30 Mean values and standard deviations of the maximum of absolute value of the undesired interaction torques between the right upper brace and the knee along the z direction

5.8.2 Knee Kinematics during Sit to Stand Task

Mean values and standard deviations of angle of the left knee for without exoskeleton, unlocked, and locked case during sit to stand task can be seen from Figure 5.31. One-way repeated measures ANOVA with Post-Hoc Tukey was conducted to study the effect of the self-aligning on the knee angle range for sit-to-stand task. The effect of self-aligning was not found to be statistically significant for the sit-to-stand kinematic of the left knee at $p<0.05$ level ($F(1,14)=0.079$).

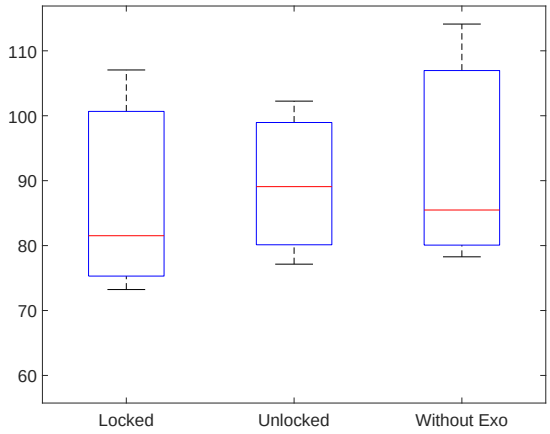

Figure 5.31 Mean values and standard deviations of angle of the left knee for different cases

Rotational motion range of left knee for different cases is shown in the Figure 5.32.

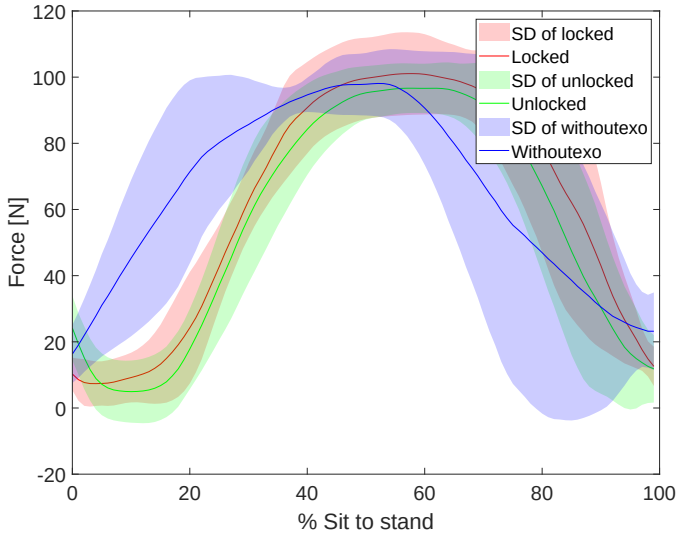

Figure 5.32 Rotational motion range of left knee for different cases

Mean values and standard deviations of angle of right knee for without exoskeleton, unlocked, and locked case during sit to stand task can be seen from Figure 5.33. One-way repeated measures ANOVA with Post-Hoc Tukey was conducted to study the effect of the self-aligning on the knee angle range for sit-to-stand task. The effect of self-aligning was not found to be statistically significant for the sit-to-stand kinematic of the right knee at $p<0.05$ level ($F(1,14)=0.368$).

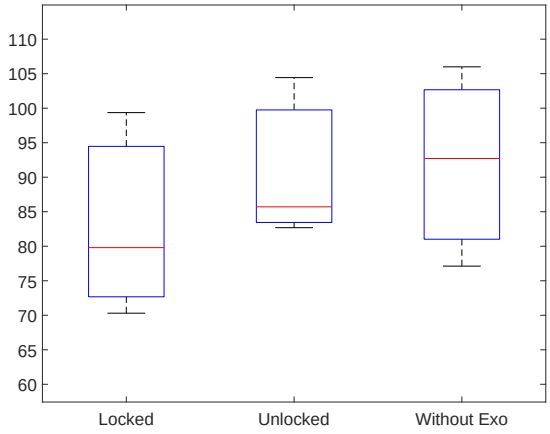

Figure 5.33 Rotational motion range of right knee for different cases

Rotational motion range of left knee for different cases is shown in the Figure 5.34.

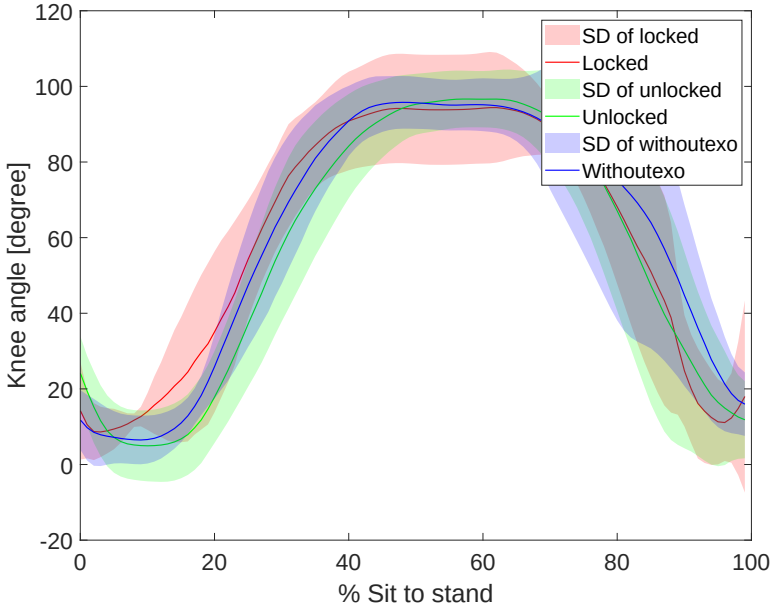

Figure 5.34 Rotational motion range of right knee for different cases

5.8.3 Comfort Rate of Sit-to-Stand Task

Comfort rate has been asked to the volunteers after each condition.

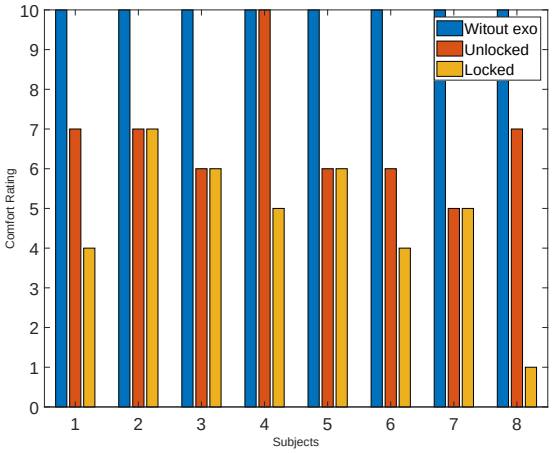

Figure 5.35 Comfort rates of different volunteers

Mean and standard deviations of comfort rates of sit-to-stand task for each condition can be seen in Figure 5.36. Also, ANOVA results with Post-Hoc Tukey for comfort rates for sit-to-stand task can be seen in Table 5.3. The effect of self-aligning was found to be statistically significant for sit-to-stand task at $p<0.05$ level ($F(1,4)=60.143$).

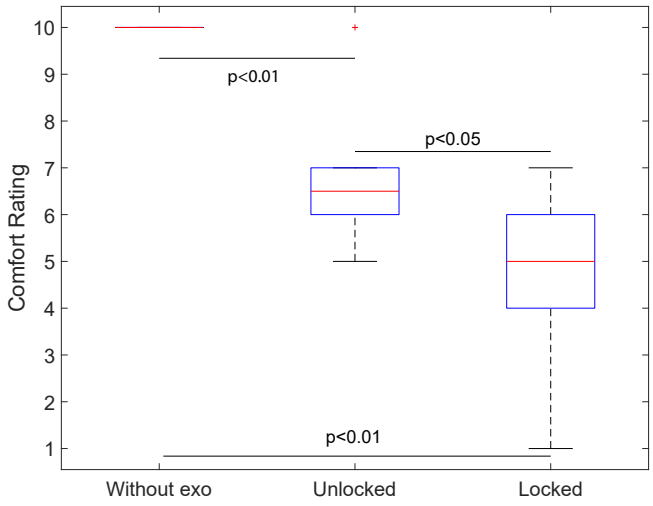

Figure 5.36 Mean and standard deviations of comfort rates for each condition

Table 5.3 ANOVA results with Post-Hoc Tukey for comfort rates of sit-to-stand task

					95 Confidence Interval	
		Main Difference	Std. Error	Sig.	Lower Bound	Upper Bound
Locked	Unlocked	-2.0000*	0,68139	0,021	-3,7175	-0,2825
	Without exo	-5.2500*	0,68139	0,000	-6,9675	-3,5325
Unlocked	Locked	2.0000*	0,68139	0,021	0,2825	3,7175
	Without exo	-3.2500*	0,68139	0,000	-4,9675	-1,5325
Without exo	Unlocked	5.2500*	0,68139	0,000	3,5325	6,9675
	Locked	3.2500*	0,68139	0,000	1,5325	4,9675

5.9 Results of Walking Task

5.9.1 Interaction Forces and Torques

The self-aligning property of the exoskeleton is evaluated by studying the undesired interaction forces. For walking task, undesired interaction forces were captured by using the force sensor attached to the upper knee brace of the volunteers. Note that all the results below are for three volunteers who have participated the walking task.

5.9.1.1 Interaction Forces along X Direction

Mean values and standard deviations of undesired interaction forces between the left upper brace and the knee along the x direction is shown in Figure 5.37.

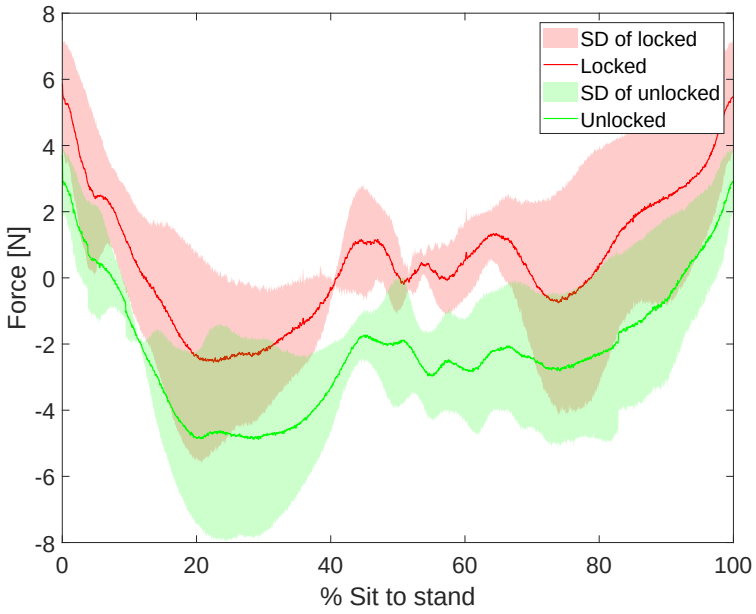

Figure 5.37 Mean values and standard deviations of undesired interaction forces between the left upper brace and the knee along the x direction

Mean values and standard deviations of the maximum of absolute value of the undesired interaction forces between the left upper brace and the knee along the x direction is shown as box plot in Figure 5.38. One-way repeated measures ANOVA was conducted to study the effect of the self-aligning on the interaction forces along y direction between left knee and exoskeleton. The effect of self-aligning was found to be statistically significant for this forces at $p<0.05$ level ($F(1,4)=0.005$).

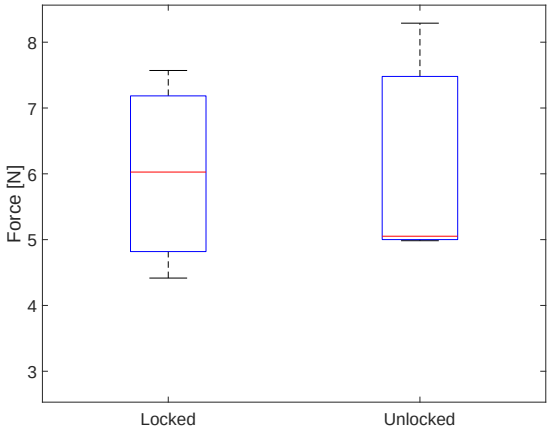

Figure 5.38 Mean values and standard deviations of the maximum of absolute value of the undesired interaction forces between the left upper brace and the knee along the x direction

Table 5.4 Effect size of undesired interaction forces between left upper brace and knee in x direction

	Point Estimate	95 Confidence Interval	
		Lower	Upper
Eta-squared	0,107	0,000	0,403
Epsilon-squared	0,043	-0,071	0,361
Omega-squared Fixed-effect	0,040	-0,067	0,346
Omega-squared Random-effect	0,040	-0,067	0,346

Mean values and standard deviations of undesired interaction forces between the right upper brace and the knee along the x direction is shown in Figure 5.39.

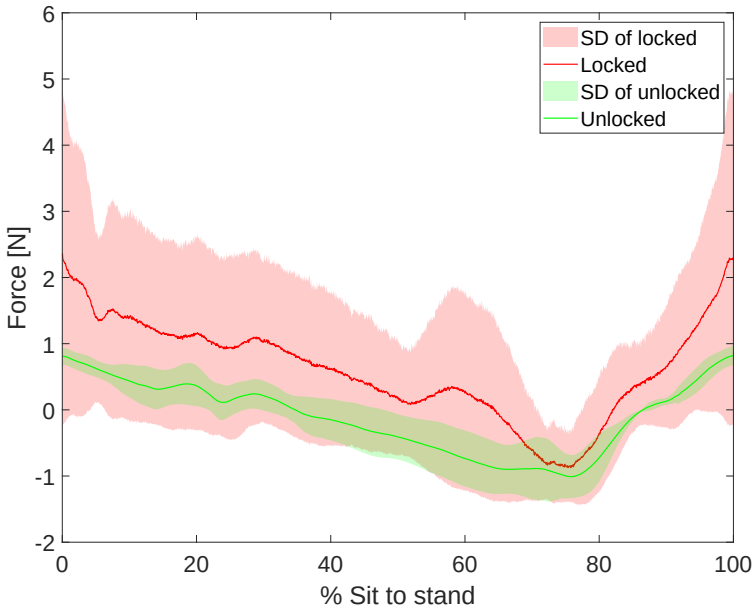

Figure 5.39 Mean values and standard deviations of undesired interaction forces between the right upper brace and the knee along the x direction

Mean values and standard deviations of the maximum of absolute value of the undesired interaction forces between the right upper brace and the knee along the x direction is shown as box plot in Figure 5.40. One-way repeated measures ANOVA was conducted to study the effect of the self-aligning on the interaction forces along y direction between left knee and exoskeleton. The effect of self-aligning was found to be statistically significant for this forces at $p<0.05$ level ($F(1,4)=1.011$).

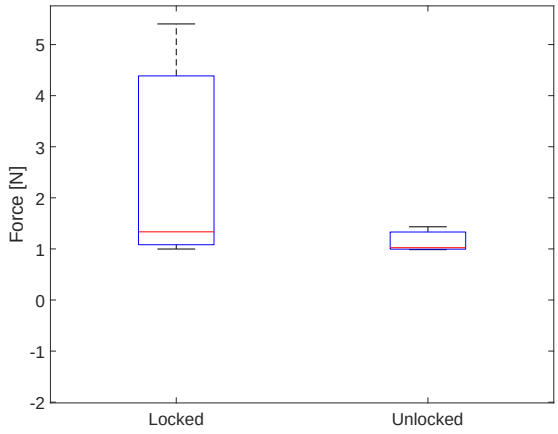

Figure 5.40 Mean values and standard deviations of the maximum of absolute value of the undesired interaction forces between the right upper brace and the knee along the X direction

Table 5.5 ANOVA effect sizes of interaction forces along x direction for the right knee

	Point Estimate	95 Confidence Interval	
		Lower	Upper
Eta-squared	0,057	0,000	0,343
Epsilon-squared	-0,011	-0,071	0,296
Omega-squared Fixed-effect	-0,010	-0,067	0,282
Omega-squared Random-effect	-0,010	-0,067	0,282

5.9.1.2 Interaction Forces along the Y Direction

Mean values and standard deviations of undesired interaction forces between the left upper brace and the knee along the y direction is shown in Figure 5.41.

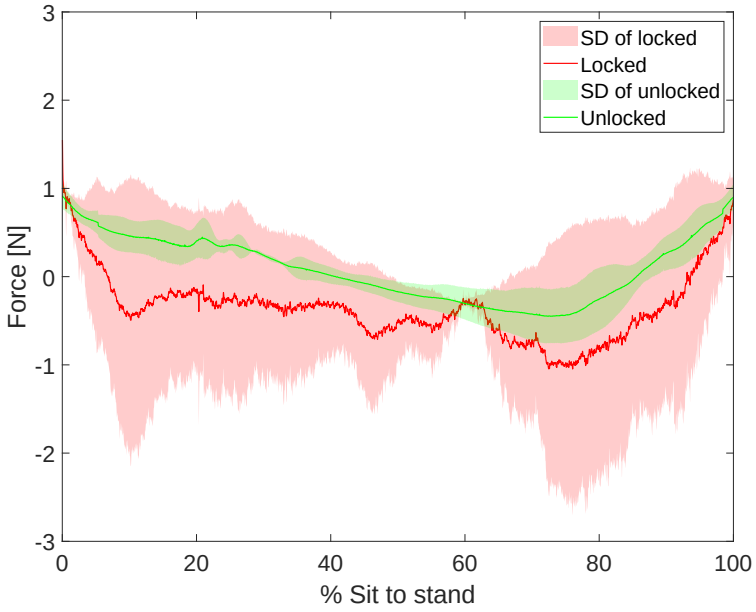

Figure 5.41 Mean values and standard deviations of undesired interaction forces between the left upper brace and the knee along the y direction

Mean values and standard deviations of the maximum of absolute value of the undesired interaction forces between the left upper brace and the knee along the y direction is shown as box plot in Figure 5.42. One-way repeated measures ANOVA was conducted to study the effect of the self-aligning on the interaction forces along y direction between left knee and exoskeleton. The effect of self-aligning was not found to be statistically significant for this forces at $p<0.05$ level ($F(1,4)=1.278$).

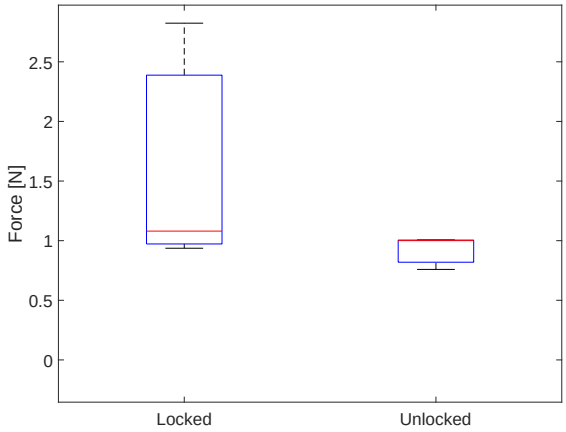

Figure 5.42 Mean values and standard deviations of the maximum of absolute value of the undesired interaction forces between the left upper brace and the knee along the y direction

Mean values and standard deviations of undesired interaction forces between the right upper brace and the knee along the y direction is shown in Figure 5.47.

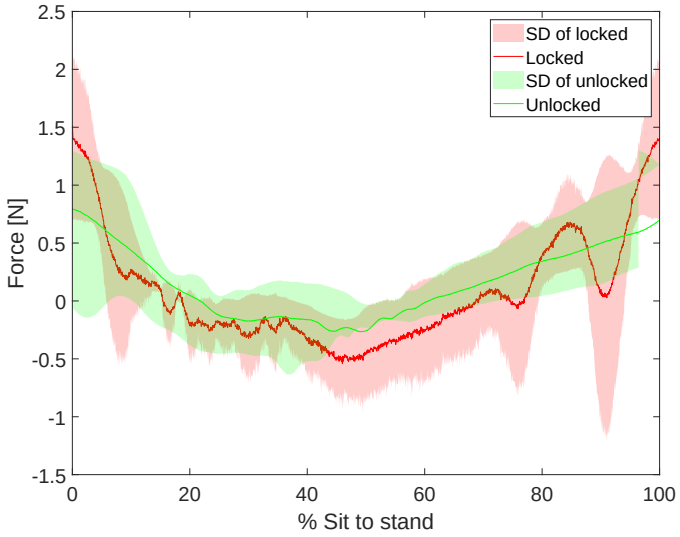

Figure 5.43 Mean values and standard deviations of undesired interaction forces between the right upper brace and the knee along the y direction

Mean values and standard deviations of the maximum of absolute value of the undesired interaction forces between the right upper brace and the knee along the y direction is shown as box plot in Figure 5.44. One-way repeated measures ANOVA was conducted to study the effect of the self-aligning on the interaction forces along

y direction between right knee and exoskeleton. The effect of self-aligning was not found to be statistically significant for this forces at $p<0.05$ level ($F(1,4)=1.515$).

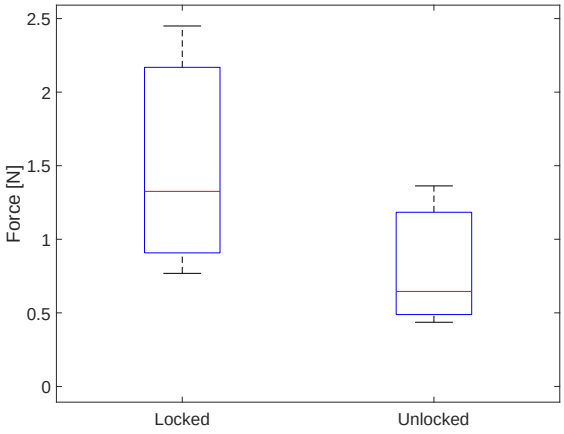

Figure 5.44 Mean values and standard deviations of the maximum of absolute value of the undesired interaction forces between the right upper brace and the knee along the y direction

5.9.1.3 Interaction Forces along the Z Direction

Mean values and standard deviations of undesired interaction forces between the left upper brace and the knee along the z direction is shown in Figure 5.15.

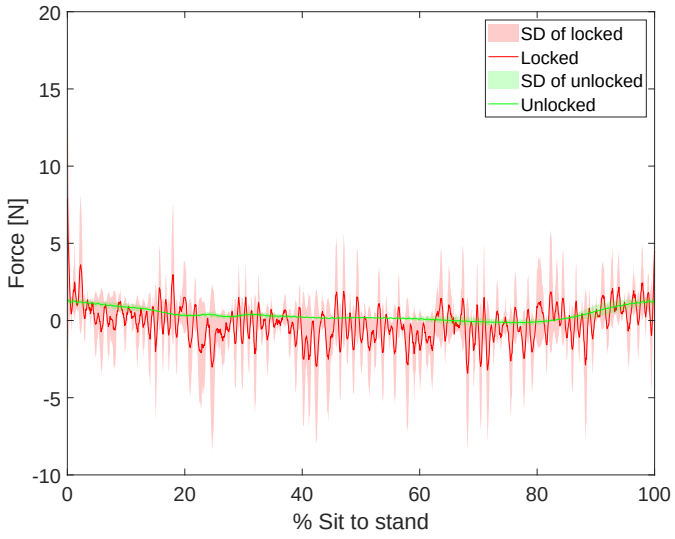

Figure 5.45 Mean values and standard deviations of undesired interaction forces between the left upper brace and the knee along the z direction

Mean values and standard deviations of the maximum of absolute value of the

undesired interaction forces between the left upper brace and the knee along the z direction is shown as box plot in Figure 5.46. One-way repeated measures ANOVA was conducted to study the effect of the self-aligning on the interaction forces along z direction between left knee and exoskeleton. The effect of self-aligning was not found to be statistically significant for this forces at $p<0.05$ level ($F(1,4)=0.940$).

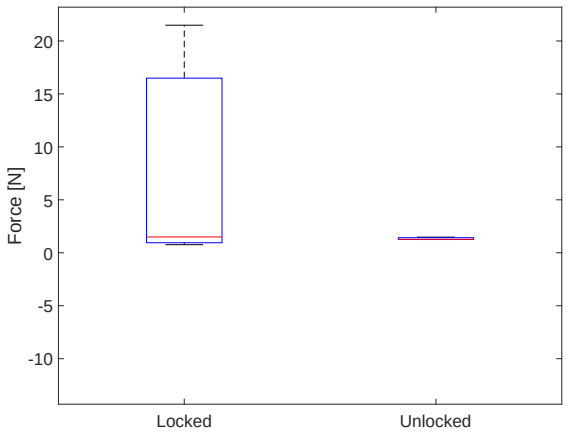

Figure 5.46 Mean values and standard deviations of the maximum of absolute value of the undesired interaction forces between the left upper brace and the knee along the z direction

Mean values and standard deviations of undesired interaction forces between the right upper brace and the knee along the z direction is shown in Figure 5.47.

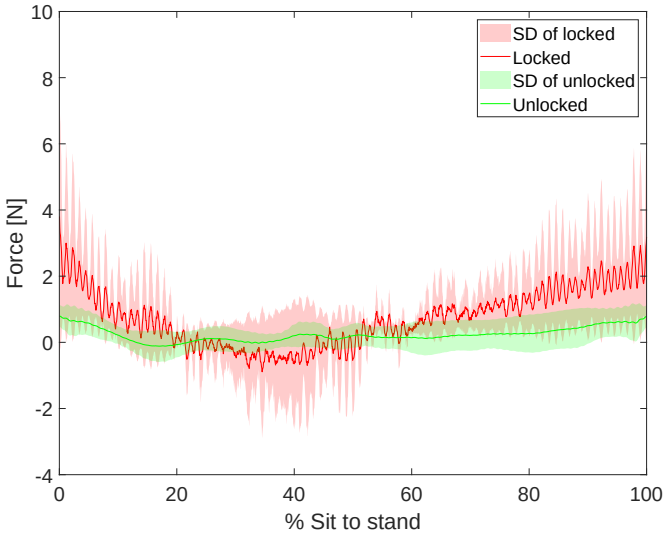

Figure 5.47 Mean values and standard deviations of undesired interaction forces between the right upper brace and the knee along the z direction

Mean values and standard deviations of the maximum of absolute value of the undesired interaction forces between the right upper brace and the knee along the z direction is shown as box plot in Figure 5.48. One-way repeated measures ANOVA was conducted to study the effect of the self-aligning on the interaction forces along z direction between right knee and exoskeleton. The effect of self-aligning was not found to be statistically significant for this forces at $p<0.05$ level ($F(1,4)=1.420$).

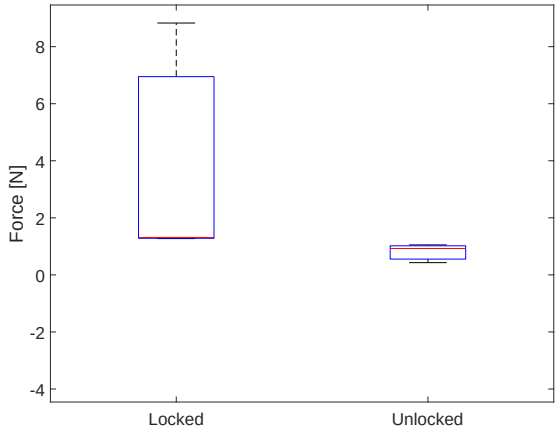

Figure 5.48 Mean values and standard deviations of the maximum of absolute value of the undesired interaction forces between the right upper brace and the knee along the z direction

5.9.1.4 Interaction Torques along the X Direction

Mean values and standard deviations of undesired interaction torques between the left upper brace and the knee along the x direction is shown in Figure 5.49.

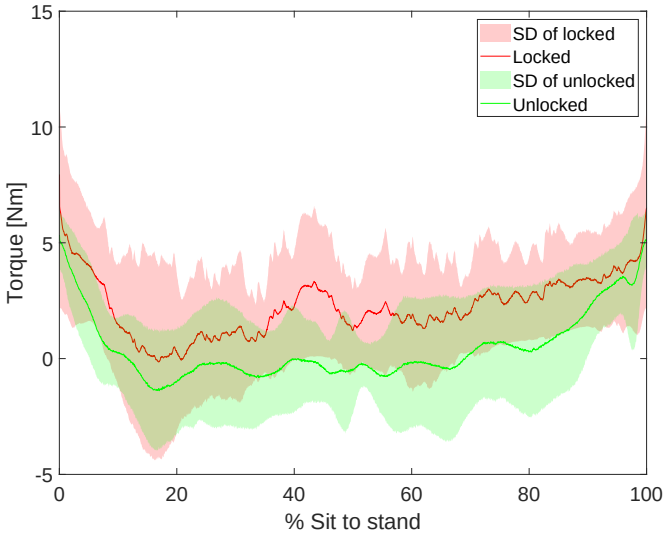

Figure 5.49 Mean values and standard deviations of undesired interaction torques between the left upper brace and the knee along the x direction

Mean values and standard deviations of the maximum of absolute value of the undesired interaction torques between the left upper brace and the knee along the x direction is shown as box plot in Figure 5.50. One-way repeated measures ANOVA was conducted to study the effect of the self-aligning on the interaction torques along x direction between left knee and exoskeleton. The effect of self-aligning was not found to be statistically significant for this torques at $p<0.05$ level ($F(1,4)=0.528$).

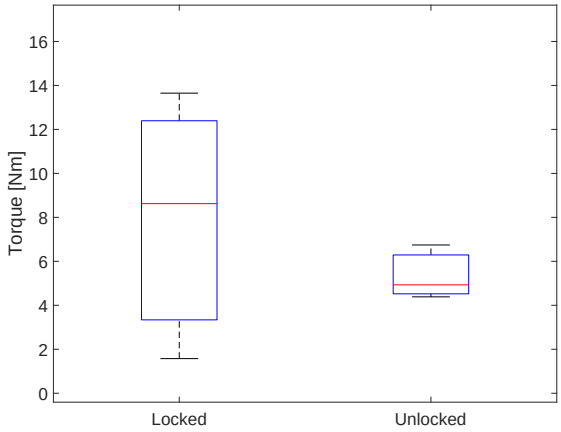

Figure 5.50 Mean values and standard deviations of the maximum of absolute value of the undesired interaction torques between the left upper brace and the knee along the x direction

Mean values and standard deviations of undesired interaction torques between the right upper brace and the knee along the x direction is shown in Figure 5.51.

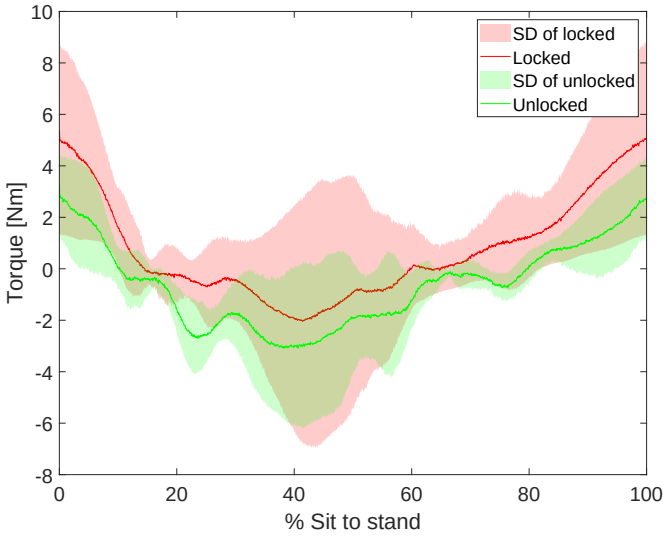

Figure 5.51 Mean values and standard deviations of undesired interaction torques between the right upper brace and the knee along the x direction

Mean values and standard deviations of the maximum of absolute value of the undesired interaction torques between the right upper brace and the knee along the x direction is shown as box plot in Figure 5.52. One-way repeated measures ANOVA was conducted to study the effect of the self-aligning on the interaction torques along

x direction between right knee and exoskeleton. The effect of self-aligning was not found to be statistically significant for this torques at $p<0.05$ level ($F(1,4)=0.149$).

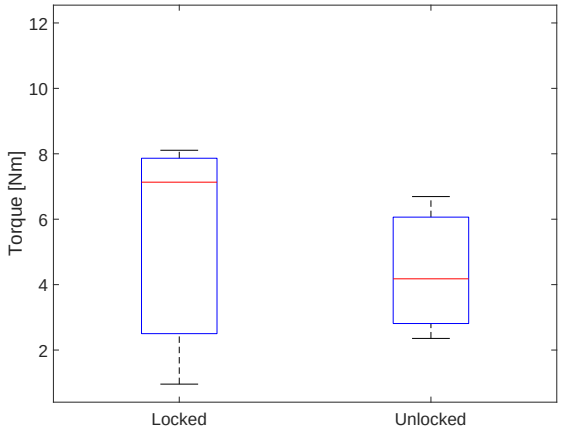

Figure 5.52 Mean values and standard deviations of the maximum of absolute value of the undesired interaction torques between the right upper brace and the knee along the x direction

5.9.1.5 Interaction Torques along the Y Direction

Mean values and standard deviations of undesired interaction torques between the left upper brace and the knee along the y direction is shown in Figure 5.53.

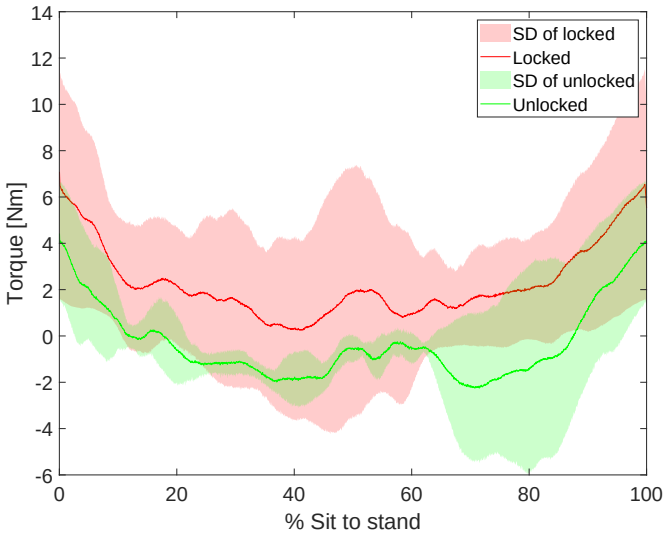

Figure 5.53 Mean values and standard deviations of undesired interaction torques between the left upper brace and the knee along the y direction

Mean values and standard deviations of the maximum of absolute value of the

undesired interaction torques between the left upper brace and the knee along the y direction is shown as box plot in Figure 5.54. One-way repeated measures ANOVA was conducted to study the effect of the self-aligning on the interaction torques along y direction between left knee and exoskeleton. The effect of self-aligning was not found to be statistically significant for this torques at $p<0.05$ level ($F(1,4)=0.132$).

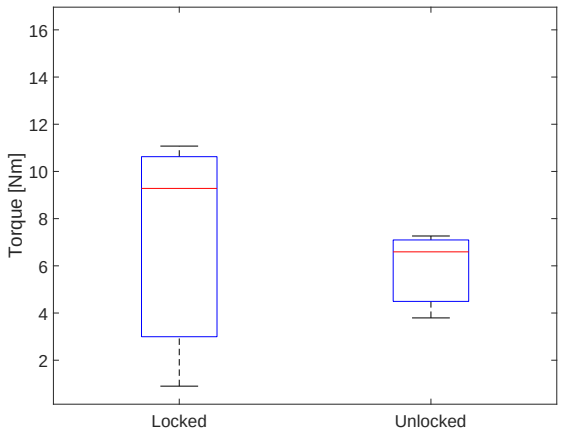

Figure 5.54 Mean values and standard deviations of the maximum of absolute value of the undesired interaction torques between the left upper brace and the knee along the y direction

Mean values and standard deviations of undesired interaction torques between the right upper brace and the knee along the y direction is shown in Figure 5.55.

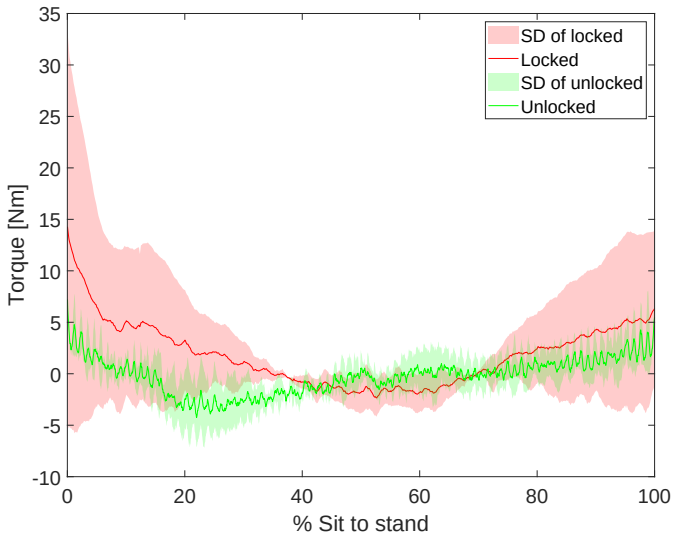

Figure 5.55 Mean values and standard deviations of undesired interaction torques between the right upper brace and the knee along the y direction

Mean values and standard deviations of the maximum of absolute value of the undesired interaction torques between the right upper brace and the knee along the y direction is shown as box plot in Figure 5.56. One-way repeated measures ANOVA was conducted to study the effect of the self-aligning on the interaction torques along y direction between right knee and exoskeleton. The effect of self-aligning was not found to be statistically significant for this torques at $p<0.05$ level ($F(1,4)=0.411$).

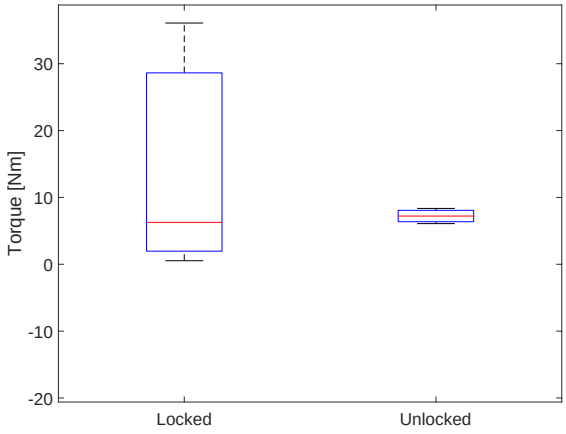

Figure 5.56 Mean values and standard deviations of the maximum of absolute value of the undesired interaction torques between the right upper brace and the knee along the y direction

5.9.1.6 Interaction Torques along the Z Direction

Mean values and standard deviations of undesired interaction torques between the left upper brace and the knee along the z direction is shown in Figure 5.57.

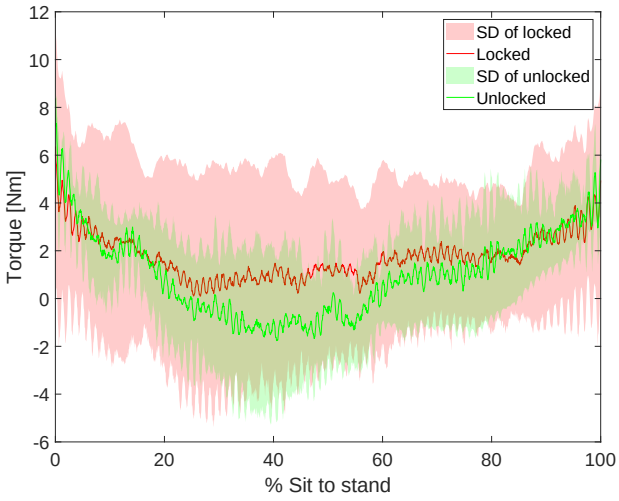

Figure 5.57 Mean values and standard deviations of undesired interaction torques between the left upper brace and the knee along the z direction

Mean values and standard deviations of the maximum of absolute value of the undesired interaction torques between the left upper brace and the knee along the z direction is shown as box plot in Figure 5.58. One-way repeated measures ANOVA was conducted to study the effect of the self-aligning on the interaction torques along z direction between left knee and exoskeleton. The effect of self-aligning was not found to be statistically significant for this torques at $p<0.05$ level ($F(1,4)=0.374$).

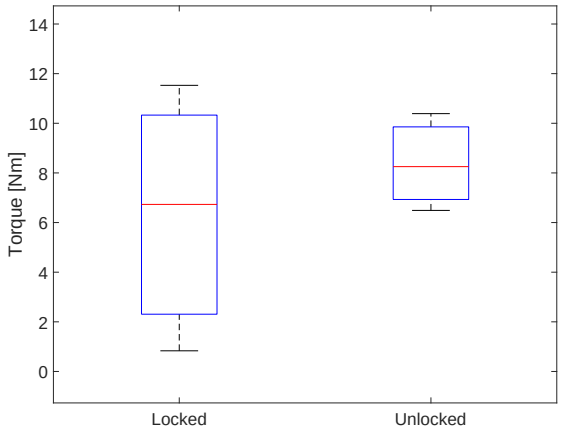

Figure 5.58 Mean values and standard deviations of the maximum of absolute value of the undesired interaction torques between the left upper brace and the knee along the z direction

Mean values and standard deviations of undesired interaction torques between the right upper brace and the knee along the z direction is shown in Figure 5.59.

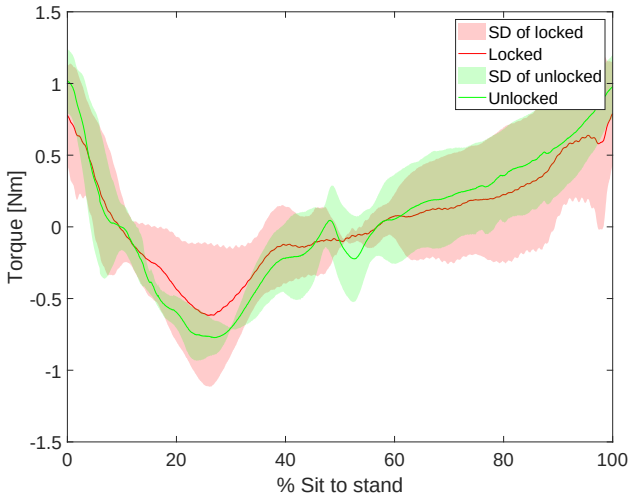

Figure 5.59 Mean values and standard deviations of undesired interaction torques between the right upper brace and the knee along the z direction

Mean values and standard deviations of the maximum of absolute value of the undesired interaction torques between the right upper brace and the knee along the z direction is shown as box plot in Figure 5.60. One-way repeated measures ANOVA was conducted to study the effect of the self-aligning on the interaction torques along z direction between right knee and exoskeleton. The effect of self-aligning was not found to be statistically significant for this torques at $p<0.05$ level ($F(1,4)=1.010$).

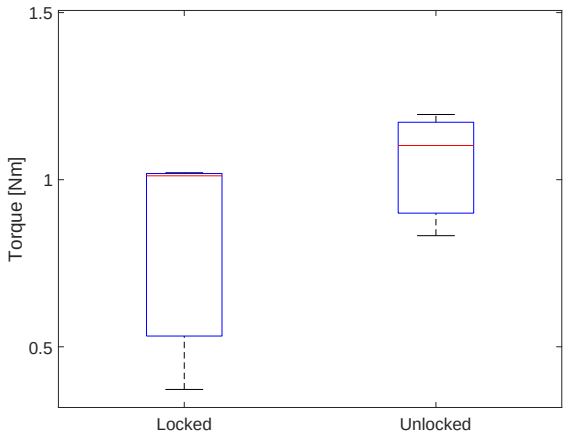

Figure 5.60 Mean values and standard deviations of the maximum of absolute value of the undesired interaction torques between the right upper brace and the knee along the z direction

5.9.2 Knee Kinematics during Walking Task

Mean values and standard deviations of angle of the left knee for without exoskeleton, unlocked, and locked case during walking task can be seen from Figure 5.61. One-way repeated measures ANOVA with Post-Hoc Tukey was conducted to study the effect of the self-aligning on the knee angle range for walking task. The effect of self-aligning was not found to be statistically significant for the sit-to-stand kinematic of the left knee at $p<0.05$ level ($F(1,14)=0.652$).

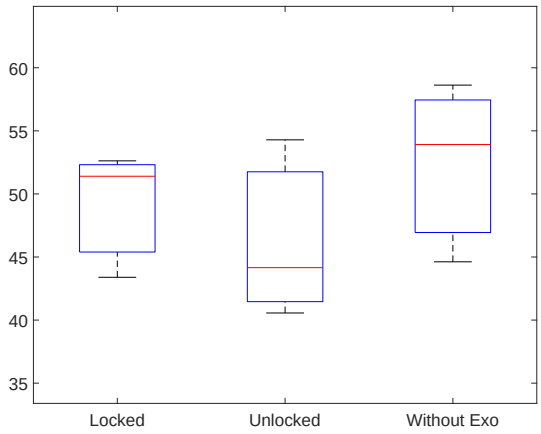

Figure 5.61 Mean values and standard deviations of angle of the left knee for different cases

Rotational motion range of left knee for different cases is shown in the Figure 5.62.

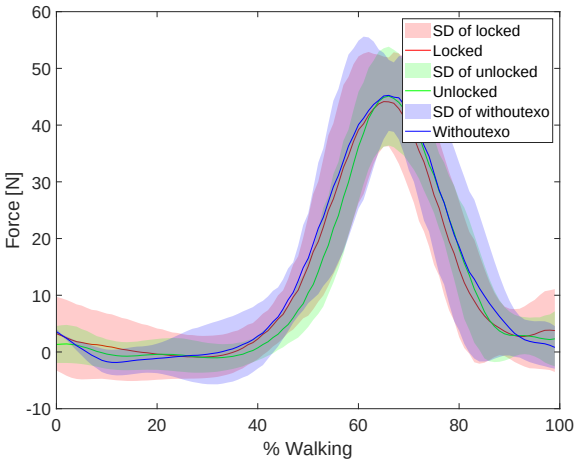

Figure 5.62 Rotational motion range of left knee for different cases

Mean values and standard deviations of angle of right knee for without exoskeleton,

unlocked, and locked case during sit to stand task can be seen from Figure 5.63. One-way repeated measures ANOVA with Post-Hoc Tukey was conducted to study the effect of the self-aligning on the knee angle range for walking task. The effect of self-aligning was not found to be statistically significant for the sit-to-stand kinematic of the right knee at $p<0.05$ level ($F(1,14)=1.675$).

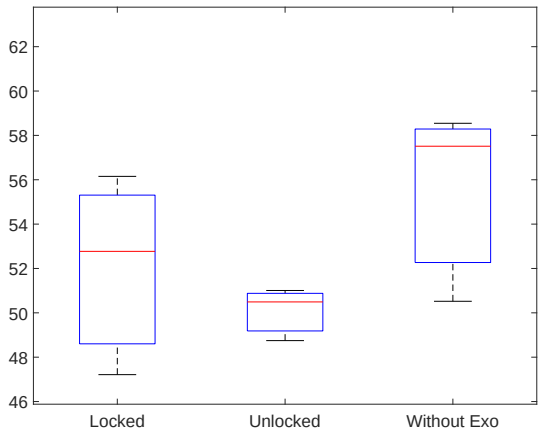

Figure 5.63 Rotational motion range of right knee for different cases

Rotational motion range of left knee for different cases is shown in the Figure 5.64.

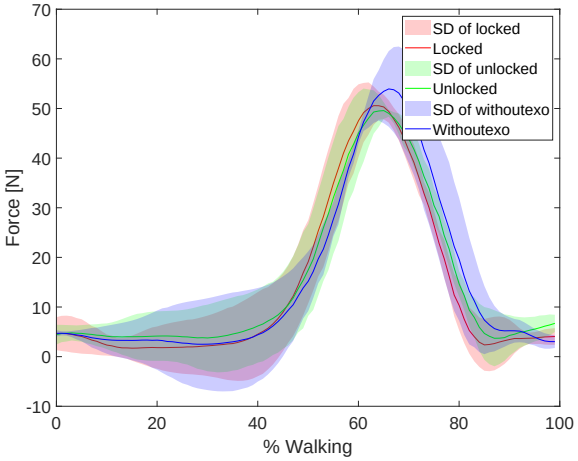

Figure 5.64 Rotational motion range of right knee for different cases

5.9.3 Comfort Rate of Walking Task

Comfort rate has been asked to the volunteers after each condition, as in Figure 5.65.

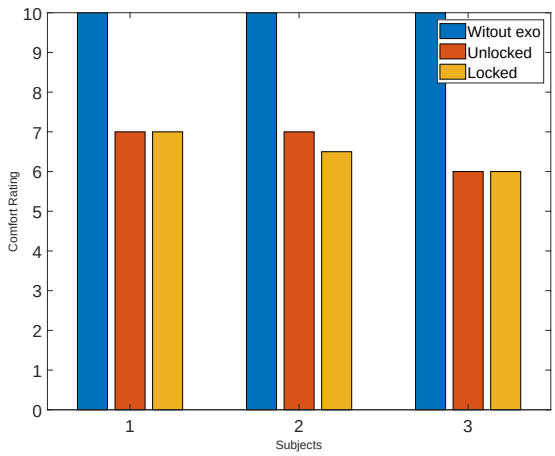

Figure 5.65 Comfort rates of different volunteers

Mean and standard deviations of comfort rates of walking task can be seen in Figure 5.66 for each condition. One-way repeated measures ANOVA with Post-Hoc Tukey was conducted to study the effect of the self-aligning on comfort level. The effect of self-aligning was not found to be statistically significant for walking task at $p<0.05$ level ($F(1,4)=60.143$).

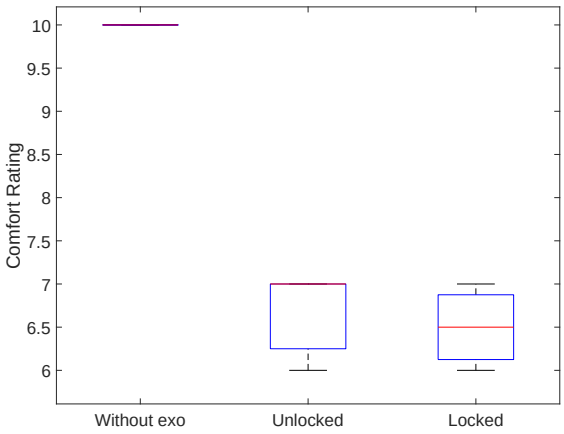

Figure 5.66 Mean and standard deviations of comfort rates for each condition

5.9.4 Discussion of Results

As it can be seen from results of sit-to-stand task, undesired interaction forces along the X direction are significantly lower when self-aligning mechanism is used. Note that undesired interaction forces along Y direction becomes lower thanks to self-aligning mechanism but this change is not significant. This is because translational motion of axis of human knee along x direction of sagittal plane is higher than motion along y direction.

Moreover, undesired interaction forces along z direction and undesired interaction torques along x, y and z directions are not significantly different for both locked and unlocked case of self-aligning mechanism. Since the self-aligning mechanism allows motion only in sagittal plane, motions of human knee along other directions are restricted for both unlocked and locked cases of self-aligning mechanism. Therefore, interaction forces/torques have not changed significantly for both cases.

Furthermore, the results of comfort rate for the sit-to-stand task show that unlocked case of the self-aligning mechanism is significantly more comfortable than the locked case. This shows the ergonomic improvement of the self-aligning mechanism for sit-to-stand task. Also, unlocked case is slightly more comfortable according to mean values of comfort rates of walking task, but this difference is not significant.

Also, results of the knee kinematics for both walking and sit-to-stand tasks show that there is not significant difference between locked, unlocked and without exoskeleton cases. Therefore, it can be concluded that self-aligning knee exoskeleton does not interfere with human knee kinematics.

Chapter 6

Conclusions and Future Work

We have presented the self-aligning compliant mechanism design, interaction control, experimental characterization, and user evaluations of a powered compliant self-aligning knee exoskeleton.

To solve the misalignment problem between the human knee and the knee exoskeleton, a large stroke XY stage compliant mechanism with low backlash and friction, and high rotational and low translational stiffness is designed in a compact and light form.

Thanks to its self-aligning property, the knee exoskeleton enables the translational movements of knee joint in the sagittal plane as well as the main flexion/extension movements. An ideal match between human knee and the exoskeleton axis is achieved by automatically aligning its joint axes so that the parasitic forces are reduced. Self-alignment of the knee exoskeleton not only guarantees ergonomy and comfort throughout the therapy, but also significantly shortens the setup time required to attach a patient to the exoskeleton.

By using a Bowden cable-driven series elastic actuator, the knee exoskeleton actively controls the rotational movement of the knee joint. Actuator and harmonic reduction unit are placed to a remote location through Bowden cable transmission to lower the inertia of exoskeleton on the human. Moreover, the knee exoskeleton provides good torque tracking characteristics, active back-driveability within its control bandwidth, and passive compliance for excitations above this bandwidth.

We present a comprehensive set of human subject experiments designed to evaluate the self-aligning feature of the self-aligning knee exoskeleton. Our human subject experiments provide evidence that the self-aligning knee exoskeleton does not significantly interfere with the gait kinematics and its self-alignment property significantly

reduces parasitic interaction forces, when compared with the case with no self alignment.

Our future work includes improving of the mechanical design of the prototype to enable application of higher torques and performing case studies with assistant torques.

For a more compact design, the self-aligning compliant mechanism will be produced with Al 7075 material by using an EDM machine, instead of the low-cost 3D printing with PLA material. To improve transmission efficiency, flexible shafts may be employed for the power transmission, instead of Bowden cables. For more secure connection, human connections may be designed to feature two attachment parts for the upper leg and two attachment parts for the lower leg.

BIBLIOGRAPHY

[1] W. Hasenkamp Carreira, "Flexible micro/nanofabricated systems for medical devices and implants," EPFL, Tech. Rep., 2013.

[2] H. Wang, C. Yang, W. Yang, M. Deng, Z. Ma, and Q. Wei, "A rehabilitation gait for the balance of human and lower extremity exoskeleton system based on the transfer of gravity center," *Industrial Robot: the international journal of robotics research and application*, 2019.

[3] L. Zhang, G. Liu, B. Han, Z. Wang, H. Li, and Y. Jiao, "Assistive devices of human knee joint: A review," *Robotics and Autonomous Systems*, vol. 125, p. 103394, 2020.

[4] C. Fleischer, A. Wege, K. Kondak, and G. Hommel, "Application of emg signals for controlling exoskeleton robots," 2006.

[5] Z. Yang, Y. Bai, and X. Chen, "Simultaneous optimal design of topology and size for a flexure-hinge-based guiding mechanism to minimize mass under stiffness and frequency constraints," *Engineering Optimization*, vol. 49, no. 6, pp. 948–961, 2017.

[6] S. Awtar, "Novel single-axis flexure mechanism designs with improved bearing stiffness."

[7] Q. Xu, "Design and development of a compact flexure-based xy precision positioning system with centimeter range," *IEEE Transactions on Industrial Electronics*, vol. 61, no. 2, pp. 893–903, 2013.

[8] D. F. Machekposhti, N. Tolou, and J. Herder, "A statically balanced fully compliant power transmission mechanism between parallel rotational axes," *Mechanism and Machine Theory*, vol. 119, pp. 51–60, 2018. [Online]. Available: https://www.sciencedirect.com/science/article/pii/S0094114X17304871

[9] L. H. Larry, S. P. Magleby, and B. M. OLsen, "Handbook of compliant mechanisms," *John Wiley & Sons Ltd, Hoboken*, 2013.

[10] P. Spanoudakis, L. Kiener, F. Cosandier, P. Schwab, L. Giriens, J. Kruis, D. Grivon, G. Psoni, C. Vrettos, and N. Bencheikh, "Large angle flexure pivot development for future science payloads for space applications," in *MATEC Web of Conferences*, vol. 304. EDP Sciences, 2019, p. 07016.

[11] A. F. Azocar, L. M. Mooney, L. J. Hargrove, and E. J. Rouse, "Design and characterization of an open-source robotic leg prosthesis," in *2018 7th IEEE International Conference on Biomedical Robotics and Biomechatronics (Biorob)*, 2018, pp. 111–118.

[12] H. Zhu, J. Doan, C. Stence, G. Lv, T. Elery, and R. Gregg, "Design and validation of a torque dense, highly backdrivable powered knee-ankle orthosis,"

in *2017 IEEE international conference on robotics and automation (ICRA)*. IEEE, 2017, pp. 504–510.

[13] M. K. Shepherd and E. J. Rouse, "Design and validation of a torque-controllable knee exoskeleton for sit-to-stand assistance," *IEEE/ASME Transactions on Mechatronics*, vol. 22, no. 4, pp. 1695–1704, 2017.

[14] A. Khalilian Motamed Bonab, "Simulation based optimal design of exoskeletons to reduce metabolic cost and improve energy efficiency," Ph.D. dissertation, 2021.

[15] F. E. Tosun and V. Patoglu, "Necessary and sufficient conditions for the passivity of impedance rendering with velocity-sourced series elastic actuation," *IEEE Transactions on Robotics*, vol. 36, no. 3, pp. 757–772, 2020.

[16] K. Kong, J. Bae, and M. Tomizuka, "A compact rotary series elastic actuator for human assistive systems," *IEEE/ASME transactions on mechatronics*, vol. 17, no. 2, pp. 288–297, 2011.

[17] J. Apkarian, S. Naumann, and B. Cairns, "A three-dimensional kinematic and dynamic model of the lower limb," *Journal of biomechanics*, vol. 22, no. 2, pp. 143–155, 1989.

[18] L. Blankevoort and R. Huiskes, "Validation of a three-dimensional model of the knee," *Journal of biomechanics*, vol. 29, no. 7, pp. 955–961, 1996.

[19] J. Bellemans, M. D. Ries, and J. M. Victor, *Total knee arthroplasty*. Springer, 2005.

[20] K.-M. Lee and J. Guo, "Kinematic and dynamic analysis of an anatomically based knee joint," *Journal of biomechanics*, vol. 43, no. 7, pp. 1231–1236, 2010.

[21] A. Williams and M. Logan, "Understanding tibio-femoral motion," *The Knee*, vol. 11, no. 2, pp. 81–88, 2004.

[22] K. Luttgens, "Kinesiology scientific basis of human motion," 1997.

[23] A. Sunderland, D. Tinson, E. Bradley, D. Fletcher, R. L. Hewer, and D. Wade, "Enhanced physical therapy improves recovery of arm function after stroke. a randomised controlled trial." *Journal of Neurology, Neurosurgery & Psychiatry*, vol. 55, no. 7, pp. 530–535, 1992.

[24] G. Kwakkel, B. J. Kollen, and H. I. Krebs, "Effects of robot-assisted therapy on upper limb recovery after stroke: a systematic review," *Neurorehabilitation and neural repair*, vol. 22, no. 2, pp. 111–121, 2008.

[25] J. Mehrholz, T. Platz, J. Kugler, and M. Pohl, "Electromechanical and robot-assisted arm training for improving arm function and activities of daily living after stroke," *Stroke*, vol. 40, no. 5, pp. e392–e393, 2009.

[26] W. Huo, S. Mohammed, J. C. Moreno, and Y. Amirat, "Lower limb wearable robots for assistance and rehabilitation: A state of the art," *IEEE systems Journal*, vol. 10, no. 3, pp. 1068–1081, 2014.

[27] B. Celebi, M. Yalcin, and V. Patoglu, "Assiston-knee: A self-aligning knee exoskeleton," in *2013 IEEE/RSJ International Conference on Intelligent Robots and Systems*. IEEE, 2013, pp. 996–1002.

[28] K. A. Witte, A. M. Fatschel, and S. H. Collins, "Design of a lightweight, tethered, torque-controlled knee exoskeleton," in *2017 international conference on rehabilitation robotics (ICORR)*. IEEE, 2017, pp. 1646–1653.

[29] M. A. Ergin and V. Patoglu, "A self-adjusting knee exoskeleton for robot-assisted treatment of knee injuries," in *2011 IEEE/RSJ International Conference on Intelligent Robots and Systems*. IEEE, 2011, pp. 4917–4922.

[30] H. Rifaï, S. Mohammed, W. Hassani, and Y. Amirat, "Nested saturation based control of an actuated knee joint orthosis," *Mechatronics*, vol. 23, no. 8, pp. 1141–1149, 2013. [Online]. Available: https://www.sciencedirect.com/science/article/pii/S0957415813001669

[31] H. Rifaï, S. Mohammed, K. Djouani, and Y. Amirat, "Toward lower limbs functional rehabilitation through a knee-joint exoskeleton," *IEEE Transactions on Control Systems Technology*, vol. 25, no. 2, pp. 712–719, 2016.

[32] J.-H. Kim, M. Shim, D. H. Ahn, B. J. Son, S.-Y. Kim, D. Y. Kim, Y. S. Baek, and B.-K. Cho, "Design of a knee exoskeleton using foot pressure and knee torque sensors," *International Journal of Advanced Robotic Systems*, vol. 12, no. 8, p. 112, 2015.

[33] M. Khamar and M. Edrisi, "Designing a backstepping sliding mode controller for an assistant human knee exoskeleton based on nonlinear disturbance observer," *Mechatronics*, vol. 54, pp. 121–132, 2018. [Online]. Available: https://www.sciencedirect.com/science/article/pii/S0957415818301259

[34] Y. Liao, Z. Zhou, and Q. Wang, "Biokex: A bionic knee exoskeleton with proxy-based sliding mode control," in *2015 Ieee International Conference on Industrial Technology (Icit)*. IEEE, 2015, pp. 125–130.

[35] K. Knaepen, P. Beyl, S. Duerinck, F. Hagman, D. Lefeber, and R. Meeusen, "Human–robot interaction: Kinematics and muscle activity inside a powered compliant knee exoskeleton," *IEEE transactions on neural systems and rehabilitation engineering*, vol. 22, no. 6, pp. 1128–1137, 2014.

[36] G. G. A. Elliott, "Design and evaluation of a quasi-passive robotic knee brace: on the effects of parallel elasticity on human running," Ph.D. dissertation, Massachusetts Institute of Technology, 2012.

[37] G. Elliott, G. S. Sawicki, A. Marecki, and H. Herr, "The biomechanics and energetics of human running using an elastic knee exoskeleton," in *2013 IEEE 13th international conference on rehabilitation robotics (ICORR)*. IEEE, 2013, pp. 1–6.

[38] A. M. Dollar and H. Herr, "Design of a quasi-passive knee exoskeleton to assist running," in *2008 IEEE/RSJ international conference on intelligent robots and systems*. IEEE, 2008, pp. 747–754.

[39] E. Rogers, P. Polygerinos, S. Allen, F. A. Panizzolo, C. J. Walsh, and D. P. Holland, "A quasi-passive knee exoskeleton to assist during descent," in *Wearable Robotics: Challenges and Trends*. Springer, 2017, pp. 63–67.

[40] K. Shamaei, P. C. Napolitano, and A. M. Dollar, "A quasi-passive compliant stance control knee-ankle-foot orthosis," in *2013 IEEE 13th International Conference on Rehabilitation Robotics (ICORR)*. IEEE, 2013, pp. 1–6.

[41] K. Shamaei, M. Cenciarini, A. A. Adams, K. N. Gregorczyk, J. M. Schiffman, and A. M. Dollar, "Design and evaluation of a quasi-passive knee exoskeleton for investigation of motor adaptation in lower extremity joints," *IEEE Transactions on Biomedical Engineering*, vol. 61, no. 6, pp. 1809–1821, 2014.

[42] R. Chaichaowarat, D. F. P. Granados, J. Kinugawa, and K. Kosuge, "Passive knee exoskeleton using torsion spring for cycling assistance," in *2017 IEEE/RSJ International Conference on Intelligent Robots and Systems (IROS)*. IEEE, 2017, pp. 3069–3074.

[43] R. Chaichaowarat, J. Kinugawa, and K. Kosuge, "Unpowered knee exoskeleton reduces quadriceps activity during cycling," *Engineering*, vol. 4, no. 4, pp. 471–478, 2018. [Online]. Available: https://www.sciencedirect.com/science/article/pii/S2095809917306835

[44] B. Yuan, B. Li, Y. Chen, B. Tan, M. Jiang, S. Tang, Y. Wei, Z. Wang, B. Ma, and J. Huang, "Designing of a passive knee-assisting exoskeleton for weight-bearing," in *International Conference on Intelligent Robotics and Applications*. Springer, 2017, pp. 273–285.

[45] B. Li, B. Yuan, S. Tang, Y. Mao, D. Zhang, C. Huang, and B. Tan, "Biomechanical design analysis and experiments evaluation of a passive knee-assisting exoskeleton for weight-climbing," *Industrial Robot: An International Journal*, 2018.

[46] R. Ranaweera, R. Gopura, T. Jayawardena, and G. K. Mann, "Development of a passively powered knee exoskeleton for squat lifting." *J. Robotics Netw. Artif. Life*, vol. 5, no. 1, pp. 45–51, 2018.

[47] H. Kawamoto, S. Lee, S. Kanbe, and Y. Sankai, "Power assist method for hal-3 using emg-based feedback controller," in *SMC'03 Conference Proceedings. 2003 IEEE International Conference on Systems, Man and Cybernetics. Conference Theme-System Security and Assurance (Cat. No. 03CH37483)*, vol. 2. IEEE, 2003, pp. 1648–1653.

[48] C. Fleischer and G. Hommel, "Embedded control system for a powered leg exoskeleton," in *Embedded Systems–Modeling, Technology, and Applications*. Springer, 2006, pp. 177–185.

[49] Y. Wang and S. Makeig, "Predicting intended movement direction using eeg from human posterior parietal cortex," in *International Conference on Foundations of Augmented Cognition*. Springer, 2009, pp. 437–446.

[50] E. Lew, R. Chavarriaga, S. Silvoni, and J. d. R. Millán, "Detection of self-paced reaching movement intention from eeg signals," *Frontiers in neuroengineering*, vol. 5, p. 13, 2012.

[51] C. Hintermüller, C. Guger, and G. Edlinger, "Brain-computer interface: generic control interface for social interaction applications," in *International Work-Conference on Artificial Neural Networks*. Springer, 2011, pp. 386–392.

[52] A. H. Do, P. T. Wang, C. E. King, S. N. Chun, and Z. Nenadic, "Brain-computer interface controlled robotic gait orthosis," *Journal of neuroengineering and rehabilitation*, vol. 10, no. 1, pp. 1–9, 2013.

[53] J. L. Pons, "Rehabilitation exoskeletal robotics," *IEEE Engineering in Medicine and Biology Magazine*, vol. 29, no. 3, pp. 57–63, 2010.

[54] D. J. Reinkensmeyer and M. L. Boninger, "Technologies and combination therapies for enhancing movement training for people with a disability," *Journal of neuroengineering and rehabilitation*, vol. 9, no. 1, pp. 1–10, 2012.

[55] S. Musallam, B. Corneil, B. Greger, H. Scherberger, and R. A. Andersen, "Cognitive control signals for neural prosthetics," *Science*, vol. 305, no. 5681, pp. 258–262, 2004.

[56] G. Santhanam, S. I. Ryu, B. M. Yu, A. Afshar, and K. V. Shenoy, "A high-performance brain–computer interface," *nature*, vol. 442, no. 7099, pp. 195–198, 2006.

[57] M. A. Lebedev and M. A. Nicolelis, "Brain–machine interfaces: past, present and future," *TRENDS in Neurosciences*, vol. 29, no. 9, pp. 536–546, 2006.

[58] A. J. Casson, D. C. Yates, S. J. Smith, J. S. Duncan, and E. Rodriguez-Villegas, "Wearable electroencephalography," *IEEE engineering in medicine and biology magazine*, vol. 29, no. 3, pp. 44–56, 2010.

[59] C. Fleischer, C. Reinicke, and G. Hommel, "Predicting the intended motion with emg signals for an exoskeleton orthosis controller," in *2005 IEEE/RSJ International Conference on Intelligent Robots and Systems*. IEEE, 2005, pp. 2029–2034.

[60] A. Zoss and H. Kazerooni, "Design of an electrically actuated lower extremity exoskeleton," *Advanced Robotics*, vol. 20, no. 9, pp. 967–988, 2006.

[61] S. K. Banala, S. K. Agrawal, S. H. Kim, and J. P. Scholz, "Novel gait adaptation and neuromotor training results using an active leg exoskeleton," *IEEE/ASME Transactions on mechatronics*, vol. 15, no. 2, pp. 216–225, 2010.

[62] J. Ghan, R. Steger, and H. Kazerooni, "Control and system identification for the berkeley lower extremity exoskeleton (bleex)," *Advanced Robotics*, vol. 20, no. 9, pp. 989–1014, 2006.

[63] J. Wang, X. Li, T.-H. Huang, S. Yu, Y. Li, T. Chen, A. Carriero, M. Oh-Park, and H. Su, "Comfort-centered design of a lightweight and backdrivable knee exoskeleton," *IEEE Robotics and Automation Letters*, vol. 3, no. 4, pp. 4265–4272, 2018.

[64] I. Kardan and A. Akbarzadeh, "Robust output feedback assistive control of a compliantly actuated knee exoskeleton," *Robotics and Autonomous Systems*, vol. 98, pp. 15–29, 2017. [Online]. Available: https://www.sciencedirect.com/science/article/pii/S0921889017300015

[65] D. Maeda, K. Tominaga, T. Oku, H. T. Pham, S. Saeki, M. Uemura, H. Hirai, and F. Miyazaki, "Muscle synergy analysis of human adaptation to a variable-stiffness exoskeleton: human walk with a knee exoskeleton with pneumatic artificial muscles," in *2012 12th IEEE-RAS International Conference on Humanoid Robots (Humanoids 2012)*. IEEE, 2012, pp. 638–644.

[66] F. el Zahraa Wehbi, W. Huo, Y. Amirat, M. El Rafei, M. Khalil, and S. Mohammed, "Active impedance control of a knee-joint orthosis during swing phase," in *2017 International Conference on Rehabilitation Robotics (ICORR)*. IEEE, 2017, pp. 435–440.

[67] P. Félix, J. Figueiredo, C. P. Santos, and J. C. Moreno, "Powered knee orthosis for human gait rehabilitation: first advances," in *2017 IEEE 5th Portuguese Meeting on Bioengineering (ENBENG)*. IEEE, 2017, pp. 1–4.

[68] P. Félix, J. Figueiredo, C. P. Santos, and J. C. Moreno, "Electronic design and validation of powered knee orthosis system embedded with wearable sensors," in *2017 IEEE International Conference on Autonomous Robot Systems and Competitions (ICARSC)*, 2017, pp. 110–115.

[69] J. Nikitczuk, A. Das, H. Vyas, B. Weinberg, and C. Mavroidis, "Adaptive torque control of electro-rheological fluid brakes used in active knee rehabilitation devices," in *Proceedings 2006 IEEE International Conference on Robotics and Automation, 2006. ICRA 2006.* IEEE, 2006, pp. 393–399.

[70] H. Shan, C. Jiang, Y. Mao, and X. Wang, "Design and control of a wearable active knee orthosis for walking assistance," in *2016 IEEE 14th International Workshop on Advanced Motion Control (AMC)*. IEEE, 2016, pp. 51–56.

[71] Y. Luo, C. Wang, Z. Wang, Y. Ma, C. Wang, and X. Wu, "Design and control for a compliant knee exoskeleton," in *2017 IEEE International Conference on Information and Automation (ICIA)*. IEEE, 2017, pp. 282–287.

[72] M. Chandrapal, X. Chen, and W. Wang, "Intelligent assistive knee exoskeleton," *Mechatronics*, pp. 195–237, 2013.

[73] I. Kardan and A. Akbarzadeh, "Assistive control of a compliantly actuated single axis stage," in *2016 4th International Conference on Robotics and Mechatronics (ICROM)*. IEEE, 2016, pp. 313–318.

[74] S. Sridar, Z. Qiao, N. Muthukrishnan, W. Zhang, and P. Polygerinos, "A soft-inflatable exosuit for knee rehabilitation: Assisting swing phase during walking," *Frontiers in Robotics and AI*, vol. 5, p. 44, 2018.

[75] S. Sridar, P. H. Nguyen, M. Zhu, Q. P. Lam, and P. Polygerinos, "Development of a soft-inflatable exosuit for knee rehabilitation," in *2017 IEEE/RSJ International Conference on Intelligent Robots and Systems (IROS)*. IEEE, 2017, pp. 3722–3727.

[76] M. R. Tucker, A. Moser, O. Lambercy, J. Sulzer, and R. Gassert, "Design of a wearable perturbator for human knee impedance estimation during gait," in *2013 IEEE 13th International Conference on Rehabilitation Robotics (ICORR)*. IEEE, 2013, pp. 1–6.

[77] M. R. Tucker, C. Shirota, O. Lambercy, J. S. Sulzer, and R. Gassert, "Design and characterization of an exoskeleton for perturbing the knee during gait," *IEEE Transactions on Biomedical Engineering*, vol. 64, no. 10, pp. 2331–2343, 2017.

[78] Z. Zhou, Y. Liao, C. Wang, and Q. Wang, "Preliminary evaluation of gait assistance during treadmill walking with a light-weight bionic knee exoskeleton," in *2016 IEEE International Conference on Robotics and Biomimetics (ROBIO)*, 2016, pp. 1173–1178.

[79] L. Saccares, I. Sarakoglou, and N. G. Tsagarakis, "it-knee: An exoskeleton with ideal torque transmission interface for ergonomic power augmentation," in *2016 IEEE/RSJ International Conference on Intelligent Robots and Systems (IROS)*, 2016, pp. 780–786.

[80] L. Saccares, A. Brygo, I. Sarakoglou, and N. G. Tsagarakis, "A novel human effort estimation method for knee assistive exoskeletons," in *2017 International Conference on Rehabilitation Robotics (ICORR)*. IEEE, 2017, pp. 1266–1272.

[81] A. Esquenazi, M. Talaty, A. Packel, and M. Saulino, "The rewalk powered exoskeleton to restore ambulatory function to individuals with thoracic-level motor-complete spinal cord injury," *American journal of physical medicine & rehabilitation*, vol. 91, no. 11, pp. 911–921, 2012.

[82] G. Colombo, M. Joerg, R. Schreier, V. Dietz *et al.*, "Treadmill training of paraplegic patients using a robotic orthosis," *Journal of rehabilitation research and development*, vol. 37, no. 6, pp. 693–700, 2000.

[83] M. Freeman, "How the knee moves," *Current Orthopaedics*, vol. 15, no. 6, pp. 444–450, 2001.

[84] Y. Niu, Z. Song, and J. Dai, "Design of the planar compliant five-bar mechanism for self-aligning knee exoskeleton," in *2018 International Conference on Reconfigurable Mechanisms and Robots (ReMAR)*. IEEE, 2018, pp. 1–7.

[85] X. Tang and L. Chen, "Structural design of a novel wearable knee exoskeleton," in *2018 8th International Conference on Manufacturing Science and Engineering (ICMSE 2018)*. Atlantis Press, 2018, pp. 348–353.

[86] R. Mallat, M. Khalil, G. Venture, V. Bonnet, and S. Mohammed, "Human-exoskeleton joint misalignment: A systematic review," in *2019 Fifth International Conference on Advances in Biomedical Engineering (ICABME)*. IEEE, 2019, pp. 1–4.

[87] N. Jarrassé and G. Morel, "Connecting a human limb to an exoskeleton," *IEEE Transactions on Robotics*, vol. 28, no. 3, pp. 697–709, 2011.

[88] B. Lee, S. C. Lee, and C.-s. Han, "Design of fixations for an exoskeleton device with joint axis misalignments," *International Journal of Precision Engineering and Manufacturing*, vol. 21, no. 7, pp. 1291–1298, 2020.

[89] V. Bartenbach, D. Wyss, D. Seuret, and R. Riener, "A lower limb exoskeleton research platform to investigate human-robot interaction," in *2015 IEEE International Conference on Rehabilitation Robotics (ICORR)*. IEEE, 2015, pp. 600–605.

[90] S. C. Cevik, M. Derman, R. Unal, B. Ugurlu, and O. Bebek, "A custom brace design to connect a user limb to an exoskeleton link with minimal discomfort," in *2021 IEEE 19th International Conference on Industrial Informatics (INDIN)*, 2021, pp. 1–6.

[91] J. Wang, X. Li, T.-H. Huang, S. Yu, Y. Li, T. Chen, A. Carriero, M. Oh-Park, and H. Su, "Comfort-centered design of a lightweight and backdrivable knee exoskeleton," *IEEE Robotics and Automation Letters*, vol. 3, no. 4, pp. 4265–4272, 2018.

[92] B. Choi, Y. Lee, J. Kim, M. Lee, J. Lee, S.-G. Roh, H. Choi, Y.-J. Kim, and J.-Y. Choi, "A self-aligning knee joint for walking assistance devices," in *2016 38th Annual International Conference of the IEEE Engineering in Medicine and Biology Society (EMBC)*. IEEE, 2016, pp. 2222–2227.

[93] S. V. Sarkisian, M. K. Ishmael, and T. Lenzi, "Self-aligning mechanism improves comfort and performance with a powered knee exoskeleton," *IEEE Transactions on Neural Systems and Rehabilitation Engineering*, vol. 29, pp. 629–640, 2021.

[94] V. A. D. Cai, P. Bidaud, V. Hayward, F. Gosselin, and E. Desailly, "Self-adjusting, isostatic exoskeleton for the human knee joint," in *2011 Annual International Conference of the IEEE Engineering in Medicine and Biology Society*. IEEE, 2011, pp. 612–618.

[95] Y. Lee, Y.-J. Kim, J. Lee, M. Lee, B. Choi, J. Kim, Y. J. Park, and J. Choi, "Biomechanical design of a novel flexible exoskeleton for lower extremities," *IEEE/ASME Transactions on Mechatronics*, vol. 22, no. 5, pp. 2058–2069, 2017.

[96] A. H. Slocum, *Precision machine design*. Society of Manufacturing Engineers, 1992.

[97] S. T. Smith, *Foundations of ultra-precision mechanism design*. CRC Press, 2003, vol. 2.

[98] S. Awtar, A. H. Slocum, and E. Sevincer, "Characteristics of beam-based flexure modules," 2007.

[99] N. B. Hubbard, J. W. Wittwer, J. A. Kennedy, D. L. Wilcox, and L. L. Howell, "A novel fully compliant planar linear-motion mechanism," in *International Design Engineering Technical Conferences and Computers and Information in Engineering Conference*, vol. 46954, 2004, pp. 1–5.

[100] J. Seggelen, P. Rosielle, P. Schellekens, H. Spaan, R. Bergmans, and G. Kotte, "An elastically guided machine axis with nanometer repeatability," *CIRP annals*, vol. 54, no. 1, pp. 487–490, 2005.

[101] G. Parmar, K. Barton, and S. Awtar, "Large dynamic range nanopositioning using iterative learning control," *Precision engineering*, vol. 38, no. 1, pp. 48–56, 2014.

[102] R. Legtenberg, A. Groeneveld, and M. Elwenspoek, "Comb-drive actuators for large displacements," *Journal of Micromechanics and microengineering*, vol. 6, no. 3, p. 320, 1996.

[103] M. Olfatnia, S. Sood, J. J. Gorman, and S. Awtar, "Large stroke electrostatic comb-drive actuators enabled by a novel flexure mechanism," *Journal of Microelectromechanical Systems*, vol. 22, no. 2, pp. 483–494, 2012.

[104] R. Alami, A. Albu-Schaeffer, A. Bicchi, R. Bischoff, R. Chatila, A. De Luca, A. De Santis, G. Giralt, J. Guiochet, G. Hirzinger, and et al., "Safe and dependable physical human-robot interaction in anthropic domains: State of the art and challenges," *2006 IEEE/RSJ International Conference on Intelligent Robots and Systems*, 2006.

[105] S. Eppinger and W. Seering, "[pdf] understanding bandwidth limitations in robot force control: Semantic scholar," Jan 1987. [Online]. Available: https://www.semanticscholar.org/paper/Understanding-bandwidth-limitations-in-robot-force-Eppinger-Seering/b8ee657ea908903b600262bc70f0adf4eb23376a

[106] G. Pratt and M. Williamson, "Series elastic actuators," *Proceedings 1995 IEEE/RSJ International Conference on Intelligent Robots and Systems. Human Robot Interaction and Cooperative Robots*, 1995.

[107] H. P. Crowell III, A. C. Boynton, and M. Mungiole, "Exoskeleton power and torque requirements based on human biomechanics," Army Research Lab Aberdeen Proving Ground Md, Tech. Rep., 2002.

[108] S. Awtar, A. H. Slocum, and E. Sevincer, "Characteristics of beam-based flexure modules," *Journal of Mechanical Design*, vol. 129, no. 6, p. 625–639, 2006.

[109] Q. Xu, "New flexure parallel-kinematic micropositioning system with large workspace," *IEEE Transactions on Robotics*, vol. 28, no. 2, pp. 478–491, 2011.

[110] M. Rad Golchin Mashhadi and H. Moeenfard, "Load-displacement behavior of fundamental flexure modules interconnected with compliant elements," *Mechanism and Machine Theory*, vol. 120, no. 1, pp. 120–139, January 2017.

[111] K. Shamaei, G. S. Sawicki, and A. M. Dollar, "Estimation of quasi-stiffness of the human knee in the stance phase of walking," *PloS one*, vol. 8, no. 3, p. e59993, 2013.

[112] C. U. Kenanoglu and V. Patoglu, "Passivity of series elastic actuation under model reference force control during null impedance rendering," *IEEE Transactions on Haptics*, vol. 15, no. 1, pp. 51–56, 2022.

[113] R. W. Parmentier, "Design and control of a low cost and compliant assistive knee exoskeleton," Arizona State University, Tech. Rep., 2020.

[114] M. Roebroeck, C. Doorenbosch, J. Harlaar, R. Jacobs, and G. Lankhorst, "Biomechanics and muscular activity during sit-to-stand transfer," *Clinical Biomechanics*, vol. 9, no. 4, pp. 235–244, 1994.

[115] M. K. Shepherd and E. J. Rouse, "Design and validation of a torque-controllable knee exoskeleton for sit-to-stand assistance," *IEEE/ASME Transactions on Mechatronics*, vol. 22, no. 4, pp. 1695–1704, 2017.

[116] R. Baud, A. R. Manzoori, A. Ijspeert, and M. Bouri, "Review of control strategies for lower-limb exoskeletons to assist gait," *Journal of NeuroEngineering and Rehabilitation*, vol. 18, no. 1, pp. 1–34, 2021.

[117] R. D. Howard, "Joint and actuator design for enhanced stability in robotic force control," Ph.D. dissertation, Massachusetts Institute of Technology, 1990.

[118] G. A. Pratt and M. M. Williamson, "Series elastic actuators," in *Proceedings 1995 IEEE/RSJ International Conference on Intelligent Robots and Systems. Human Robot Interaction and Cooperative Robots*, vol. 1. IEEE, 1995, pp. 399–406.

[119] A. Erdogan, B. Celebi, A. C. Satici, and V. Patoglu, "Assist on-ankle: a reconfigurable ankle exoskeleton with series-elastic actuation," *Autonomous Robots*, vol. 41, no. 3, pp. 743–758, 2017.

[120] J. E. Colgate and N. Hogan, "Robust control of dynamically interacting systems," *International journal of Control*, vol. 48, no. 1, pp. 65–88, 1988.

[121] N. Hogan, "Controlling impedance at the man/machine interface," in *1989 IEEE International Conference on Robotics and automation*. IEEE Computer Society, 1989, pp. 1626–1627.